



Turun yliopisto
University of Turku

IMAGING NEUROINFLAMMATION IN PROGRESSIVE MULTIPLE SCLEROSIS

Eero Rissanen

University of Turku

Faculty of Medicine
Department of Clinical Medicine
Department of Neurology and Turku PET Centre
Turku Doctoral Programme of Clinical Investigation
Division of clinical neurosciences, Turku University Hospital

Supervised by

Docent Laura Airas
Division of Clinical Neurosciences
Turku University Hospital and
University of Turku, Turku, Finland

Professor Juha O. Rinne
Turku PET Centre
Turku University Hospital and
University of Turku, Turku, Finland

Reviewed by

Docent Hanna Kuusisto
Department of Neurology
Kanta-Häme Central Hospital,
Hämeenlinna, Finland

Senior Lecturer Alexander Gerhard
Institute of Brain, Behaviour
and Mental Health, University of
Manchester, Manchester, UK

Opponent

Professor Bruno Stankoff
Department of Neurology,
Saint-Antoine University Hospital and
Brain & Spine Institute, University of
Pierre et Marie Curie, Paris, France

The originality of this thesis has been checked in accordance with the University of Turku quality assurance system using the Turnitin OriginalityCheck service.

Cover picture: Eero Rissanen

ISBN 978-951-29-6098-9 (PRINT)
ISBN 978-951-29-6099-6 (PDF)
ISSN 0355-9483
Painosalama Oy - Turku, Finland 2015

To my loved ones

ABSTRACT

Eero Rissanen

IMAGING NEUROINFLAMMATION IN PROGRESSIVE MULTIPLE SCLEROSIS

Faculty of Medicine, Department of Clinical Medicine, Department of Neurology and Turku PET Centre; Turku Doctoral Programme of Clinical Investigation; Division of clinical neurosciences, Turku University Hospital.

Multiple sclerosis (MS) is a chronic autoimmune disease of the central nervous system (CNS), where inflammation and neurodegeneration lead to irreversible neuronal damage. In MS, a dysfunctional immune system causes auto-reactive lymphocytes to migrate into CNS where they initiate an inflammatory cascade leading to focal demyelination, axonal degeneration and neuronal loss. One of the hallmarks of neuronal injury and neuroinflammation is the activation of microglia. Activated microglia are found not only in the focal inflammatory lesions, but also diffusely in the normal-appearing white matter (NAWM), especially in progressive MS. The purine base, adenosine is a ubiquitous neuromodulator in the CNS and also participates in the regulation of inflammation. The effect of adenosine mediated via adenosine A_{2A} receptors has been linked to microglial activation, whereas modulating A_{2A} receptors may exert neuroprotective effects. In the majority of patients, MS presents with a relapsing disease course, later advancing to a progressive phase characterised by a worsening, irreversible disability. Disease modifying treatments can reduce the severity and progression in relapsing MS, but no efficient treatment exists for progressive MS.

The aim of this research was to investigate the prevalence of adenosine A_{2A} receptors and activated microglia in progressive MS by using *in vivo* positron emission tomography (PET) imaging and [^{11}C]TMSX and [^{11}C](R)-PK11195 radioligands. Magnetic resonance imaging (MRI) with diffusion tensor imaging (DTI) was performed to evaluate structural brain damage. Non-invasive input function methods were also developed for the analyses of [^{11}C]TMSX PET data. Finally, histopathological correlates of [^{11}C](R)-PK11195 radioligand binding related to chronic MS lesions were investigated in post-mortem samples of progressive MS brain using autoradiography and immunohistochemistry.

[^{11}C]TMSX binding to A_{2A} receptors was increased in NAWM of secondary progressive MS (SPMS) patients when compared to healthy controls, and this correlated to more severe atrophy in MRI and white matter disintegration (reduced fractional anisotropy, FA) in DTI. The non-invasive input function methods appeared as feasible options for brain [^{11}C]TMSX images obviating arterial blood sampling. [^{11}C](R)-PK11195 uptake was increased in the NAWM of SPMS patients when compared to patients with relapsing MS and healthy controls. Higher [^{11}C](R)-PK11195 binding in NAWM and total perilesional area of T1 hypointense lesions was associated with more severe clinical disability, increased brain atrophy, higher lesion load and reduced FA in NAWM in the MS patients. In autoradiography, increased perilesional [^{11}C](R)-PK11195 uptake was associated with increased microglial activation identified using immunohistochemistry.

In conclusion, brain [^{11}C]TMSX PET imaging holds promise in the evaluation of diffuse neuroinflammation in progressive MS. Being a marker of microglial activation, [^{11}C](R)-PK11195 PET imaging could possibly be used as a surrogate biomarker in the evaluation of the neuroinflammatory burden and clinical disease severity in progressive MS.

Key words: Multiple sclerosis, disease progression, adenosine, microglia, PET, DTI, MRI

TIIVISTELMÄ

Eero Rissanen

NEUROINFLAMMAATION KUVANTAMINEN PROGRESSIIVISESSA MS-TAUDISSA

Lääketieteellinen tiedekunta, kliininen laitos, neurologian oppiaine ja valtakunnallinen PET-keskus; Turun kliininen tutkijakoulu; Turun yliopistollisen keskussairaalan neurotoimialue.

Multipeliskleroosi eli MS-tauti on krooninen keskushermoston (KH) autoimmuunisairaus, jossa tulehdusreaktio (inflammaatio) ja hermosolujen rappeutuminen johtavat pysyvään hermoston vaurioitumiseen. Sairaudessa virheellisesti toimiva immuunipuolustus tuottaa omia KH:n rakenteita vastaan hyökkääviä valkosoluja, jotka sinne päästyään käynnistävät paikallisia inflammaatioreaktiota aiheuttaen myeliinin rappeutumista ja aksonikatoa. Yksi inflammaation tunnusmerkeistä MS-taudissa on mikroglIASolujen aktivoituminen, jota tavataan paitsi paikallisissa inflammaatio-muutoksissa, myös normaalilta näyttävässä valkeassa aineessa (normal appearing white matter; NAWM). Adenosiini on välittäjäaine, joka osallistuu muun muassa inflammaation säätelyyn KH:ssa. Adenosiini vaikuttaa myös mikroglIASolujen aktiivisuuteen adenosiinin A_{2A} -reseptorien välityksellä. A_{2A} -reseptorien toiminnan muovaamisella puolestaan voi olla neuroprotektiivisiä vaikutuksia. Suurimmalla osalla potilaista MS-tauti alkaa aaltomaisella taudinkuvalla, mutta siirtyy progressiiviseen taudin vaiheeseen, jossa toimintakyky vähitellen heikkenee vääjäämättä. Aaltomaisen taudin kulkuun voidaan vaikuttaa immuunipuolustusta muovaavilla lääkityksillä, mutta progressiivisen MS-taudin ei ole tehoavaa hoitoa.

Tämän tutkimuksen tarkoituksena oli selvittää aivojen A_{2A} -reseptoreiden ja aktivoituneiden mikroglIASolujen merkitystä etenevässä MS taudissa positroni-emissiotomografian (PET) sekä A_{2A} -reseptoreihin sitoutuvan [^{11}C]TMSX- ja aktivoituneisiin mikroglIASoluihin sitoutuvan [^{11}C](R)-PK11195-merkkiaineen avulla. Magneettikuvantamista ja diffuusiotensorikuvantamista (DTI) käytettiin aivojen rakenteellisten vaurioiden arviointiin. Tavoitteena oli myös kehittää verinäytteiden otosta riippumattoman [^{11}C]TMSX-kuvantamisen mahdollistavia analyysimenetelmiä. Lisäksi kroonisiin MS-plakkeihin liittyvää mikroglIASolujen aktivaatiota tutkittiin [^{11}C](R)-PK11195-autoradiografian ja immunohistokemian avulla progressiivista MS-tautia sairastaneiden potilaiden ruumiinavausnäytteistä.

[^{11}C]TMSX-sitoutuminen A_{2A} -reseptoreihin oli lisääntynyt sekundaaris-progressiivista MS-tautia (SPMS) sairastavien potilaiden NAWM:ssa. Lisääntynyt [^{11}C]TMSX-sitoutuminen NAWM:ssa korreloi voimakkaampaan valkean aineen atrofiaan ja alentuneeseen fraktionaaliseen anisotropiaan (FA) NAWM:issa merkinä valkean aineen radastovauriosta. [^{11}C]TMSX:n sitoutumispotentiaalın arvioimiseen kehitetyt ei-kajoavat menetelmät osoittautuivat luotettaviksi mahdollistaen valtimoverinäytteiden otosta luopumisen jatkossa. [^{11}C](R)-PK11195 sitoutuminen oli voimakkaampaa SPMS-potilaiden NAWM:ssa verrattuna aaltomaista MS-tautia sairastaviin potilaisiin ja terveisiin. Suurempi [^{11}C](R)-PK11195 sitoutuminen NAWM:ssa ja kroonisia MS-plakkeja ympäröivässä valkeassa aineessa korreloi vaikeampaan kliiniseen taudinkuvaan, lisääntyneeseen aivoatrofiaan, ja alentuneeseen FA:han NAWM:ssa. Autoradiografia-tutkimuksissa [^{11}C](R)-PK11195:n lisääntynyt sitoutuminen plakkeja ympäröivässä valkeassa aineessa liittyi immunohistokemiallisesti tunnistettujen, aktivoituneiden mikroglIASolujen suurentuneeseen määrän vastaavilla alueilla.

Tulosten perusteella voidaan todeta, että [^{11}C]TMSX PET -kuvantaminen on lupaava menetelmä aivojen laaja-alaisen inflammaation arviointiin etenevässä MS-taudissa. Lisäksi [^{11}C](R)-PK11195 PET -kuvantamista voidaan käyttää laaja-alaisen tulehduskuorman mittarina sekä mahdollisesti etenevän MS-taudin tunnistamiseen ja sen vaikeusasteen arvioimiseen.

Avainsanat: MS-tauti, taudin eteneminen, adenosiini, mikroglia, PET, DTI, MRI

TABLE OF CONTENTS

ABSTRACT	4
TIIVISTELMÄ	5
TABLE OF CONTENTS	6
ABBREVIATIONS	8
LIST OF ORIGINAL PUBLICATIONS	11
1. INTRODUCTION	12
2. REVIEW OF THE LITERATURE	14
2.1 Multiple sclerosis	14
2.1.1 Epidemiology	14
2.1.2 Risk factors	14
2.1.3 Disease course, clinical diagnosis and treatment in MS	15
2.1.4 Pathogenesis	19
2.1.4.1 Neuroinflammation	19
2.1.4.2 Neurodegeneration	23
2.2 Role of microglia and adenosine in MS	24
2.2.1 Microglia in neuroinflammation and MS	24
2.2.2 Adenosine in neuroinflammation and MS	27
2.3 Imaging methods of neuroinflammation in MS	30
2.3.1 Magnetic resonance imaging (MRI)	30
2.3.1.1 Physical basis of conventional MRI	30
2.3.1.2 Applications of conventional MRI in MS	31
2.3.1.3 Physical basis of diffusion tensor imaging (DTI)	32
2.3.1.4 Applications of DTI in MS	34
2.3.2 Positron emission tomography (PET)	35
2.3.2.1 Principles of PET physics	35
2.3.2.2 PET scanner and acquisition of image data	36
2.3.2.3 Pharmacokinetic modelling of neuroreceptor binding	38
2.3.2.4 Radioligands in the imaging of neuroinflammation	40
3. AIMS OF THE STUDY	46
4. METHODS	47
4.1 Study population and clinical assessment	47
4.2 MRI	50
4.2.1 Volumetric Analyses and Evaluation of MS Lesions	51
4.2.2 DTI analyses	51
4.3 PET imaging	52
4.3.1 Radiochemical synthesis of [¹¹ C]TMSX	52
4.3.2 Radiochemical synthesis of [¹¹ C](R)-PK11195	53
4.3.3 PET Image Acquisition	54
4.3.4 Blood radioactivity and metabolite analyses	54
4.3.5 Preprocessing of MRI and PET image data	55
4.3.6 Definition of Regions of Interest (ROI)	56
4.3.7 Modelling of [¹¹ C]TMSX and [¹¹ C](R)-PK11195 image data	58
4.3.7.1 ROI analyses	58

4.3.7.2	Parametric image analyses	59
4.3.7.3	Visual evaluation of [¹¹ C](R)-PK11195 binding in T1-lesions	59
4.4	Developing non-invasive input functions for [¹¹ C]TMSX analyses.....	60
4.4.1	Population based input function.....	60
4.4.2	Clustered Reference Region Acquisition	60
4.5	Post-mortem [¹¹ C](R)-PK11195 autoradiography and immunohistochemistry of progressive MS brain samples.....	61
4.6	Statistical methods	62
5.	RESULTS.....	64
5.1	Demographics and clinical characteristics.....	64
5.2	MRI and DTI in healthy controls and MS patients	64
5.2.1	Increased atrophy, lesion load and DTI abnormalities in SPMS	64
5.2.2	Association of brain atrophy and reduced FA to disability and age..	66
5.3	<i>In vivo</i> imaging of adenosine A _{2A} receptors with [¹¹ C]TMSX.....	67
5.3.1	Increased [¹¹ C]TMSX binding in NAWM of SPMS patients in comparison to healthy controls.....	67
5.3.2	Automated reference region extraction and non-invasive input functions for [¹¹ C]TMSX image analyses	69
5.3.2.1	Reference region extraction	70
5.3.2.2	[¹¹ C]TMSX distribution volumes in SCgm and cerebellum reference regions with OPIF and PBIFs.....	70
5.3.2.3	Performance of PBIFs and SCgm in the estimation of [¹¹ C]TMSX binding in target regions.....	73
5.4	<i>In vivo</i> imaging of activated microglia with [¹¹ C](R)-PK11195.....	77
5.4.1	Increased [¹¹ C](R)-PK11195 binding in NAWM and thalami of SPMS patients in comparison to healthy controls.....	77
5.4.2	[¹¹ C](R)-PK11195 PET in determining clinical severity and disease type in RRMS and SPMS.....	79
5.4.2.1	ROI specific [¹¹ C](R)-PK11195 binding.....	79
5.4.2.2	Correlations of [¹¹ C](R)-PK11195 binding to clinical and MRI parameters in all MS patients.....	80
5.5	Post-mortem [¹¹ C](R)-PK11195 autoradiography and immunohistochemistry of progressive MS brain samples.....	85
6.	DISCUSSION.....	88
6.1	Summary of the main findings	88
6.2	Methodological considerations.....	89
6.3	Adenosine A _{2A} receptors in progressive MS.....	91
6.4	TSPO and activated microglia in progressive MS.....	92
6.5	MRI and DTI abnormalities in progressive MS	96
7.	CONCLUSIONS.....	97
8.	ACKNOWLEDGEMENTS.....	98
9.	REFERENCES.....	100
	ORIGINAL PUBLICATIONS.....	113

ABBREVIATIONS

ABSS	Arterial blood sampling system
AD	Alzheimer's disease
AAL	Anatomic automatic labelling
BBB	Blood brain barrier
BET	Brain extraction tool
B_{\max}	Receptor availability
BP	Binding potential
BP_{ND}	Non-displaceable binding potential
BSA	Body surface area
C	Cytosine
cAMP	Cyclic adenosine monophosphate
CAMs	Cell adhesion molecules
CB2	Cannabinoid receptor 2
CD	Cluster of differentiation
C_F	Free compartment
CIS	Clinically isolated syndrome
CNS	Central nervous system
C_{ND}	Non-displaceable compartment
C_{NS}	Non-specific compartment
COX1	Cyclo-oxygenase 1
C_P	Plasma compartment
CSF	Cerebrospinal fluid
CV	Coefficient of variance
DAWM	Dirty appearing white matter
DIT	Dissemination in time
DIS	Disseminations in space
DMT	Disease modifying therapy
DNA	Deoxyribonucleic acid
DTI	Diffusion tensor imaging
DV	Distribution volume
DVR	Distribution volume ratio
DWI	Diffusion weighted imaging
EAE	Experimental autoimmune encephalitis
EDSS	Expanded disability status scale
FA	Fractional anisotropy
FDT	FMRIB's Diffusion Toolbox
FLAIR	Fluid attenuated inversion recovery

FLIRT	FMRIB's Linear Image Registration Tool
FMRIB	Functional Magnetic Resonance Imaging of the Brain
FNIRT	FMRIB's Nonlinear Image Registration Tool
FSL	FMRIB software library
FWHM	Full width half maximum
GABA	Gamma aminobutyric acid
GFAP	Glial fibrillary acidic protein
GM	Gray matter
HAB	High affinity binder
HD	Huntington's disease
HLA	Human leukocyte antigen
HPLC	High-performance liquid chromatography
HRRT	High resolution research tomography
HSB	High specific binding
IgG	Immunoglobulin G
IFN- γ	Interferon gamma
IL	Interleukin
i.m.	Intramuscular
IgG	Immunoglobulin G
IQR	Interquartile range
i.v.	Intravenous
K_d	Dissociation constant
LAB	Low affinity binder
LFB	Luxol fast blue
LBD	Lewy Body Dementia
LOR	Line of response
LPC	Lysophosphatidylcholine
LPS	Lipopolysaccharide
LST	Lesion segmentation tool
MAB	Medium affinity binder
MD	Mean diffusivity
MMP	Matrix metalloproteinase
MNI	Montreal Neurological Institute
MRI	Magnetic resonance imaging
MS	Multiple sclerosis
MSSS	Multiple sclerosis severity score
MTR	Magnetisation transfer ratio
NAGM	Normal appearing gray matter
NAWM	Normal appearing white matter
NRF2	Nuclear factor erythroid 2 -related factor 2

OPIF	Original plasma input function
PBIF	Population based input function
PBIFis	Population based input function; invasive, individually scaled
PBIFnis	Population based input function; noninvasive, individually scaled
PBR	Peripheral benzodiazepine receptor
PD	Parkinson's disease
PET	Positron emission tomography
p.o.	Peroral
PPMS	Primary progressive MS
PS	Phosphatidylserine
RF	Radiofrequency
ROI	Region of interest
RRMS	Relapsing remitting multiple sclerosis
S1P	Sphingosine-1-phosphate
s.c.	Subcutaneous
SCgm	supervised clustering derived gray matter reference region
SD	Standard deviation
SIENAX	Structural image evaluation, using normalization, of atrophy
SPECT	Single photon emission computed tomography
SPM	Statistical parametric mapping
SPMS	Secondary progressive multiple sclerosis
SUV	Standardised uptake value
SVCA	Supervised cluster algorithm
T	Thymidine
TAC	Time activity curve
TBSS	Tract based spatial statistics
Th1	T-helper 1 cell
Th2	T-helper 2 cell
TNF	Tumour necrosis factor
Treg	T-regulatory cell
TSPO	Translocator protein
UPDRS	Unified Parkinson's disease rating scale
VBM	Voxel based morphometry
VCAM1	Vascular cell adhesion molecule 1
VLA-4	Very late antigen 4
V_T	Total distribution volume
WM	White matter

LIST OF ORIGINAL PUBLICATIONS

This thesis is based on the following publications, which are referred to in the text by the Roman numerals I-IV:

- I Rissanen E, Virta JR, Paavilainen T, Tuisku J, Helin S, Luoto P, Parkkola R, Rinne JO, Airas L. Adenosine A2A receptors in secondary progressive multiple sclerosis: a [¹¹C]TMSX brain PET study. *J Cereb Blood Flow Metab* 2013;33:1394-1401 [epub 2013 May 22].
- II Rissanen E, Tuisku J, Luoto P, Arponen E, Johansson J, Oikonen V, Parkkola R, Airas L, Rinne JO. Automated Reference Region Extraction and Population Based Input Function for Brain [¹¹C]TMSX PET Image Analyses. *J Cereb Blood Flow Metab* 2015;35:157-65 [epub 2014 Nov 5].
- III Rissanen E, Tuisku J, Rokka J, Paavilainen T, Parkkola R, Rinne JO, Airas L. In Vivo Detection of Diffuse Inflammation in Secondary Progressive Multiple Sclerosis Using PET Imaging and the Radioligand [¹¹C]PK11195. *J Nucl Med* 2014;55:939-944 [epub 2014 April 7].
- IV Rissanen E, Tuisku J, Gardberg M, Dickens A, Sucksdorff M, Rokka J, Paavilainen T, Parkkola R, Rinne JO, Airas L. Microglial activation correlates with disease progression in multiple sclerosis. Submitted.

The original publications have been reprinted with the permission of the copyright holders.

1. INTRODUCTION

Multiple sclerosis (MS) is an autoimmune disease of the central nervous system (CNS), where neuroinflammation and neurodegeneration are the two main components in the pathogenesis. Even though the initial cause of the disease is not entirely understood, several environmental and genetic predisposing factors have been identified. The clinical presentation of the MS is heterogeneous, with the most typical form at the onset of the disease being relapsing remitting MS (RRMS) which is characterised by acute worsening of symptoms followed by a full or partial recovery. In the majority of patients, RRMS shifts into to the secondary progressive MS (SPMS), where slowly cumulating symptoms cause an irreversible and progressive disability (Compston and Coles 2008).

The inflammatory activity in RRMS can be suppressed with disease modifying therapies; these can reduce the numbers of acute worsening of symptoms, (relapses) , and the progression of the disease can be slowed down to some extent (Costello et al. 2014). Tragically, there is no curative treatment for MS and moreover, no effective treatment available to prevent the cumulative disability in the progressive forms of the disease. Since it is the most common disability causing neurological disease in young adults (Kutzelnigg and Lassmann 2014), the socioeconomic impact of MS is considerable both in terms of individual suffering and its burden on the health service budget (Compston and Coles 2008, Kobelt et al. 2006). Thus, more research is clearly needed in order to understand the pathophysiology, to develop alternative biomarkers for the evaluation of disease activity, and to seek alternative pathways for therapeutic development in the treatment of progressive MS.

According to current understanding, both neuroinflammation and neurodegeneration occur during all stages of MS. However, despite increasing evidence that neuroinflammation is the driving force behind neurodegeneration, it is still debated whether neurodegeneration in MS can propagate independently of neuroinflammation (Frischer et al. 2009, Kutzelnigg and Lassmann 2014, Lassmann et al. 2012, Trapp and Nave 2008). Although axonal loss underlies the transition from relapsing to progressive MS, neurodegeneration with axonal transections is known to occur already in the very early course of the disease (Compston and Coles 2008, Trapp et al. 1998). On the other hand, by studying progressive MS, one may gain important insights about the degenerative component of MS present in all stages of the disease. Activation of microglia, the intrinsic cells of innate immunity in the CNS, is one of the key inflammatory components which can be detected not only in active, but also in the borders of chronic lesions, and even in areas of the brain appearing normal in conventional magnetic resonance imaging (MRI). (Frischer et al. 2009, Lassmann et al. 2012) When microglia are activated following an insult, they become mobile and capable of phagocytosis and antigen presentation. It has been proposed that in chronic neuroinflammation, the equilibrium between “resting” and activated states of

microglia becomes unbalanced, and the overactivated microglia cause uncontrolled neuronal damage resulting in a self-propagating vicious cycle and progressive neurodegeneration (Gao and Hong 2008).

Another viewpoint for understanding neuroinflammation in MS is to study adenosine-related phenomena. Adenosine is an endogenous purine nucleotide which participates in the regulation of numerous physiological functions, including neuronal survival and the regulation of inflammation in the central nervous system CNS. There are four known subtypes of adenosine receptors; of these, the A₁ and A_{2A} subtypes are the most abundant in CNS and are located in the neuronal synapses (Blackburn et al. 2009, Chen et al. 2014). Based on studies conducted in animal models, it has been postulated that treatment with A_{2A} antagonists might be beneficial in late stage neurodegenerative diseases (Sebastião and Ribeiro 2009). Moreover, the beneficial effects of A_{2A} antagonism in reducing neuroinflammation may be partially mediated by their effects to limit microglial activation (Rebola et al. 2011, Saura et al. 2005).

It is not possible to examine specific molecular pathophysiology and neuroreceptor binding with magnetic resonance imaging (MRI), even though this technique remains the cornerstone of modern clinical diagnostics and follow-up of MS, also being widely used in MS research. In contrast, positron emission tomography (PET) imaging has the capability to allow molecular and neuroreceptor imaging *in vivo*. In the PET imaging of activated microglia, several radioligands binding to the translocator protein (TSPO) – a protein structure expressed on the outer mitochondrial membrane of activated, but not resting microglia – have been developed (Ching et al. 2012). Similarly, the estimation of adenosine A_{2A} receptors can be evaluated with PET tracers binding selectively to A_{2A} receptors (Mishina and Ishiwata 2014).

The aim of this study was to investigate the role of activated microglia and adenosine A_{2A} receptors in progressive MS by using *in vivo* PET imaging with radioligands [¹¹C](R)-PK11195 and [¹¹C]TMSX, respectively, in healthy controls and in patients with SPMS and RRMS. In addition, it was evaluated whether the findings in [¹¹C](R)-PK11195 and [¹¹C]TMSX PET imaging would correlate with the clinical parameters of disease severity and with the pathological findings in conventional MRI and diffusion tensor imaging (DTI). Finally, histopathological correlates of [¹¹C](R)-PK11195 binding in post mortem brains of patients with progressive MS were sought between the results of autoradiography and immunohistochemistry.

2. REVIEW OF THE LITERATURE

2.1 Multiple sclerosis

2.1.1 Epidemiology

MS is an autoimmune disease of the central nervous system, where inflammation and neurodegeneration lead to irreversible neuronal damage inflicting permanent disability on its carriers. In 2002, it was estimated that about 2,5 million people were suffering from MS all around the world (Compston and Coles 2002) corresponding to an overall prevalence of 120/100 000, the annual incidence being 7/100 000 inhabitants. However, MS is a rather unevenly distributed disease depending on the geographical location. Generally, MS is rare in the latitudes near to the equator. The highest prevalence rates are found in populations of Northern European descent, especially in Scandinavia, the British Isles, northern parts of the United States and Southern Canada (Compston 1997).

In Finland, the prevalence of MS has been estimated to be approximately 130/100 000, and the annual incidence is 7/100 000 inhabitants (Remes et al. 2014), but focal areas with as many as double that prevalence are found in southwest Finland (Sumelahti et al. 2000, Sumelahti et al. 2001, Tienari et al. 2004). Women are affected 2–3 times more often than men, and the disease is more common in Caucasian people than in other racial groups (Evans et al. 2013). The age at onset of the disease is typically between 20–40 years, but in about 7% of cases, the disease begins before the age of 16 years (Compston and Coles 2002). MS is the most common autoimmune disease of the CNS, and one of the most ubiquitous disability-causing diseases in Western world, and thus it poses a major socioeconomic burden on society in addition to the suffering it inflicts on the patients and their loved ones (Compston and Coles 2002, Kobelt et al. 2006).

2.1.2 Risk factors

The origin of MS is considered as both multifactorial and heterogeneous. Several independent risk factors for MS have been identified, and they can be clustered into genetic, environmental and hormonal contributors. However, it is evident that there are also complex interactions between the different risk factors. The risk for an individual to develop MS can be defined as a timeline, where several additive steps are required for the development of the disease. In addition to the static risk factors present at the time of birth (i.e. inherited genetic traits, ethnic origin, sex, time of birth, latitude of birth/childhood), dynamic (environmental) risk factors as well as protective factors can alter an individual's risk for MS during childhood and adolescence. Over time, when the individual is exposed to the dynamic risk factors, immunological changes in the periphery take place,

increasing the probability for developing MS, until a biological threshold is reached and the immunological changes start to appear in the CNS. (Ramagopalan et al. 2010).

According to epidemiological studies, the familial recurrence risk for MS in first degree relatives is generally 10–25 times greater than in the general population (Ramagopalan et al. 2010), being highest in monozygotic twins (~25%), followed by dizygotic twins (~5%), siblings (~3–5%), parents (~2%), children (~2%) and second and third degree relatives (~1%). The genetic susceptibility for MS has been traditionally linked to human leukocyte antigen (HLA) class II haplotypes HLA-DW2 and HLA-DR2 (Olerup and Hillert 1991), but also other HLA II as well as HLA I and numerous non-HLA related genetic associations have been identified (Dyment et al. 2005, Gourraud et al. 2012).

The environmental risk factors for MS can be further divided into infectious and non-infectious factors. With respect to the infectious risk factors, the most likely contributing organism is the Epstein-Barr virus (EBV), the seroprevalence of which has been attributed to confer an over four fold risk for developing MS (Almohmeed et al. 2013). The commonly known non-infectious environmental risk factors include low D-vitamin intake or blood levels (Duan et al. 2014, Munger et al. 2004, Munger et al. 2006), low sunlight exposure and high latitudes of birth, (Simpson et al. 2011), month of birth (children born in May having the highest and those born in November having the lowest susceptibility for MS) (Willer et al. 2005), and cigarette smoking (Hawkes 2007). Even though the female-to-male sex ratio in the incidence of MS has been increasing for the past five decades, this has been due to the increasing incidence in women but not in men (Orton et al. 2006), and no specific sex-related risk factor has yet been detected. Female physiology and hormone related factors (Ramagopalan et al. 2010, Whitacre 2001) as well as gene-environment interactions (Orton et al. 2006) have been proposed to underlie these changes.

2.1.3 Disease course, clinical diagnosis and treatment in MS

In the majority (80%) of cases, MS presents initially with a relapsing disease course, where the first acute episode or relapse is referred to as the clinically isolated syndrome (CIS), if the diagnostic criteria for RRMS are not readily met (Compston and Coles 2008). The probability for a CIS patient to develop RRMS, if the MRI findings at baseline refer to demyelinating disease, increases from 50% at two years up to 82% at 20 years (Fisniku et al. 2008). RRMS is characterised by relapses, which are defined as attacks of new or recurrent neurological signs or symptoms consistent with a demyelinating event in the CNS lasting for at least 24 hours and followed by full or partial recovery (Polman et al. 2011). Depending on the neuroanatomical location of the culprit MS lesion or lesions in the CNS, the symptoms may include sensory disturbances, motor weakness, clumsiness (dysmetria, ataxia), tremor, vertigo, impaired vision (due to optic neuritis),

diplopia, dysarthria or other speech difficulties, dysphagia, bladder or bowel dysfunction, cognitive impairment or fatigue (Compston and Coles 2008).

As the disease progresses, recovery from relapses remains incomplete, and permanent symptoms begin to accumulate. After approximately 10–15 years, in 50–65% of the of RRMS patients, the disease advances into the secondary progressive phase, where gradual progression of the disease leads to increasing disability, and this stage may or may not be superimposed with relapses. In a minority (20%) of cases, the disease presents as primary progressive MS (PPMS) where a progressive accumulation of disability is evident already from the very onset of the symptoms. The median age at the time of assignment of irreversible disability has been reported to be approximately 44 years (Compston and Coles 2008) irrespective of the initial course of the disease (Compston and Coles 2008, Confavreux and Vukusic 2006). Before the era of modern disease-modifying therapies, at 15 years from the diagnosis approximately 50% of the patients required a cane or crutch in order to walk, less than 20% were confined to wheelchair and less than 5% had died as a consequence of the disease (Weinshenker et al. 1989).

The clinical diagnosis and differential diagnosis of relapsing MS is based on clinical, imaging (MRI) and laboratory (cerebrospinal fluid (CSF)) parameters with evidence of the disease's dissemination in time (DIT) and space (DIS) (Polman et al. 2011). The presence of demyelinating inflammatory activity can be further confirmed by positive CSF findings characterised by an elevated immunoglobulin IgG index and/or two or more oligoclonal bands. However, a positive CSF finding is not required for the diagnosis of MS, but the analyses may aid in the differential diagnosis and in evaluating the risk of CIS patient to develop clinically definite MS (Polman et al. 2011). The current 2010 McDonald diagnostic criteria for MS based on clinical and MRI parameters are summarised in Table 1.

The diagnosis of SPMS cannot be defined as categorically as it is for RRMS, since the progression of the disease is often slow and insidious, and thus the definitions can vary. According to the current treatment guidelines in Finland, relapsing MS can be regarded to have shifted to SPMS, when progressive, permanent worsening of disability is evident (measured with the expanded disability status scale, EDSS (Kurtzke 1983)) between or without relapses (Remes et al. 2014). EDSS is the most widely used rating system for assessing the clinical severity of the disease; it has a scale ranging from 0 to 10, with 0 corresponding to no disability and 10 to death due to MS. An EDSS score of 6.0 denotes the threshold of being dependent on a walking aid. A summary of the EDSS scores and the related clinical disability is provided in Table 2. The diagnosis of PPMS can be made if the patient has had progressive symptoms without relapses for at least one year, and has at least two of the following three criteria: evidence for DIS in brain MRI, evidence for DIS in the spinal cord MRI, or positive CSF. However, if the patient has a spinal cord or brain stem syndrome, all the symptomatic lesions are excluded from the MRI criteria. (Polman et al. 2011).

Table 1. The 2010 McDonald diagnostic criteria for MS (modified from Polman et al. 2011).

<i>Clinical presentation</i>	<i>Additional data needed for MS diagnosis</i>
≥2 attacks; objective clinical evidence of ≥2 lesions or objective clinical evidence of 1 lesion with reasonable historical evidence of a prior attack	None
≥2 attacks; objective clinical evidence of 1 lesion	DIS, demonstrated by: ≥1 T2 lesion in at least 2 of 4 MS-typical regions of the CNS (periventricular, juxtacortical, infratentorial, or spinal cord); or Await a further clinical attack implicating a different CNS site
1 attack; objective clinical evidence of ≥2 lesions	DIT, demonstrated by: Simultaneous presence of asymptomatic gadolinium-enhancing and non-enhancing lesions at any time; or A new T2 and/or gadolinium-enhancing lesion(s) on follow-up MRI, irrespective of its timing with reference to a baseline scan; or Await a second clinical attack
1 attack; objective clinical evidence of 1 lesion (CIS)	DIS and DIT, demonstrated by: For DIS: ≥1 T2 lesion in at least 2 of 4 MS-typical regions of the CNS (periventricular, juxtacortical, infratentorial, or spinal cord); or Await a second clinical attack implicating a different CNS site; and For DIT: Simultaneous presence of asymptomatic gadolinium-enhancing and non-enhancing lesions at any time; or A new T2 and/or gadolinium-enhancing lesion(s) on follow-up MRI, irrespective of its timing with reference to a baseline scan; or Await a second clinical attack
Insidious neurological progression suggestive of MS (PPMS)	1 year of disease progression (retrospectively or prospectively determined) plus 2 of 3 of the following criteria: 1. Evidence for DIS in the brain based on ≥1 T2 lesions in the MS-characteristic (periventricular, juxtacortical, or infratentorial) regions 2. Evidence for DIS in the spinal cord based on ≥2 T2 lesions in the cord 3. Positive CSF (isoelectric focusing evidence of oligoclonal bands and/or elevated IgG index)

DIS = dissemination in space; DIT = dissemination in time; CNS = central nervous system; MRI = magnetic resonance imaging; PPMS; primary progressive multiple sclerosis; CSF = cerebrospinal fluid; IgG = immunoglobulin G

According to the revised definitions of the clinical phenotype of the disease (Lublin et al. 2014), more emphasis has been put on the definition of active vs. non-active disease states both in the relapsing and progressive diseases types, the activity being defined clinically the presence of relapses or in MRI with new

Table 2. EDSS in the evaluation of clinical disability in MS. Summary of the rating scale modified from Kurtzke et al 1983 and from neurostatus.net (rating scale Version 04/10.2).

EDSS	Definition
0.0	Normal neurological exam
1.0	No disability, minimal signs in one FS
1.5	No disability, minimal signs in more than one FS
2.0	Minimal disability in one FS
2.5	Minimal disability in two FS
3.0	Moderate disability in one FS though fully ambulatory; or mild disability in three or four FS though fully ambulatory
3.5	Fully ambulatory but with moderate disability in one FS and mild disability in one or two FS and others 0 or 1; or fully ambulatory with two FS grade; or fully ambulatory with five FS grade 2
4.0	Ambulatory without aid or rest for ≥ 500 meters; up and about some 12 hours a day despite relatively severe disability consisting of one FS grade 4 or combinations of lesser grades exceeding limits of previous steps
4.5	Ambulatory without aid or rest for ≥ 300 meters; up and about much of the day, characterised by relatively severe disability usually consisting of one FS grade 4 and combination of lesser grades exceeding limits of previous steps
5.0	Ambulatory without aid or rest for ≥ 200 meters
5.5	Ambulatory without aid or rest for ≥ 100 meters
6.0	Unilateral assistance (cane or crutch) required to walk at least 100 meters with or without resting (see chapter 8, Ambulation)
6.5	Constant bilateral assistance (canes or crutches) required to walk at least 20 meters without resting (see chapter 8, Ambulation)
7.0	Unable to walk 5 meters even with aid, essentially restricted to wheelchair; wheels self and transfers alone; up and about in wheelchair some 12 hours a day
7,5	Unable to take more than a few steps; restricted to wheelchair; may need some help in transferring and in wheeling self
8.0	Essentially restricted to bed or chair or perambulated in wheelchair, but out of bed most of day; retains many self-care functions; generally has effective use of arms
8.5	Essentially restricted to bed much of the day; has some effective use of arm(s); retains some self-care functions
9.0	Helpless bed patient; can communicate and eat
9.5	Totally helpless bed patient; unable to communicate effectively or eat/swallow
10.0	Death due to MS

EDSS = Expanded disability status scale; FS = functional system (EDSS consists of visual, brainstem, pyramidal, cerebellar, sensory, bowel and bladder, and cerebral functional systems, which are scored separately according to more detailed definitions).

gadolinium-enhancing T1, new T2, or enlarging T2 lesions. Defining the clinical course of MS is especially relevant in the clinical practice, since options for treatment differ according to the type of the disease. With modern therapies, it is possible to reduce the clinical and radiological activity in the relapsing (active) forms of MS to some extent, but there are still neither curative nor progression halting therapies (Costello et al. 2014).

The primary aim of all current disease modifying treatments (DMTs) in relapsing MS is to reduce inflammation and thus to slow down the accumulation of new MS lesions, to decrease the number of relapses, and to prevent disability caused by unresolved relapses and thus to slow disease progression. In contrast, the neurodegenerative component cannot be primarily targeted with current DMTs. The indications and the proposed mechanisms of actions of the currently available DMTs are summarised in Table 3. Generally, with the first line treatment options, the annual relapse rate can be reduced by approximately 30% as compared with placebo, and the proportion of patients with sustained disability progression has also been reduced by about a third. (Costello et al. 2014). For second line treatments, the treatment effect is more impressive: for example, with natalizumab a 68% reduction in the relapse rate and 42% decrease in the risk for confirmed disability progression can be achieved (Polman et al. 2006).

However, the optimal time window of treatment for long term disability is during the early phase of relapsing MS (Freedman et al. 2013), since an EDSS score >3 has been considered to be the turning point of irreversible cumulative disability (Andersen 2010, Leray et al. 2010). Moreover, no effective treatment which could slow down the accumulation of disability in progressive MS is available.

2.1.4 Pathogenesis

As a result of the complex interplay of genetic, environmental and hormonal contributors, a dysfunction of the immune system in MS gives rise to auto-reactive T-lymphocytes, which are primed in the peripheral lymphatic system, from where they transmigrate across the blood-brain barrier (BBB) into the CNS, and upon recognising and reacting to the self-antigens - e.g. the structures of myelin - they initiate focal inflammation causing degradation of myelin, axonal degeneration and neuronal loss. The focal inflammatory lesions cause the typical demyelinating plaques appearing sclerotic in autopsy, after which the disease was originally named (f. sclérose en plaques) by Jean-Martin Charcot (1825–1893). However, even today, the ultimate trigger which initiates the pathogenic cascade in MS is not fully understood.

2.1.4.1 Neuroinflammation

According to the current paradigm, the CNS damage in MS is mainly considered to result from an immune-mediated process including both the components of innate and adaptive immunity (Koch et al. 2013). The role of infections in triggering the autoimmune reactions against CNS structures has been postulated to be explained by two alternative pathways: by molecular mimicry with auto-reactive T-cells cross-reacting between the foreign pathogens and self-antigens,

Table 3. Currently available disease modifying therapies in MS and their proposed mechanism of action and indication. Modified from Costello et al 2014 and supplemented with Neuhaus et al. 2007 and Coles 2013.

<i>Drug (delivery route)</i>	<i>Proposed mechanism of action</i>	<i>Indication</i>
Interferon β 1a/1b (s.c. or i.m.)	Promotion of shift from Th1 to Th2, reduction of trafficking across BBB, restoration of Treg, inhibition of antigen presentation, enhancement of apoptosis of autoreactive T-cells.	First line treatment for relapsing forms of MS
Glatiramer acetate (s.c.)	Promotion of differentiation to Th2 and Treg-cells, increased release of neurotrophic factors from immune cells, deletion of myelin-reactive T-cells.	First line treatment for relapsing forms of MS
Teriflunomide (p.o.)	Metabolite of leflunomide; inhibition of de novo pyrimidine synthesis, cytostatic effect on rapidly dividing peripheral T- and B-cells.	First line treatment for relapsing forms of MS
Dimethyl fumarate (p.o.)	Promotion of anti-inflammatory and cytoprotective functions mediated by Nrf2 pathway.	First line treatment for relapsing forms of MS
Fingolimod (p.o.)	Blockade of S1P receptors on lymphocytes preventing egress from secondary lymphoid organs.	Second line treatment for relapsing forms of MS
Natalizumab (i.v.)	Monoclonal VLA-4 antibody; blocking α 4-integrin on lymphocytes resulting in reduced trafficking of lymphocytes into CNS.	Second line treatment for relapsing forms of MS
Alemtuzumab (i.v.)	Monoclonal CD52 antibody, binds to CD52 on the surface of T- and B-cells, monocytes and macrophages; depletion of these CD52 cells by complement-mediated lysis, antibody dependent cell toxicity and induction of apoptosis, with resulting leukopenia (Coles 2013)	Second line treatment for relapsing forms of MS
Mitoxantrone (i.v.)	Disruption of DNA synthesis and repair, inhibition of B-cell, T-cell and macrophage proliferation, antigen presentation impairment, reduction of IFN- γ , TNF and IL-2 secretion	Third line treatment for relapsing forms of MS and aggressive secondary progressive MS
Azathioprine (p.o.)	Purine analogue; depression of both cellular and humoral immunity by targeting activation, proliferation, and differentiation of T- and B-cells by competition of its metabolites with DNA nucleotides (Neuhaus et al. 2007)	Fourth line treatment for relapsing forms of MS and aggressive secondary progressive MS

s.c. = subcutaneous; i.m. = intramuscular; p.o. = peroral; i.v. = intravenous; Th1 = T-helper 1 cell; Th2 = T-helper 2 cell; Treg = T-regulatory cell; Nrf2 = Nuclear factor erythroid 2 -related factor 2; S1P = sphingosine-1-phosphate; VLA-4 = very late antigen 4; CD52 = cluster of differentiation 52; IFN- γ = interferon gamma; TNF = tumour necrosis factor; IL-2 = interleukin 2

or by bystander activation with auto-reactive cells being activated due to nonspecific inflammatory events occurring during infections (Sospedra and Martin 2005). In addition, epitope spreading facilitates a wider array of antigens being capable of inducing immune response and propagating the progression of the disease cascade (Vanderlugt and Miller 2002).

The triggering step in the initiation of the inflammatory cascade in MS (Figure 1) is considered to be the activation of autoreactive CD4+ type T helper lymphocytes (Th1) reacting against CNS antigens in the peripheral tissues (Milo and Miller 2014). First, autoreactive (e.g. myelin specific) T-lymphocytes are primed in the peripheral lymphatic system, and the CD4+ T-helper cells (Th-cells) and CD8+ cytotoxic T-cells (Tc-cells) become activated. The presentation of antigens to the naïve CD4+ lymphocytes initiates the differentiation of various T cell populations depending on the presented antigen, cytokine environment and presence of co-stimulatory molecules. These lymphocyte cell populations include Th1 and Th17 cells as well as Th2 and T-regulatory (T-reg) cells. The T1 cells mediate the immunity against intracellular, and Th17 cells against the extracellular pathogens by producing inflammatory cytokines that activate macrophages and opsonizing antibodies. The main role of the Th2 cells is to promote humoral immunity and secretion of anti-inflammatory cytokines, whereas T-reg cells modulate immune responses and the host's tolerability to self-antigens (Koch et al. 2013, Lubetzki and Stankoff 2014). In MS patients, there is a bias towards a Th1 and Th17 cell environment accompanied by a dysfunction of T-reg cells, which promotes the predominance of inflammation (Durelli et al. 2009, Vigiotta et al. 2004).

After being activated, the autoreactive immune cells transmigrate across the blood brain barrier (BBB) into the CNS. The transmigration is enabled by the adhesion of integrins on the leukocyte surface to the cell adhesion molecules (CAMs) expressed on endothelial cells (Cannella and Raine 1995). In addition, the activated cells upregulate cytokine receptors and secrete pro-inflammatory cytokines (e.g. interleukin-2, interferon gamma and tumour necrosis factor alpha), chemokines and matrix metalloproteinases (MMP) (Milo and Miller 2014), which disrupt the BBB further facilitating the transmigration (Obermeier et al. 2013). After entering the brain, the T-cells are re-activated by the presentation of CNS self-antigens, which in turn initiates the damaging inflammatory cascade involving multiple cell types – including macrophages and microglia (Figure 2). Additionally, CD8+ T lymphocytes are crucial effectors in the detrimental neuroinflammation, having been identified as the predominant T-cell type in active MS-lesions (Babbe et al. 2000). Furthermore, B-cells contribute to the CNS damage by producing antibodies injuring myelin, oligodendrocytes and other neuronal structures and by acting as antigen presenting cells. Further demyelination and damage to oligodendrocytes is evoked by mitochondrial damage, which is considered to result from the production of free radicals, reactive oxygen species and nitrous oxide which are encountered during microglial activation and associated with iron deposition (Costello et al. 2014). In

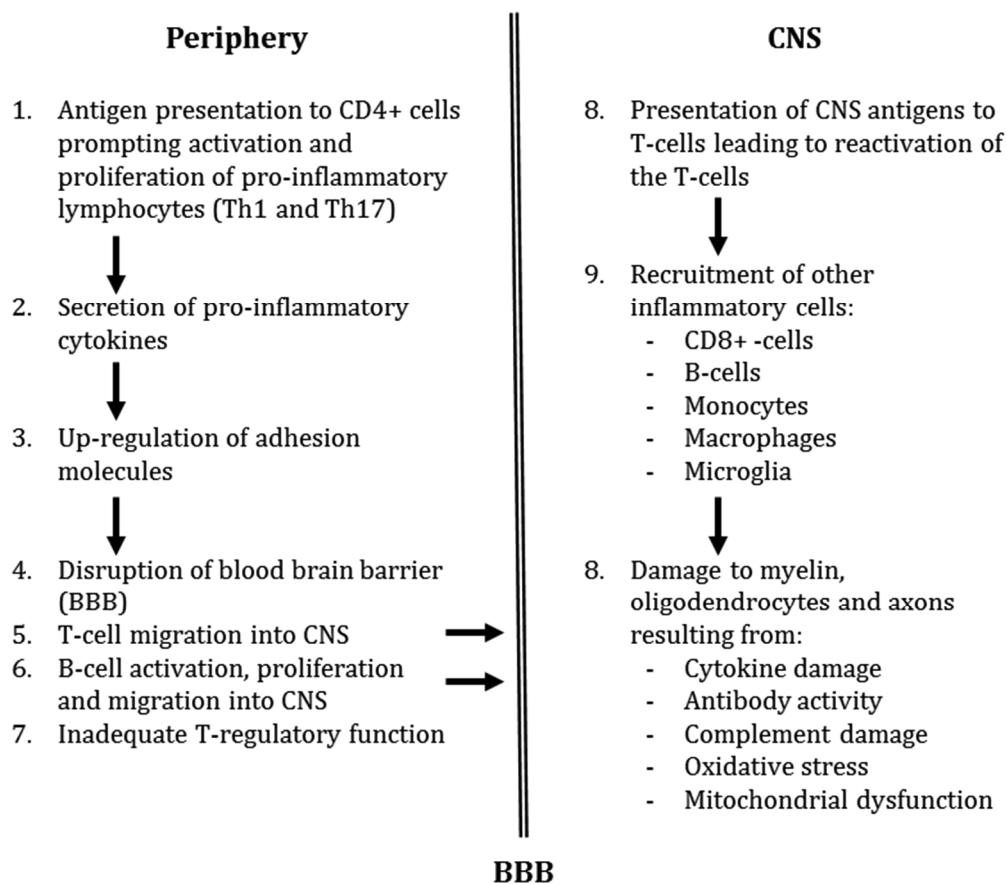


Figure 1. Key events in the inflammatory cascade of multiple sclerosis. Modified from (Costello et al. 2014)

addition to demyelination, the neuroinflammatory events listed above are also considered responsible for axonal loss, which has been shown to occur already in the early phase of the disease (Trapp et al. 1998).

Thus, the pathological hallmarks of MS lesions are inflammation, demyelination, axonal damage and gliosis. However, these events are unevenly distributed, and therefore four different MS lesion patterns can be recognised (Compston and Coles 2008, Lucchinetti et al. 2000, Lucchinetti et al. 1996). Pattern I is characterised with T-cell infiltrates and macrophages associated to demyelination, whereas in pattern II, the demyelination is linked with antibody and complement mediated immune reactions against oligodendroglial cells and myelin. The typical findings exhibited in pattern III are hypoxia-like damage, with impaired mitochondrial function due to inflammatory vascular damage or macrophage toxins, and with oligodendrocyte dystrophy, apoptosis and myelin protein dysregulation. In contrast, pattern IV is characterised by a primary susceptibility of oligodendrocytes to immune mediated injury, more resembling

that of toxin- or viral-induced damage than that of autoimmune origin. Patterns I and II have been proposed to be the dominant types. Originally, it was postulated that each MS patient would have only one predominant lesion pattern and that the patterns would differ between individuals or disease subtypes, whereas later it has been shown that acute lesions demonstrate pattern II in all individuals and other patterns are more rare (Compston and Coles 2008, Kutzelnigg and Lassmann 2014).

Acute and chronic MS lesions can also be classified according to the presence and distribution of macrophages and activated microglia. Acute lesions are densely infiltrated by macrophages containing myelin degradation products throughout the lesion, whereas chronically active lesions contain a broad rim of macrophages with myelin degradation products at the edge and with later stage myelin degradation products in the centre of the lesion. Chronic, slowly expanding lesions have an inactive centre surrounded by a rim of activated microglia with only some macrophages at the lesion margin containing little myelin degradation products. Inactive lesions show a sharp lesion border without macrophages or activated microglia (Frischer et al. 2009, Kutzelnigg and Lassmann 2014). In relapsing MS, the WM lesions are typically of the active lesion type, being the likely correlate with the clinical attacks (Bruck et al. 1995). In SPMS, majority of the plaques are of the chronic active or slowly expanding (smouldering), or chronically inactive type. Additionally, there is diffuse inflammation with scattered activated microglial cells and lymphocytes widely in the white and gray matter and B-cell follicle-like structures in the meninges (Kutzelnigg et al. 2005, Magliozzi et al. 2010, Moll et al. 2011).

2.1.4.2 Neurodegeneration

The accumulation of axonal damage is considered as the hallmark of neurodegeneration and the primary culprit for progressive disability (Compston and Coles 2008). According to the classical paradigm, neuroinflammation has been regarded as the key component in the pathology in RRMS, slowly subsiding as neurodegeneration becomes the predominant feature with the progression of the disease (Hauser and Oksenberg 2006). However, it is still being argued about whether neuroinflammation is the propagating force behind neurodegeneration, or whether neurodegeneration can occur independently of neuroinflammation (Kutzelnigg and Lassmann 2014, Trapp and Nave 2008). Loss of myelin and inflammatory activity, as well as axonal transections and neurodegeneration can be observed in all phases of MS (Trapp et al. 1998). On the other hand, considerable inflammation can be observed also in the progressive and late stage MS, where inflammation may occur independently of the BBB breakdown (Hochmeister et al. 2006). For instance, aggregates of inflammatory cells can be detected in the meninges and perivascular spaces in progressive MS without concomitant damage to BBB (Lassmann et al. 2012). Consequently, a concept of compartmentalised inflammation trapped behind an intact BBB and independent of peripheral autoimmune activation has been proposed (Lassmann et al. 2012).

SPMS is pathologically characterized by a slow expansion of the pre-existing demyelinating white matter plaques, the new onset of cortical demyelination, and a diffuse injury in normal-appearing white matter (NAWM; areas of white matter appearing normal in conventional MRI), where pronounced microglial activation and perivascular inflammation can be found. In addition to the brain parenchyma, inflammatory activity can be detected also in the meninges (Kutzelnigg et al. 2005, Lassmann 2007). The observed close correlation between inflammation and axonal injury suggests that inflammation plays a central role in contributing to neurodegeneration and disease progression (Frischer et al. 2009, Magliozzi et al. 2010, Prineas et al. 2001), even though it has not been established whether neurodegeneration is a secondary or independent component. In fact, it has been hypothesised that the partly compartmentalised disease process within the brain and spinal cord in progressive MS might explain the failure of current DMTs, which predominantly target the peripheral immune response.

2.2 Role of microglia and adenosine in MS

2.2.1 Microglia in neuroinflammation and MS

Microglia are myeloid cells of the CNS, that are derived from early embryonic erythromyeloid progenitor cells and have migrated into the developing nervous tissue, where they have begun the maturation process into brain resident microglial cells (Biber et al. 2014). Microglia constitute approximately 10 percent of the total cell population in a human brain. The key tasks performed by microglia include phagocytosis of extracellular debris, antigen presentation to host immune cells, and secretion of inflammatory mediators (Minghetti and Levi 1998). In addition, microglia may have a vital role in neurodevelopment and maintenance via synaptic pruning, where synaptic elements and apoptotic neurons are being phagocytised by microglia. These events are not only integral in postnatal development, but appear to take place also in the mature and aging brain (Paolicelli et al. 2011, Sierra et al. 2010).

Microglia express two different phenotypes, which are characterised by the alterations in their cytoplasmic processes: in the ramified state they are immobile and present long dendritic-like processes, whereas in the de-ramified state, they are mobile and capable of phagocytosis. In normal healthy brain, the majority of microglia are in their ramified phenotype. In a reaction to external stimuli (such as pathogens or inflammatory mediators) or neural signals (either via direct neuron-microglia contact or via diffusible mediators) the microglia retract their ramified processes and become motile and take on an amoebic appearance resembling that of phagocytic macrophages. When activated, microglia begin to function as phagocytic cells, and the morphological reaction is accompanied by increases in their migratory and proliferative capabilities (Biber et al. 2014, Gehrman et al. 1995). Earlier the ramified microglia were considered as being inactive and were referred to as “resting” microglia, but it has become evident,

that even in the non-mobile state, they serve several homeostatic and immunosurveillance tasks and thus are by no means inactive, and that this “surveying” state could better be described as a tolerant or pro-homeostatic state. (Biber et al. 2014, Graeber and Streit 2010) However, microglia in the mobile and injury responsive state are still generally referred to as “active” microglia (or the process is termed “microglial activation”) in the literature; this terminology will be applied also in this thesis.

In the early phase of multiple sclerosis, microglial activation promotes the recruitment of naïve T-cells, which are activated by the dendritic cells functioning as antigen presenting cells. Microglia also act as antigen presenting cells, re-stimulating the auto-reactive memory-T-cells invading through the BBB into the CNS, which is considered a key event in maintaining the chronic inflammation in the CNS (Gao and Tsirka 2011, McMahan et al. 2005). In active white matter lesions, there is a profound infiltration of activated microglia and blood borne macrophages throughout the lesion, whereas in slowly expanding (smouldering) or chronic active lesions, the microglia and macrophages are concentrated as a dense rim around the lesions (Breij et al. 2008, Frischer et al. 2009). Microglia can also be found diffusely in the non-lesional white and gray matter with concomitant axonal degeneration and meningeal inflammation. Thus, chronic activation of microglia has been linked to neurodegeneration in the progressive phase of the disease (Howell et al. 2010, Kutzelnigg et al. 2005, Magliozzi et al. 2010).

However, it is still not established whether the functions of activated microglia in MS and other neuroinflammatory and neurodegenerative diseases are ultimately detrimental or beneficial. Instead of their role in the maintenance of damaged CNS (e.g. in phagocytosis of extracellular debris and limiting inflammation), it has been postulated that interactions between dysregulated and overactive microglia and injured neurons would lead to a vicious cycle of self-propagating, prolonged inflammation thus driving the chronic progression of the disease (Gao and Hong 2008). On the other hand, the differentiation between activated brain resident microglia and blood derived macrophages - which may possess different functions - is not without challenges, which might distort the interpretation of *in vitro* and *in vivo* studies on the role of microglia in health and disease. Nevertheless, whether being the culprit or an innocent bystander in the disease process, the presence of activated microglia is well established in the MS brain.

Activated microglia express the translocator protein (TSPO), or as it was named earlier, the peripheral benzodiazepine receptor (PBR) on the outer membrane of mitochondria. Several functions have been attributed to TSPO, either directly or indirectly, including immunomodulation, regulation of cholesterol transport, synthesis of steroid hormones, apoptosis, cell proliferation, porphyrin and anion transport, regulation of mitochondrial functions and heme synthesis (Papadopoulos et al. 2006). Structurally, TSPO is an 18 kDa protein with a structure of five alpha-helices spanning the membrane lipid bilayer. Two

archetypal ligands binding to TSPO have been identified, namely Ro5-4864, the 4-chloro-derivative of diazepam, and PK11195, the isoquinoline carboxamide (Casellas et al. 2002), the latter having been used as a marker for *in vivo* PET imaging of activated microglia (see also chapter 2.3.2.3 for the review of TSPO radioligands).

Whereas TSPO is highly expressed in activated microglia, in the “resting” or surveying microglia, it is expressed at a very low level, and mainly in the gray matter (Doble et al. 1987). As a marker of microglial activation, TSPO expression has been shown to be increased in many cerebral pathological states, such as Huntington’s disease (HD) (Schoemaker et al. 1982), brain ischemia (Stephenson et al. 1995) and MS (Vowinckel et al. 1997). In Parkinson’s disease (PD) and Alzheimer’s disease (AD), some neuropathological studies have found evidence of increased microglial activation (McGeer et al. 1988), in line with the *in vivo* findings of increased TSPO binding in PD (Gerhard et al. 2006, Ouchi et al. 2005) and AD (Cagnin et al. 2001, Edison et al. 2008). In addition, TSPOs are highly expressed in gliomas (Broaddus and Bennett 1990, Vlodaysky and Soustiel 2007), with the majority of the expression being accounted for by tumour cells instead of microglia (Su et al. 2015). In non-neoplastic CNS damage without BBB breakdown, microglia are the main cell population expressing TSPO (Banati et al. 1997). In focal damage with BBB breakdown, also TSPO expressing activated macrophages – cells which have invaded from the peripheral blood into brain parenchyma – are present (Banati et al. 2000).

PET imaging of activated microglia with TSPO binding radioligands is being increasingly utilised in MS research. The first *in vivo* TSPO PET pilot study in MS patients with [^{11}C]PK11195 revealed that TSPO binding was increased in acute lesions but was low in chronic lesions (Vowinckel et al. 1997). Thereafter, another study detected a pattern of increased TSPO binding in scattered areas related to demyelinating lesions in MRI (excluding black holes) and also in NAWM and central gray matter (thalami and brainstem); the majority of the subjects in the study were RRMS patients (Banati et al. 2000). Subsequently Debruyne and colleagues (Debruyne et al. 2002, Debruyne et al. 2003) reported that TSPO binding was elevated in gadolinium enhancing active plaques, and in non-enhancing T2 lesions during relapse, when compared to T2 lesions in patients without relapse. However the T2 lesional binding was at a similar or lower level than in NAWM. Interestingly, the TSPO binding in NAWM showed an increasing trend which associated to longer disease duration. However, the patient characteristics were heterogeneous, with patients representing both RRMS and SPMS as well as PPMS subtypes of the disease. Further analyses by the same group showed that increasing brain atrophy was associated with higher TSPO binding in NAWM but lower binding in T2 lesional brain (Versijpt et al. 2005). Only one treatment study investigating TSPO in RRMS has been published. In that study, one year treatment with glatiramer acetate reduced TSPO binding significantly in both cortical GM and cerebral WM (Ratchford et al. 2011). In a more recent study conducted by Politis and colleagues (Politis et al. 2012), SPMS

and RRMS patients were shown to have increased [¹¹C](R)-PK11195 binding also in the cerebral cortex in addition to WM when compared to healthy controls. Moreover, the cortical TSPO binding correlated with the clinical disability, with the correlation being more evident in patients with SPMS than in those with RRMS. However, similar correlations were not found for WM.

To summarize, it seems that diffuse activation of microglia in normal-appearing brain structures as well as related to focal lesions in MS represents a potential surrogate marker of disease activity and neuroinflammation. However, the studies conducted thus far have been somewhat scarce and heterogeneous, which is one of the reasons which stimulated the initiation of this research.

2.2.2 Adenosine in neuroinflammation and MS

Adenosine is an endogenous purine nucleotide regulating several physiological phenomena in the CNS and peripheral organs such as heart, kidney, and vascular smooth muscle. Adenosine is also an important regulator of inflammation in both the peripheral tissues and the CNS, and adenosine release is increased as a response to tissue damage. (Blackburn et al. 2009, Fredholm et al. 1994, Sebastião and Ribeiro 2009). In the CNS, adenosine contributes critically to the neuromodulatory control of a variety of normal and abnormal brain functions, ranging from synaptic plasticity to cognition, sleep, motor activity, neuroinflammation, and cell death. Adenosine regulates the activity of the central nervous system by controlling neuronal activity and neurotransmitter release and uptake in synapses especially those utilizing glutamate and gamma-aminobutyric acid (GABA). Adenosine's homeostatic effects are mediated via paracrine functions and cellular signalling. Thus, adenosine is not a classical neurotransmitter, since it is not enriched and stored in vesicles, and is not released in response to action but instead is produced both intra- and extracellularly. (Chen et al. 2014)

There are two sources for extracellular adenosine: the release of adenosine with aided diffusion from intracellular sites into the extracellular space, and the conversion of extracellular adenine nucleotides into adenosine by a series of ectoenzymes, of which CD73 (ecto-5'-nucleotidase) is the last and rate-limiting step in the conversion (Zimmermann and Braun 1999). The effects of adenosine are mediated through G-protein-coupled cell membrane receptors with four recognised subtypes, A₁, A_{2A}, A_{2B} and A₃. The effects of A₁ and A₃ receptors in the intracellular signal transduction are inhibitory, and lead to reduced levels of the intracellular second messenger, cyclic adenosine monophosphate (cAMP). On the contrary, the activation of A_{2A} and A_{2B} receptors leads to an increase in intracellular cAMP, and thus the effect is considered as excitatory (Sebastião and Ribeiro 2009). In the CNS, adenosine receptors are mainly located in the neuronal synapses, and A₁ and A_{2A} are the predominant adenosine receptor subtypes. A₁ receptors are most abundant in neurons in hippocampi, cerebral cortex, and cerebellum, but are also expressed at intermediate levels in other regions, and are present both pre- and post-

synaptically. (Chen et al. 2014) A_{2A} receptors are primarily concentrated in striatum, olfactory tubercle and nucleus accumbens, but are also present in lower amounts in the hippocampi and cortex (Dunwiddie and Masino). In striatum, the A_{2A} receptors are highly concentrated and co-localized post-synaptically with dopamine receptors, especially as A_{2A} - D_2 -heteromer complexes in the striatopallidal, GABAergic medium spiny neurons where A_{2A} stimulation reduces the binding of dopamine into D_2 receptors (Ferré et al. 2004). In addition, the A_{2A} receptors are co-localized presynaptically with A_1 receptors in glutamatergic striatal terminals and participate in the fine tuning of glutamate release (Ciruela et al. 2006). In the sites of lower expression in corticostriatal terminals and hippocampi, the A_{2A} receptors are localised pre-synaptically (Rebola et al. 2005). In the periphery, all immune cells express adenosine receptors. Monocytes and macrophages express all four adenosine receptors, though the levels of expression differ markedly throughout the maturation and differentiation process, whereas in human dendritic cells, only A_{1A} , A_{2A} and A_3 receptors are differentially expressed. In lymphocytes, the adenosine receptor expression level depends on the cell type; $CD4+$ and $CD8+$ T lymphocytes have been the cells most extensively studied and being shown to express A_2 , A_{2B} , and A_3 receptors. (Blackburn et al. 2009) In peripheral organs, A_1 receptors are present in heart, kidney, adipose tissue and testis. While A_{2A} receptors are scarce in peripheral organs, A_{2B} receptors are widely distributed with an especially rich expression in the gastrointestinal tract. A_3 receptors, in turn, are not abundant in the periphery, being mainly found in testis (Fredholm et al. 1994). With respect to the peripheral organs, probably the effects of adenosine on the heart have been best investigated; adenosine is involved in the regulation of heart rate, contractility, and coronary flow (Mustafa et al. 2009) and tissue protection from myocardial injury due to myocardial ischemia reperfusion damage (Headrick and Lasley 2009).

In peripheral tissues, the activation of adenosine receptors in immune cells leads to the net effect of suppression of inflammatory mediators (Ohta and Sitkovsky 2001). In the CNS, the effects of A_1 receptors are generally considered as being anti-inflammatory and neuroprotective, whereas the A_{2A} mediated actions can vary depending on the pathological circumstances (Sebastião and Ribeiro 2009). However, selective A_{2A} antagonism appears to exert neuroprotective effects. For example, the neurological defect caused by middle cerebral artery occlusion in A_{2A} knockout mice has been reported to be milder than in wild type mice (Chen et al. 1999), and the neuroinflammation induced by peripheral injection of lipopolysaccharide (LPS) could be attenuated by intracerebro-ventricular injection of A_{2A} antagonist in rats (Rebola et al. 2011).

Adenosine may have a significant involvement in the neuroinflammation present in MS. Patients with MS have been shown to have reduced levels of adenosine in their peripheral blood when compared to healthy controls (Mayne et al. 1999). In addition, the expression of A_1 receptors in the monocytes and macrophages in the peripheral blood and brain of MS patients is lower than in control subjects (Johnston et al. 2001). However, in support of the evidence of A_1 -mediated

immunosuppressive effects in MS, adenosine A₁-receptor knockout mice have been shown to develop more severe experimental autoimmune encephalitis (EAE) than the wild type mice (Tsutsui et al. 2004). Because of the immunosuppressive properties of adenosine mediated via A₁ receptors in the EAE model, it could have been anticipated that CD73-deficient mice would develop severe EAE in view of the crucial role of CD73 in regulating adenosine signalling. Surprisingly, CD73-knockout mice have been found to be resistant to EAE when compared to the wild type mice. Moreover, A_{2A}-receptor antagonism has been shown to protect wild type mice from EAE induction (Mills et al. 2008). In contrast, A_{2A} receptor knockout mice display more severe EAE symptoms than their wild type counterparts (Mills et al. 2012, Yao et al. 2012). However, according to experiments conducted on bone marrow chimeric EAE mice, it appears that normally functioning A_{2A} receptors – apparently in the CNS – are needed for the development of EAE, whereas the expression of A_{2A} receptors on lymphocytes is integral for controlling the severity of the inflammatory response (Mills et al. 2012). Finally, it has been demonstrated that A_{2A} receptors are upregulated in the peripheral lymphocytes of MS patients, and that A_{2A} stimulation of these cells resulted in marked inhibition of several inflammatory mediators (such as TNF- α , IFN- γ , IL-6 and IL-17) and also led to reduced VLA-4 expression (Vincenzi et al. 2013).

Interestingly, treatment with interferon-beta has been shown to increase CD73 expression in microvascular endothelial cells and astrocytes of MS-patients. Interferon-beta also increased the levels of soluble CD73 in the serum of MS patients, and this also correlated with the clinical outcome. Thus, up-regulation of CD73 enzyme activity and the subsequent increase in adenosine production might contribute to the beneficial effects of interferon-beta on MS via enhancing the endothelial barrier function. (Airas et al. 2007, Niemelä et al. 2008). Adenosine may also play an important role in myelination, since adenosine has been shown to inhibit the proliferation of oligodendrocyte progenitor cells and promote their differentiation and myelination (Stevens et al. 2002).

Another interesting link between adenosine and the modulation of neuroinflammation is provided by microglial activation. As well as adenosine receptors, microglia express many purinergic receptors including two purinoreceptors, P2X and P2Y, which can mediate the effects of ATP (Färber and Kettenmann 2006). It has been shown that *in vitro* inflammatory stimuli induce up-regulation of A_{2A} receptors on microglia, and that stimulation of A_{2A} receptors leads to morphological and functional changes including deramification in microglia (Orr et al. 2009). Moreover, the protective effects of A_{2A} antagonism in neuroinflammatory conditions induced by LPS in animal models appear to be partly mediated by the suppression of microglial activation and attenuation of microglial nitric oxide production (Rebola et al. 2011, Saura et al. 2005).

In conclusion, it appears that adenosine signalling can affect microglial activation via A_{2A} receptors at least *in vitro* and *in vivo* in animal models. Whether or not the A_{2A}-mediated effects of adenosine are protective or harmful in MS patients is a

largely unanswered question. Thus, more studies would be needed to explore these relationships *in vivo* in humans.

2.3 Imaging methods of neuroinflammation in MS

2.3.1 Magnetic resonance imaging (MRI)

2.3.1.1 Physical basis of conventional MRI

Conventional structural MRI is based on the detection of angular momentum of subatomic particles in a strong external magnetic field. Since the nucleus of a hydrogen atom (H^1) has only one proton and has the highest energy, and is present in water (H_2O) and fat which make up the majority of human body, it is the most widely used nucleus in clinical MR imaging. In the terms of quantum mechanics, a subatomic particle has a quantized angular momentum, called its spin. The spin, in turn, is associated with a magnetic momentum. The strong magnetic field applied by an MRI scanner forces the magnetic moments of the subatomic particles (e.g. protons) to align in a direction parallel or anti-parallel to the external magnetic field B_0 . However, it is not feasible to define the properties of a single proton; instead, one has to observe the average behaviour of a large number of similar protons. The behaviour of these spins can be considered as the equivalent to a quantum average, which can also be defined as a macroscopic magnetisation M_0 . (Hendee and Morgan 1984a, Hendee and Morgan 1984b, Nitz 2003)

If one applies another magnetic field B_1 , that is perpendicular to B_0 , then this will cause a rotation to the macroscopic magnetisation. By varying the duration and the amplitude of the B_1 field, different radio frequency (RF) pulses can be created. When the B_1 field is switched off, the magnetisation will continue to rotate and return to the original alignment thus inducing a so-called free induction decay signal which can be detected by a coil in the MRI scanner. The relaxation time, i.e. the time to return to the original alignment, differs depending on the molecular structures of the tissue and the number of protons involved i.e. the proton density. The time required for the longitudinal realignment of the magnetisation with the B_0 is dependent on the tissue specific relaxation rate, and is called the T1 relaxation time. In contrast, the transverse relaxation time, T2, reflects the interaction between the nuclei and is dependent on the dephasing caused by the dipole-dipole interaction between the transverse magnetic moments. (Hendee and Morgan 1984a, Hendee and Morgan 1984b, Nitz 2003)

T1-weighted image sequences are most commonly used in the clinical setting because of their good discrimination between fat and water, fat being shown as bright (hyperintense) and water as dark (hypointense). In T2-weighted sequences, the signals of fat and water are opposite i.e. fat appears to be hypointense whereas water is hyperintense. In brain imaging, T2-weighted

imaging is also widely used especially due to its better sensitivity to pathological changes, whereas the strength of T1-weighted imaging lies in its better structural resolution and differentiation of white and gray matter. Fluid attenuated inversion recovery (FLAIR) is a further refinement of T2 weighted imaging, where the signal of free water (e.g. CSF) can be nullified thus providing a better visualisation of periventricular lesions, which are easily obscured by the adjacent CSF signal in normal T2 images. (Hendee and Morgan 1984a, Hendee and Morgan 1984b, Nitz 2003)

2.3.1.2 Applications of conventional MRI in MS

Demyelinating MS plaques, both acute and chronic, are visualised as hyperintense lesions in T2-weighted MRI imaging. In acute lesions, the borders are relatively poorly defined on T2 and FLAIR sequences, whereas the borders of chronic lesions are more sharply defined. The visibility of MS lesions near to CSF containing structures, such as sulci and ventricles and appearing bright in T2 images, can be increased in comparison to normal T2 sequences by using FLAIR showing CSF as dark, thus offering better discrimination. Acute lesions may also be detected by their uptake of contrast medium (e.g. gadolinium) which is seen as a hyperintense signal in T1 images. In non-contrast T1 images, acute lesions may be of the same or darker intensity than in the adjacent white matter, whereas chronic lesions appear as well defined hypointense, dark regions, and thus are also called “black holes” and representing longer standing disease with axonal destruction. Chronic T1 black holes do not significantly take up contrast medium. If one wishes to have better contrast of lesions in deep gray matter nuclei, brain stem and cerebellum, then proton density weighted imaging can be used, since proton density sequencing produces a grayscale directly proportional to the concentration of hydrogen nuclei, which are abundant in inflammatory lesions but more scarce elsewhere, especially in deep gray matter and brain stem. In conclusion, in the clinical setting, the recommended brain MR imaging protocol of MS patients includes pre- and post-contrast T1, T2, proton density and FLAIR sequences. (Bricker and Jones 2013, Simon et al. 2006)

Conventional MRI has established its role in the clinical routine of imaging MS patients due to the wide availability of MRI scanners, the good reproducibility of the results when using similar protocols, and the method's sensitivity for detecting macroscopic brain abnormalities. In addition to being the cornerstone in the initial diagnosis and differential diagnosis of the disease, it is used in the assessment of disease activity in RRMS patients. Both the accumulation of new T2 hyperintense lesions and the number of new gadolinium-enhancing lesions are known to correlate to clinically active relapsing disease (Filippi et al. 1995, Kappos et al. 1999), and thus the imaging findings can guide the treatment choices when combined with the clinical presentation of the disease (Fazekas et al. 2007, Remes et al. 2014). In patients with CIS, the presence and amount of T2 lesions also affect the probability for developing RRMS. In long-term longitudinal studies with median follow-up times ranging from 6.5 to 20 years, 72–88% of CIS patients

with at least one demyelinating lesion in the MRI developed RRMS, whereas with normal MRI, the corresponding percentage was only 8–20% (Brex et al. 2002, Fisniku et al. 2008, Tintore et al. 2006). However, no reliable conventional MRI markers to predict the progression of cumulative disability are available when evaluating an individual patient in a clinical setting.

In clinical trials designed as longitudinal studies with serial follow-up imaging, other MRI parameters acquired from conventional MRI sequences, but not yet in routine clinical use, have been exploited as surrogate markers of disease activity or disease progression. Both new T2 lesions and gadolinium enhancing lesions have been shown to be fairly reliable surrogate markers for clinical relapses (Sormani et al. 2010, Sormani et al. 2011). Increasing GM atrophy has been claimed to predict clinically detectable progression of the disease both in relapsing and progressive MS (Jacobsen and Farbu 2014). Increased WM atrophy has been demonstrated to be more clearly associated to secondary progressive than to relapsing MS (Tedeschi et al. 2005). A high total volume of T1 lesions, or lesion load, has been associated with the progressive disease type, and increasing lesion load of black holes correlated to accumulating disability in a long term clinical follow-up (Hickman et al. 2001, Truyen et al. 1996, van Walderveen et al. 2001). On the other hand, the association between GM atrophy and WM lesions has been shown to be weaker in progressive than in relapsing MS, which has been suggested to indicate that the neurodegenerative disease process may be more independent of lesion and atrophy evolution (Steenwijk et al. 2014).

However, when evaluating an individual patient in the clinical setting, the associations between the clinical disability to the conventional MRI parameters and their predictive value are known to be weak or unconvincing (Bakshi et al. 2008, Miki et al. 1999, Nijeholt et al. 1998), a phenomenon which is named the clinico-radiological paradox (Barkhof 1999, Barkhof 2002). One advance in trying to resolve the clinico-radiological paradox has been the introduction of the term dirty-appearing white matter (DAWM), which refers to brain regions with intermediate signal intensity between those of focal lesions and normal-appearing white matter (NAWM) in T2- and proton density -weighted imaging (Filippi and Rocca 2010). The pathology in diffusely abnormal white matter corresponding to DAWM in MRI is characterized by gliosis, demyelination, axonal loss, and the presence of macrophages and activated microglia (Allen and McKeown 1979, Seewann et al. 2009, Vos et al. 2005). Moreover, marked DAWM changes have been demonstrated in progressive MS with more prominent findings in SPMS than RRMS, and thus DAWM has been postulated to contribute considerably to disease progression (Seewann et al. 2009, Vrenken et al. 2010).

2.3.1.3 Physical basis of diffusion tensor imaging (DTI)

Diffusion can be defined as the random motion – also known as Brownian motion – of particles as a result of the thermal energy possessed by the molecules (Le Bihan et al. 2001, Le Bihan 2003). MRI is sensitive to thermal Brownian motion,

which is characterized by the diffusion coefficient $[D[x,y]]$ and which describes the ability of water molecules (H_2O) to perform random translational motion within a given tissue. By applying a magnetic field gradient for a short duration, a temporary change in resonance frequencies is produced, resulting in a corresponding dephasing of the transverse magnetisation. By repeating the same gradient for the same duration, but with an opposite polarity, results in a rephasing of the transverse magnetization for a stationary tissue, and the net magnetization returns to the original level. Instead, in an un-stationary tissue, for those molecules (protons) which have changed their position before the repeated gradient, and are thus not exposed to the exactly opposing gradient, the rephasing of the transverse magnetization remains incomplete, leading to signal loss. As a result, un-stationary tissue areas in which there has been increased diffusion and the resulting signal loss due to movement of protons, appear as hypointense regions in diffusion weighted imaging (DWI). A diffusion weighted image, in which the signal attenuation is not dependent on the directionality of diffusion, is called a trace-weighted or isotropic diffusion weighted image. (Le Bihan et al. 2001, Le Bihan 2003, Nitz 2003)

Diffusion tensor imaging (DTI) is an advanced application of DWI, and is based on detecting the directionality of the diffusion. Thus, DTI, investigates how free (i.e. isotropic) or in some way mechanically restricted (anisotropic) the diffusion is within the area of interest. In other words, the distance and directions of diffusion of H_2O molecules decrease in an anisotropic environment. In healthy brain tissue, diffusion in the white matter is generally more restricted than in the gray matter, because myelinated axons allow diffusion primarily along the longitudinal axis of the axons. Consequently, in the areas of normal white matter tracts, diffusion is regarded as being highly anisotropic. (Le Bihan et al. 2001, Le Bihan 2003)

Technically, DTI is an advanced application of DWI, in which gradients are applied in pulses of linear inhomogeneous magnetic fields in a minimum of six different directions. This allows the creation of a mathematical model of the diffusion in three-dimensional space, a so-called diffusion tensor (Alexander et al. 2007). From the diffusion tensor, the main directions and distances of diffusivities can be calculated as eigenvectors (ϵ) and their respective eigenvalues (λ), annotated with 1, 2 and 3 from largest to smallest according to the principal axes of the ellipsoid (Figure 2.) (Alexander et al. 2007, Jellison et al. 2004). Several different parameters can be used to describe the properties of the diffusion tensor. Mean diffusivity (MD) is the mean of all three eigenvalues ($MD=(\lambda_1+\lambda_2+\lambda_3)/3$). Thus, MD reflects the mean magnitude of diffusional displacement, but is insensitive to the directionality of the diffusion. Diffusion anisotropy correlates to the degree to which the three eigenvalues differ from each another (i.e. to the extent to which the shape of the tensor ellipsoid deviates from that of a sphere), and thus is a measure of the directionality of the diffusion. Although there are many various anisotropy parameters, one of the most commonly used is fractional anisotropy (FA). FA measures the magnitude of anisotropic diffusion in a relative

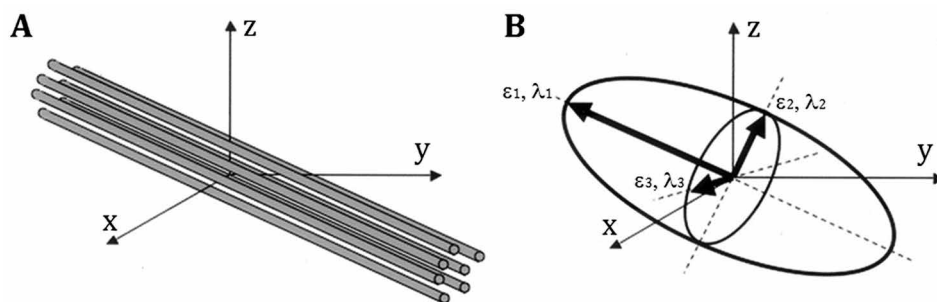


Figure 2. A) Simplified diagram of neuronal fiber tracts with an arbitrary orientation with respect to the scanner orientation (axes x,y,z) and **B)** three-dimensional, ellipsoid diffusion tensor characterised by the main eigenvectors ($\epsilon_1, \epsilon_2, \epsilon_3$) and their eigenvalues ($\lambda_1, \lambda_2, \lambda_3$) representing the respective diffusivities. Modified from (Jellison et al. 2004)

scale from 0 to 1. When the measured diffusivities are equal in all directions, diffusion is isotropic and $FA=0$. Were diffusion to occur only in one direction (which is only a theoretical case with respect to biological tissue) with the two other measured diffusivities equaling 0, FA would have a value of 1. (Basser and Pierpaoli 1996, Le Bihan et al. 2001)

2.3.1.4 Applications of DTI in MS

DTI is not a part of the routine imaging protocol in MS patients, but it has been widely used in some clinical and pre-clinical studies. It is well established that the structural damage causing widespread reductions of FA and increases in MD in WM and NAWM do correlate to physical disability and cognitive impairment in both relapsing and progressive MS (Preziosa et al. 2011, Sbardella et al. 2013, Welton et al. 2014), although partly controversial results have been reported with respect to the correlation between disability measured with EDSS and the DTI changes (reviewed in (Sbardella et al. 2013)). Nevertheless, the white matter disintegrity has been shown to be more pronounced in SPMS than in RRMS patients (Preziosa et al. 2011, Welton et al. 2014). Furthermore, in the normal-appearing cortical and deep gray matter, the DTI abnormalities (decreased FA and increased MD) are more prominent in SPMS than RRMS. In RRMS, the normal-appearing gray matter (NAGM) changes have been stated to be characterised by increased MD , whereas both increased and decreased values for FA have been reported (reviewed in (Sbardella et al. 2013)).

Within T2 lesions, FA is generally decreased and MD is increased. Consequently, there is an overlap between the FA and MD maps and the T2 lesion distribution in the majority of MS phenotypes with the exception of PPMS patients in whom a mis-match between FA and T2 lesion maps has been observed (Preziosa et al. 2011). This has given support to the hypothesis that in PPMS, axonal damage and T2 lesions occur partially independently from each other (Sbardella et al. 2013).

Interestingly, reduced FA has been shown to correlate with increased numbers of microglia and macrophages in NAWM and slightly abnormal WM (defined as abnormal magnetisation transfer ratio (MTR) in areas surrounding MS lesions) in a post-mortem study of MS brain sections (Moll et al. 2011). Moreover, animal experiments have shown that FA values that are first reduced after Wallerian degeneration due to neuronal injury, increase gradually in the later stage after the injury, and that the reduced FA correlates with the presence of activated microglia, myelin clearance and astrogliosis as assessed in a neuropathological analysis (Qin et al. 2012). Thus, it is plausible that microglial activation might partly explain the subtle changes in WM observed with DTI.

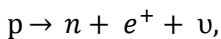
Even though DTI is a sophisticated method to reveal the disruption of structural integrity in MS, the subtle alterations detected with DTI, along with other non-conventional methods such as MTR and adiabatic sequences (Mangia et al. 2013), are more or less unspecific with regards to the neuropathology of MS. Consequently, even adoption of the non-conventional MRI techniques alone will not be sufficient to elucidate the insidious pathology behind the gradually progressing disability in MS. Thus, the exploitation of molecular imaging techniques, such as PET, may shed more light on the clinico-pathological relationships underpinning progressive MS.

2.3.2 Positron emission tomography (PET)

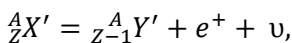
2.3.2.1 Principles of PET physics

Positron emission tomography (PET) imaging enables *in vivo* molecular imaging of physiological and pathological processes in the target organs or organisms. The methodology of PET imaging is based on the capability of the PET scanner to detect radioactivity emitted by radiolabelled ligands. The radiolabels are short-lived radioisotopes, such as ^{11}C , ^{15}O , and ^{18}F , which are first produced in a cyclotron, and then are chemically incorporated into molecules that act as the ligands for the investigated biochemical process. Thus, the accumulation of the radioligand can be quantitated as a function of time within the target tissue.

The radioisotopes used in PET imaging are isotopes with unstable radioactive nuclei, that undergo beta plus (β^+) decay (i.e. positron emission), where a proton (p) is transformed into a neutron (n) while simultaneously emitting a positron (e^+) and an electron neutrino (ν):

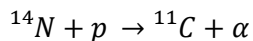


or as described by nuclear mass equation:

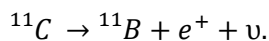


where X' is the parent's nuclear mass and Y' the daughter's nuclear mass. The positron carries a unit of positive charge from the nucleus and has the same mass as an electron, whereas the neutrino has no charge and seemingly no mass.

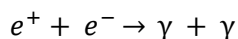
In the example of ^{11}C , it is first produced by bombarding gaseous ^{14}N with protons accelerated in a cyclotron thus inducing an alpha decay (α) of nitrogen:



The half-life of ^{11}C is approximately 20.39 minutes, and as ^{11}C undergoes β^+ -decay into ^{11}B , it emits a positron and a neutrino:



The emitted positrons possess a large amount of kinetic energy, and travel through matter until they have lost enough energy to be able to interact, or collide, with an electron (e^-). This collision is termed annihilation, and results in the emission of two photons (γ) with 511 keV energy in approximately opposite directions ($\sim 180.25^\circ$):



(Esser 2010, Turkington 2001).

2.3.2.2 PET scanner and acquisition of image data

PET imaging is based on the detection of annihilated photons (or gamma rays) by detector crystals positioned in a rim, or row of rims, in the gantry of a PET scanner (Figures 3 and 4). When annihilation occurs, and a photon pair is detected simultaneously (or almost simultaneously) by opposing detectors, annihilation can be deduced to have occurred along an imaginary line connecting the two detectors (Figure 4). This line is called the line of response (LOR), and the event of the detection is referred to as a coincidence event, or true count. Single events (false counts) are detections of single gamma rays without a simultaneous event on an opposing detector. However, if the annihilated emissions in the imaged target are scattered, the subsequently recorded LOR indicates an incorrect location of the event, thus causing a false LOR. If two single events occur so close in time (e.g. <5 nanoseconds), that the electronics of the detectors record it as a genuine coincidence, a random false LOR is registered. However, approximately 97% of singles can be eliminated by applying a coincidence window correction procedure. The remaining data of the registered true counts is recorded in a two dimensional co-ordinate system, where each LOR is located and identified by its distance and angle, and can be plotted as a discrete point on a graph. The plotted curve of the LORs has a sinusoidal shape, and is thus called a sinogram. (Esser 2010, Turkington 2001). The sinograms are collected as a

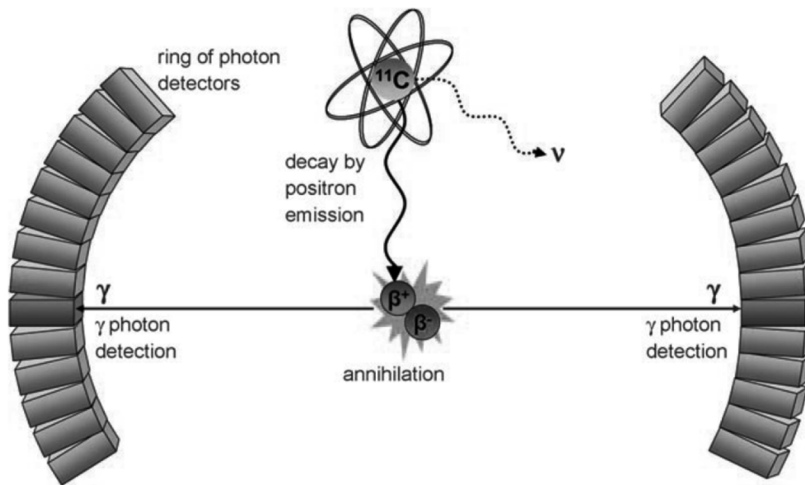


Figure 3. Illustration of an annihilation and the respective coincidence event detected in a PET scanner. An unstable nucleus (^{11}C) emits a positron, which collides into an electron causing annihilation, and the two emitted photons are detected in the detectors within the scanner gantry (for illustrative purposes, the nuclear components and the detectors are not depicted to a natural scale). Modified from (Miller et al. 2008).

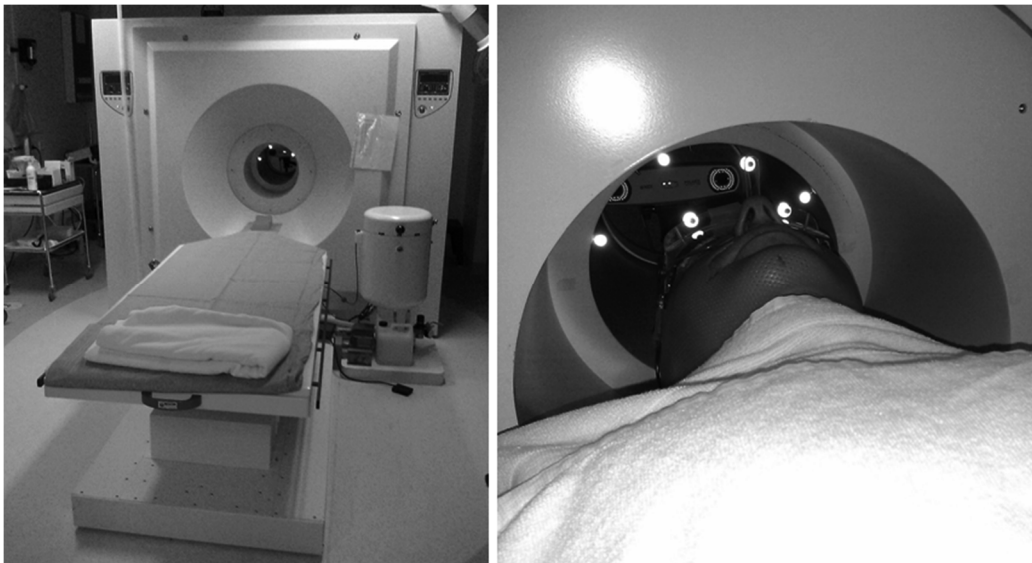


Figure 4. High resolution research tomograph (ECAT HRRT) in Turku PET Centre. General view of the scanner and scanner table on the left, and a picture of a study patient in the scanner on the right (picture used with the permission of the patient) with a thermoplastic mask and motion detection goggles (motion detection device visible on the background).

function of time, and are divided into time frames corresponding to the temporal distribution of the detected true counts.

Finally, the sinogram data is reconstructed with attenuation correction, correction for isotope decay and filtering (smoothing). The final result is a quantitative PET image representing radioactivity concentrations within the scanned object as a function of time. (Esser 2010, Turkington 2001)

2.3.2.3 Pharmacokinetic modelling of neuroreceptor binding

Brain PET imaging facilitates the indirect measurement of neuro-transmitter system components, such as neuroreceptors or transporters. A simple and robust way to measure the uptake of the radioligand into the target tissue *in vivo* is to calculate the standardised uptake value (SUV), which is calculated as the radioactivity concentration at a given time point normalised to the injected dose (corrected for decay to the time point of measurement) and body weight. Thus, SUV measurement does not require dynamic imaging or blood samples, but on the other hand, it does not allow pharmacokinetic modelling. Therefore, analyses of neurotransmitter PET data are commonly performed by applying kinetic models, which are based on assumptions of a compartmental system. With respect to the radiotracer concentrations, at least three compartments (two tissues) can be defined for brain regions containing target receptors, the first compartment being the arterial plasma (C_P). After passing through the blood brain barrier, the non-metabolised radioligand enters the second (first tissue) compartment, named the non-displaceable compartment (C_{ND}), consisting of free (C_F) and non-specifically bound (C_{NS}) sub-compartments. Anatomically, C_{ND} is likely to be constituted of several regions, including interstitial fluid and intracellular cytoplasm. The third (second tissue) compartment (C_S) represents the specific binding to receptors in the target tissue. Brain tissue devoid of high affinity target receptors for the ligand is referred to as reference tissue, where only free (C'_F) and non-specific compartments (C'_{NS}) exist (Figure 5). (Nitz 2003)

In the *in vivo* kinetic modelling, the final parameter of interest is the non-displaceable specific binding of the radioligand in target tissue as a function of time. The golden standard for acquiring the tracer plasma concentration (C_P) is to perform repeated arterial blood sampling for radioactivity and metabolite analyses of the tracer, so that the supply of the non-metabolised active tracer can be calculated as a function of time (i.e. the arterial plasma time activity curve (TAC)). When using conventional compartmental modelling for the dynamic PET image data, the specifically bound radiotracer concentration (C_S) in a target region of interest (ROI) can be estimated from differential equations with non-linear fitting and iterative computation. Consequently, simplified linear graphical methods, such as Logan plot, have been developed.

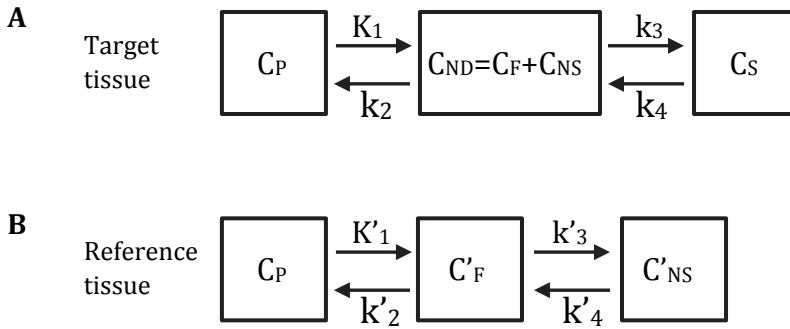


Figure 5. Two tissue (three compartment) model to depict radioligand kinetics *in vivo* in A) target tissue and B) reference tissue. K_1 , k_2 , k_3 , k_4 and K'_1 , k'_2 , k'_3 , k'_4 are the rate constants governing the exchange rates between compartments (according to Nitz 2003).

The Logan plot (Logan et al. 1990, Logan et al. 1996, Logan 2000) can be used to calculate the distribution volume (DV) of a reversibly binding radioligand in the target tissue. If a reference region (free of receptors and thus free of specific binding) is available, the specific binding of the ligand can be estimated as the distribution volume ratio (DVR), which is the ratio of DV in target region of interest (ROI) to the DV in the reference region ROI. According to Logan's equation, the distribution volume (DV) of a reversibly binding radioligand is:

$$DV = \frac{K_1}{k_2} \times \left(1 + \frac{k_3}{k_4}\right) = \frac{K_1}{K_2} \times \left(1 + \frac{B_{max}}{K_d}\right),$$

where B_{max} is the receptor availability, and K_d is the equilibrium dissociation constant (equalling to k_4/k_3), and thus the receptor affinity is $1/K_d = k_3/k_4$.

In a reference region, that is presumably free of receptors and thus free of specific binding, DV can be defined as follows:

$$DV = \frac{K'_1}{k'_2}$$

If a time activity curve (TAC) from the metabolite corrected plasma data is available, the DVs in the target and reference regions can be calculated according to the above equations. Then the specific binding of the radioligand can be calculated as a distribution volume ratio (DVR) of the DVs in a receptor-containing target region and the DV in a receptor-free reference region, resulting in the equation (Logan et al. 1990):

$$DVR = \frac{\frac{K_1}{k_2} \times \left(1 + \frac{k_3}{k_4}\right)}{\frac{K'_1}{k'_2}} = 1 + \frac{k_3}{k_4} = 1 + \frac{B_{max}}{K_d} = 1 + BP$$

where BP = binding potential. The requirement for this equation is that $K_1/k_2 = K'_1/k'_2$.

If no metabolite corrected plasma TAC is available, the plasma curve $C_t(t)$ can be replaced with a reference region curve $C_r(t)$ derived from the reference ROI. Thus, the slope of the linear phase equals DVR (Logan et al. 1996):

$$\frac{\int_0^T C_t(t) dt}{C_t(T)} = DVR \times \frac{\int_0^T C_r(t) dt}{C_t(T)} + C'$$

The precondition, however, for the equation is that $C_t(t)/C_r(t)$ must remain stable enough. The time to reach this equilibrium depends on the receptor density, areas with higher densities taking longer times. If this prerequisite does not hold, an estimate of k'_2 must be determined (e.g. from a population average) and implemented in the equation (Logan et al. 1996):

$$\frac{\int_0^T C_t(t) dt}{C_t(T)} = DVR \times \frac{\int_0^T C_r(t) dt + C_r(T)/\bar{k}_2}{C_t(T)} + C''$$

The arterial plasma input function can also be omitted by using other non-invasive models, of which the Simplified Reference Tissue Models (SRTM) are widely used in neuroreceptor studies (Gunn et al. 1997, Lammertsma and Hume 1996, Wu and Carson 2002). However, the Logan plot is independent of any particular model structure, and thus is more robust. Moreover, when using a reference Logan, no arterial input is needed. Therefore, the Logan plot was chosen as the method of choice in the studies included in this thesis.

2.3.2.4 Radioligands in the imaging of neuroinflammation

During the past decades, several radioligands have been developed in attempts to elucidate the pathological processes related to neuroinflammation. Reviewing all those ligands in detail is outside the scope of this literature review; instead a summary of the radioligands and their targets in CNS is provided in Table 4. Subsequently, only the most relevant radioligands with regard to this thesis, i.e. the TSPO and adenosine receptor ligands, will be reviewed in more detail.

TSPO radioligands

To date, the most widely used target in the PET imaging of neuroinflammation has been TSPO which is highly expressed in the outer mitochondrial membranes of activated microglia (TSPO and microglia reviewed in more detail in chapter 2.2.1).

For more than 25 years, the prototypic TSPO ligand has been [¹¹C](R)-PK11195, with the first human brain studies being conducted in patients with glioma (Junck et al. 1989), Rasmussen's encephalitis (Banati et al. 1999), and in healthy controls and MS patients (Vowinckel et al. 1997). Since then, several studies related to aging, neuroinflammation, neurodegenerative diseases and neuropsychiatric disorders have been published (Table 4).

However, the use of [¹¹C](R)-PK11195 in clinical studies has been somewhat impeded due to its relatively low signal-to-noise ratio (Schweitzer et al. 2010) despite its high specificity for the TSPO (Banati et al. 2014). The low signal-to-noise ratio has been attributed to the ligand's rather low penetration through the BBB and its low brain uptake (Ching et al. 2012), as well as to the ligand's binding to structures in the brain vasculature, where endothelial and smooth muscle cells also express TSPO (Cosenza-Nashat et al. 2009). Reactive astrocytes are also known to overexpress TSPO in response to injury (Kuhlmann and Guilarte 2000) probably adding to the non-microglial specific binding (Ji et al. 2008, Rojas et al. 2007).

Numerous 2nd generation TSPO radioligands with higher affinity and specificity than their predecessor [¹¹C](R)-PK11195 have been developed (Table 4). However, the utility of 2nd generation TSPO ligands in clinical studies in humans has so far been hampered by these ligands' mixed affinity binding phenotype, which has recently been discovered to be attributed to TSPO gene polymorphism in humans (Owen et al. 2012), a phenomenon, however, not affecting [¹¹C](R)-PK11195 binding. A single nucleotide polymorphism (22q13.2 rs6971) in the TSPO gene leads to a replacement of cytosine (C) with thymidine (T) leading to alanine being replaced with threonine in position 147 in the protein. This in turn leads to three different phenotypes with regards to the TSPO binding affinity: low affinity binders (LAB; T/T; threonine/threonine homozygote), mixed affinity binders, (MAB; C/T, alanine/threonine heterozygote) and high affinity binders (HAB; C/C, alanine/alanine homozygote), of which HAB is the most common phenotype (49%) in a Caucasian population, followed by MAB (42%) and LAB (9%) (Owen et al. 2012). In LAB subjects, the binding of the 2nd generation TSPO ligands in the brain is too low to permit a reliable quantification of activated microglia with PET (Kreisl et al. 2013). However, if the binding class is known a priori, then the LAB subjects can be excluded, and subsequently the results stratified according to MAB and HAB groups, then the within subject variability of the 2nd generation ligands is significantly lower than can be achieved with [¹¹C](R)-PK11195. Consequently, the sample sizes needed to reveal 50% differences in between-group analyses would be approximately half of those needed with [¹¹C](R)-PK11195 (Guo et al. 2012). Nevertheless, in order to acquire the binding class information, one must perform peripheral blood sampling to allow the genetic testing of the TSPO polymorphism. In addition, despite their better signal-to-noise ratio than [¹¹C](R)-PK11195, the 2nd generation TSPO ligands have also been shown to bind to reactive astrocytes (Dickens et al. 2014, Lavisse et al. 2012).

Table 4. Molecular targets and the respective radioligands in human PET imaging studies of events related to neuroinflammation.

Target	Related CNS event	Radioligand	Disease / disease model	Studies
TSPO	Microglial activation	[¹¹ C](R)-PK11195	MS	(Banati et al. 2000, Debruyne et al. 2003, Giannetti et al. 2014b, Politis et al. 2012, Ratchford et al. 2011, Vowinckel et al. 1997)
			AD, MCI	(Cagnin et al. 2001, Edison et al. 2008, Okello et al. 2009)
			PD, LBD	(Gerhard et al. 2006, Iannaccone et al. 2013, Ouchi et al. 2005)
			HD	(Pavese et al. 2006, Politis et al. 2011, Tai et al. 2007)
			ALS	(Turner et al. 2004)
			Stroke	(Gerhard et al. 2005, Pappata et al. 2000, Thiel et al. 2010)
			Glioma	(Black et al. 1990, Junck et al. 1989, Su et al. 2015)
	+TSPO in glioma cells		Rasmussen's encephalitis	(Banati et al. 1999)
		[¹¹ C]DAA1106*	MS	(Takano et al. 2013)
			AD	(Varrone et al. 2013)
			Acute neuroinflammation [§]	(Venneti et al. 2007a)
			TBI [§]	(Venneti et al. 2007b)
		[¹¹ C]vinpocetine*	MS	(Vas et al. 2008)
			AD and aging	(Gulyas et al. 2011)
			Stroke	(Gulyas et al. 2012a, Gulyas et al. 2012b)
		[¹¹ C]PBR28*	MS	(Oh et al. 2011)
			Stroke [§]	(Imaizumi et al. 2007)
		[¹⁸ F]PBR111*	Acute neuroinflammation [§]	(Van Camp et al. 2010)
			EAE [§]	(Mattner et al. 2013)
		[¹¹ C]CLINME*	Acute neuroinflammation [§]	(Boutin et al. 2007, Van Camp et al. 2010)
		[¹⁸ F]GE180*	Acute neuroinflammation [§]	(Dickens et al. 2014)
			EAE [§]	(Airas et al. 2015)
			Stroke [§]	(Boutin et al. 2014)
		[¹⁸ F]DPA714*	Acute neuroinflammation [§]	(Chauveau et al. 2009)
			EAE [§]	(Abourbeh et al. 2012)
			Herpes encephalitis [§]	(Doorduyn et al. 2009)
			Stroke [§]	(Boutin et al. 2013, Harhausen et al. 2013, Martin et al. 2010, Wang et al. 2014b)
			TBI [§]	(Wang et al. 2014a)
			Glioma [§]	(Winkeler et al. 2012)
		[¹⁸ F]FEMPA*	AD	(Varrone et al. 2014)

Table 4. continued

Target	Related CNS event	Radioligand	Disease / disease model	Studies
CB2	Microglial activation	[¹¹ C]A836339	Acute neuroinflammation [§] AD [§]	(Horti et al. 2010) (Horti et al. 2010)
COX1	Microglial activation	[¹¹ C]KD2	ALS [¶]	(Mu et al. 2013)
Myelin	De-/remyelination	[¹¹ C]ketoprofen	Acute neuroinflammation [§]	(Shukuri et al. 2011)
		[¹¹ C]BMB	EAE [§] and MS [¶]	(Stankoff et al. 2006)
		[¹¹ C]CIC	Cuprizone mouse model [§]	(de Paula Faria et al. 2014)
		[¹¹ C]MeDAS	Lysolecithin rat model [§] Cuprizone mouse model [§] Plp-Akt-DD mouse model [§]	(Wang et al. 2009) (de Paula Faria et al. 2014) (Wu et al. 2010)
A _{1A} R	Inflammation regulation	[¹¹ C]PIB	LPC-induced demyelin.	(Wu et al. 2013)
		[¹¹ C]MPDX	MS	(Stankoff et al. 2011)
A _{2A} R	Inflammation regulation	[¹⁸ F]CFFPX	Aging	(Mishina et al. 2012)
		[¹¹ C]TMSX	AD	(Fukumitsu et al. 2008)
GABA _A R	Neuronal integrity	[¹⁸ F]CFFPX	Aging	(Meyer et al. 2007)
		[¹¹ C]TMSX	Hepatic encephalopathy	(Boy et al. 2008)
Caspases	Neuronal death / apoptosis	[¹¹ C]TMSX	MS	(Study I)
		[¹¹ C]SCH442416	Aging	(Mishina et al. 2012)
PS	Neuronal apoptosis	[¹¹ C]SCH442416	(PD)	(Mishina et al. 2011)
		[¹¹ C]Flumazenil	Epilepsy	(Ramlackhansingh et al. 2011)
PS	Neuronal apoptosis	[¹⁸ C]ML-10	AD	(Juhász et al. 1999, Pascual et al. 2012)
		[¹⁸ F]DFNSH	Stroke [§]	(Pascual et al. 2012)
PS	Neuronal apoptosis	[^{99m} Tc]AnnexinV [#]	Ketamine-induced [§]	(Reshef et al. 2008)
		[^{99m} Tc]AnnexinV [#]	AD	(Zhang et al. 2011)
			Stroke	(Lampl et al. 2006) (Lorberboym et al. 2006)

A_{2A}R = adenosine A_{2A}-receptor, AD = Alzheimer's disease, CB2 = cannabinoid receptor 2, COX1 = cyclo-oxygenase 1, EAE = experimental autoimmune encephalitis, GABA_AR = GABA_A-receptor, HD = Huntington's disease, LBD = Lewy Body Dementia, LPC = lysophosphatidylcholine; MCI mild cognitive impairment; MMP = matrix metalloproteinase, PD = Parkinson's disease, PS = phosphatidylserine, TSPO = translocator protein, VCAM1 = vascular cell adhesion molecule 1, * 2nd generation TSPO ligand, § Animal model, # used in single photon emission computed tomography (SPECT) imaging, ¶ post-mortem study

Another challenge, shared by both [^{11}C](R)-PK11195 and the 2nd generation TSPO ligands, is the lack of an anatomically clearly defined reference region with presumably negligible specific binding. This is particularly difficult in neuroinflammatory and neurodegenerative diseases with diffusely dispersed pathologies – such as in MS. In order to overcome the lack of a suitable reference region, an automated method for the supervised clustering of normal gray matter reference for [^{11}C](R)-PK11195 PET images has been developed (SuperPK software; Imperial College, London, UK) (Tomasi et al. 2008, Turkheimer et al. 2007, Yaqub et al. 2012). Briefly, in this methodology, a set of predefined kinetic tissue class TACs, representing the average kinetics of the radiotracer in different types of brain tissue is first created. Thereafter, a weighted linear combination of tissue class TACs is fitted to each voxel-wise TAC of the dynamic PET image, which is standardised using frame-wise means and standard deviations (Yaqub et al. 2012). Consequently, a weight coefficient for each PET image voxel, that represents the contribution of each kinetic class to the corresponding TAC, is provided. This methodology has already been successfully applied in patients with Alzheimer's disease (Tomasi et al. 2008, Yaqub et al. 2012) and MS (Giannetti et al. 2014a, Politis et al. 2012), and it is also utilised here (studies III and IV). It is also plausible that a similar protocol could be developed for 2nd generation TSPO ligands in future studies. Moreover, for other radioligands with different targets but similar pharmacokinetic properties, the same algorithms can be utilised as demonstrated for [^{11}C]TMSX in study II.

Adenosine receptor radioligands

As reviewed in chapter (2.2.2), the adenosine receptors in CNS have an integral role in regulating inflammation. In addition, A_{2A} receptors participate in the fine tuning of motor control in striatum, being linked to dopamine D_2 receptors in heteromer receptor complexes in that part of the brain. Of the four known adenosine receptor subtypes, PET tracers have been developed for A_1 and A_{2A} receptors.

In humans, A_1 receptors were first visualised with PET using the radioligand [^{11}C]MPDX (Fukumitsu et al. 2003). [^{18}F]CPFPX is another specific A_1 receptor radioligand which has been used in humans (Bauer et al. 2003, Meyer et al. 2006). [^{18}F]CPFPX has higher affinity for A_1 receptors, but [^{11}C]MPDX is more stable in humans (Bauer et al. 2003, Fukumitsu et al. 2005). These ligands have been utilised in *in vivo* human studies related to aging (Meyer et al. 2007, Mishina et al. 2012), sleep deprivation (Elmenhorst et al. 2007), Alzheimer's disease (Fukumitsu et al. 2008), hepatic encephalopathy (Boy et al. 2008), cerebral injury (Suzuki et al. 2012), and preliminary results have also been reported from studies in patients with Parkinson's disease and epilepsy (Mishina and Ishiwata 2014).

The first produced radioligand for A_{2A} receptors was the ^{11}C -labelled xanthine analogue KF17837 (Ishiwata et al. 1996). Thereafter, several analogues of [^{11}C]KF17837 were evaluated, with [^{11}C]KF18446 ([^{11}C]TMSX) being selected for

clinical applications (Ishiwata et al. 2005, Mishina and Ishiwata 2014). [^{11}C]TMSX is a radioligand binding with high specificity to adenosine A_{2A} receptors (Ishiwata et al. 2005). Another xanthine analogue ligand, [^{11}C]KF21213, showed slightly higher affinity and even higher selectivity for A_{2A} receptors than [^{11}C]TMSX, but it has not been exploited in human studies (Wang et al. 2000).

One disadvantage of the xanthine analogue radioligands is their sensitivity to photoisomerisation, which occurs in the styryl group at the eighth position. Hence, all the procedures conducted with these radioligands need to be performed under dimmed light in order to prevent the photoisomerisation of the ligand into a non-receptor binding conformation (Ishiwata et al. 2005, Mishina and Ishiwata 2014). A non-xanthine type ligand [^{11}C]SCH442416 has also been developed (Todde et al. 2000). It was reported to have the highest affinity and specificity of the developed A_{2A} receptor ligands so far (Mishina and Ishiwata 2014). In addition, ^{18}F -labeled derivatives of SCH442416 have been developed (Bhattacharjee et al. 2011, Khanapur et al. 2014), but not yet tested in humans.

In *in vivo* brain PET studies, [^{11}C]TMSX has so far been utilised only in investigating healthy controls (Mishina et al. 2007, Mishina et al. 2011, Mishina et al. 2012, Naganawa et al. 2007) and PD patients (Mishina et al. 2011). Similarly, [^{11}C]SCH442416 has been used only in one study with healthy controls (Brooks et al. 2010) and in one study with PD patients (Ramlackhansingh et al. 2011) despite its reported superior specificity over the older A_{2A} receptor ligands.

3. AIMS OF THE STUDY

The general aims of this study were to investigate neuroinflammation and neurodegeneration *in vivo* in progressive MS using functional neuroimaging with specific radioligands binding to adenosine A_{2A} receptors and activated microglia, and to develop more automated and non-invasive analyses methods for their imaging. The specific aims of the sub-studies, referred to with the Roman numerals I–IV, were as follows:

- I To determine whether adenosine A_{2A} receptor binding is altered in the brain of SPMS patients compared to healthy controls using [¹¹C]TMSX PET, and to evaluate the possible correlations of [¹¹C]TMSX binding to clinical parameters and MRI findings including DTI abnormalities.
- II To develop and validate non-invasive input function and reference region extraction methods for the analyses of brain [¹¹C]TMSX PET images in order to obviate arterial blood sampling during imaging.
- III To examine whether microglial activation is increased in NAWM and NAGM of SPMS patients compared to healthy controls using [¹¹C](R)-PK11195 PET imaging, and to estimate whether the findings correlate to clinical and MRI parameters.
- IV To investigate microglial activation in NAWM and chronic related to T1 hypointense MS lesions in RRMS and SPMS patients *in vivo* using [¹¹C](R)-PK11195 PET, and to evaluate possible associations of the TSPO-PET imaging to clinical parameters and MRI and DTI abnormalities, and to further investigate the TSPO binding patterns from post-mortem tissue samples using [¹¹C](R)-PK11195 autoradiography and immunohistochemistry.

4. METHODS

4.1 Study population and clinical assessment

The study was conducted as an investigator initiated academic research project in Turku PET Centre and in the outpatient polyclinic of the Division of Clinical Neurosciences in Turku University Hospital. The research protocol was approved by the Ethics Committee of the Hospital District of Southwest Finland, and the study was carried out according to the ethical principles for medical research involving human subjects as stated in the World Medical Association's Declaration of Helsinki.

The patients were recruited from neurology outpatient polyclinics by collaboration with treating neurologists, and by using announcements in local MS and PD patient organisations. Healthy volunteers were recruited with announcements on notice boards of Turku University Hospital and via the MS and PD patient organisations. When contacting the study physician via telephone, the potential study subjects were provided with more information about the study, and if they agreed, they were sent the detailed study information material via mail. The possible risks related to the study were explained in detail. For example, they were informed about the possibility that arterial and venous cannulations could pose a risk for a local infection or haematoma. With a targeted injection dose of 500 MBq, the average effective radiation dose per injection was estimated to be 1.65 mSv for [¹¹C]TMSX and 2.40 mSv for [¹¹C](R)-PK11195. The total radiation exposure of 4.05 mSv for healthy controls and MS patients with both [¹¹C]TMSX and [¹¹C](R)-PK11195 PET imaging was estimated to correspond to a cumulative background radiation of approximately one year in Finland, and for PD patients with one [¹¹C]TMSX PET imaging, the radiation exposure corresponded to a cumulative background radiation of about 5 months. In comparison, one head CT scan (routinely used in clinical practice) is estimated to equal to an average effective dose of 1.3 mSv. Thus, the radiation exposure was considered acceptable for the study subjects. It was also explained that in case of significant coincidental findings were detected in the clinical status or MRI imaging, the study subjects would be referred for further investigations or treatment if needed.

After at least two days' time for consideration, the study physician contacted the study subjects via telephone, and if they agreed to participate, they were invited for the first visit with the study physician in the Turku PET centre. During the first visit, the study physician went through the written information material with the study subject, and adequate time was provided for questions or discussion. The study subjects were informed of their right to withdraw their consent at any point in the study for any reason. The study physician was also responsible for evaluating that the study subjects had sufficient cognitive capacity to understand

the purpose of the study. After having read and understood the information, the study subjects provided their written informed consent before entering the study.

The enrolled study population for the work in this thesis consisted of subpopulations of healthy controls (n=10), SPMS patients (n=10), RRMS patients (n=10) and PD patients (n=9) belonging to a larger study entity named “Imaging Central Nervous System Adenosine Receptors in Multiple Sclerosis, Parkinson’s Disease and Huntington’s Disease using Positron Emission Tomography (CadePET), where in addition to the healthy controls and MS patients, a total of 20 PD patients and 10 patients with Huntington’s disease were planned to be investigated.

A common inclusion criterion for all study subjects was that they were aged between 18–75 years. Study subjects were excluded if they had a history of notable claustrophobia and/or anxiety, ferromagnetic metallic implants or prostheses (of other material than titanium), pacemakers, stimulators and other MRI incompatible objects. The prerequisite for control subjects was that they were healthy individuals with no previous history of neurological symptoms or diagnoses. The inclusion criteria for the SPMS patients were as follows: definite diagnosis of MS at least five years before enrolment, progressive course of the disease for more than two years from the previous relapse, lesion load of >9 T2 hyperintense MS-lesions according to Barkhof criteria (Barkhof et al. 1997) in brain MRI. The criteria for the inclusion of RRMS/CIS patients were: demyelinating lesions in the brain MRI fulfilling the Barkhof criteria, and definite diagnosis of RRMS according to the revised McDonald criteria or a clinically isolated syndrome with no evidence of dissemination in time of the disease. Exclusion criteria for both MS groups were: immunomodulatory treatment within three months, or high dose corticosteroid treatment within 30 days prior to enrolling in the study, EDSS >8, active neurological or autoimmune disease other than MS, or some other significant comorbidity.

At the first visit, a complete medical history including possible current medication was acquired from all subjects by the study physician. The general inspection and cardiovascular status assessment were performed and neurological status was assessed using the Expanded Disability Status Scale (EDSS)(Kurtzke 1983) for healthy controls and MS patients. The unified Parkinson’s disease rating scale (UPDRS) (Fahn and Elton 1987) assessment was performed for all PD patients. The study physician had been trained for EDSS and UPDRS evaluations. Subsequently, brain MRI imaging (see chapter 4.2.) supervised by the study physician was performed. Depending on the imaging time schedules, the PET imaging (see chapter 4.3) was performed either on the same day or on some other day preferably within two weeks from the MRI imaging. Both [¹¹C]TMSX and [¹¹C](R)-PK11195 imaging were performed in healthy controls and MS patients, whereas only [¹¹C]TMSX imaging was conducted in the PD patients. In order to acquire repeated arterial blood samples during the PET imaging for the assessment of the radioligand’s specific activity and metabolites – used for the

estimation of arterial input for the kinetic modelling of PET image data – arterial cannulation of radial artery was performed by an anaesthesiologist prior to the scanning. To allow the administration of the radioligands, a venous cannula was placed into antecubital vein by the study physician, or by an anesthesiologist if also arterial cannulation had been performed. The need for arterial cannulation was obviated after the validation of the non-invasive input function methods for [^{11}C]TMSX (see Chapter 4.4).

One healthy control (male, age 62 years) was excluded from further studies because of unexpected, multiple vascular white matter lesions detected in the MRI. PET imaging data of another control subject (female, 44 years) with no prior history of anxiety or claustrophobia was omitted due to poor image quality caused by excessive head movements during the scan caused because of unexpected anxiety. One control subject (female, 53 years) withdrew her consent after [^{11}C](R)-PK11195 PET imaging but before the scheduled [^{11}C]TMSX PET imaging. One SPMS patient (male, 51 years) had an unexpectedly low signal in the [^{11}C]TMSX images, probably caused by photoisomerisation of the ligand before the injection. In addition, one patient's (male, 51 years) [^{11}C]TMSX PET data was lost due to technical failures in the data reconstruction. One SPMS patient (female 66 years), had a small solitary cortical occipital lesion on the right side radiologically consistent with an old ischemic infarction, but no other ischemic changes were observed. Since there had been a volume reduction due to the infarction, this patient was excluded from the volumetric MRI analyses. One healthy control (female, 61 years) had mild leukoaraiosis changes – probably of ischemic degenerative origin – without consequent tissue loss or infarctions. In the manual region of interest (ROI) analyses, the ROIs were delineated such that none of the leukoaraiotic or ischemic changes were included in the ROIs.

Consequently, in study I, 7 healthy controls (2 males, 5 females) and 8 SPMS patients (2 males, 6 females) were included in the final analyses. In study II, all the study subjects with available arterial input data for [^{11}C]TMSX PET imaging, i.e. all healthy controls and SPMS patients from study I and in addition 4 RRMS patients (1 male, 3 females) and 9 PD patients (5 males, 4 females) participating in the CadePET study were included. In study III, 10 SPMS patients (3 males, 7 females), and 8 healthy controls (2 females, 6 females) were included in the final evaluation. For study IV, 10 RRMS patients (3 males, 7 females) in addition to the controls and SPMS patients in study III were included in the final analyses. A flowchart visualising the enrolling and exclusion of study subjects is provided in Figure 6.

Finally, for post-mortem analyses of progressive MS brain (see chapter 4.5) frozen tissue samples were obtained from the UK Multiple Sclerosis Tissue Bank. The brain tissues in the UK Multiple Sclerosis Tissue Bank have been donated for the purposes of scientific research by individual patients with their informed consent for donation provided before their death. Altogether, fifteen autopsy brain

samples from eight different patients with progressive MS (1 PPMS, 7 SPMS) were obtained for analyses.

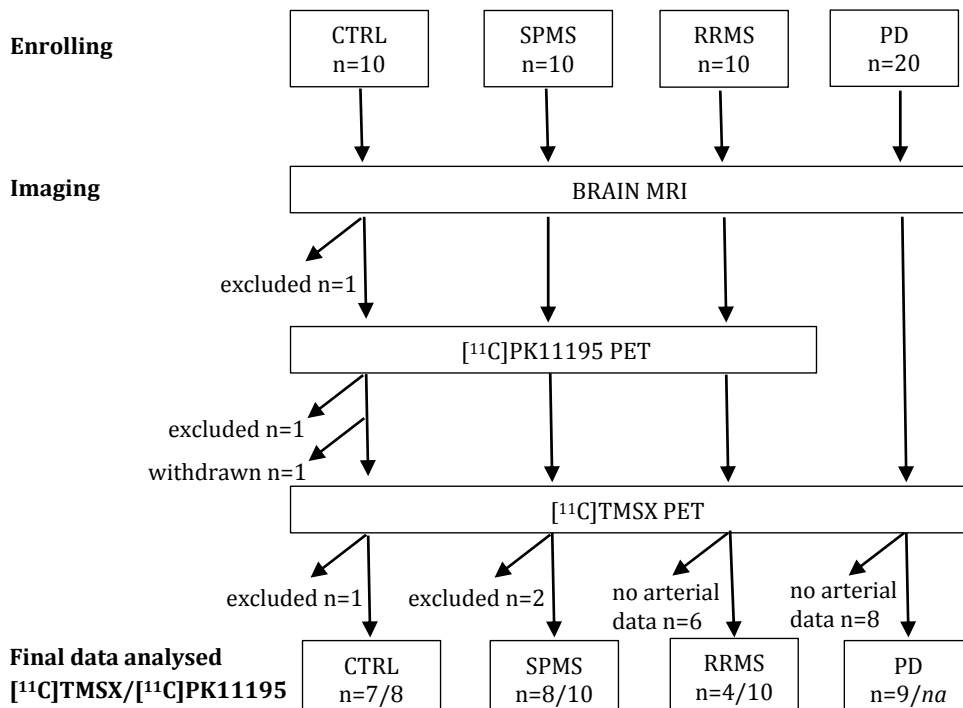


Figure 6. Study subject flowchart. CTRL = healthy controls, SPMS = secondary progressive multiple sclerosis; RRMS = relapsing remitting multiple sclerosis; PD = Parkinson's disease; PET = positron emission tomography

4.2 MRI

Brain MRI was performed in order to perform individual neuroradiological analysis on each subject, and to acquire anatomical reference for the PET image analyses. In addition, the MR imaging was utilised for DTI analyses and further assessment of the MS lesions and normal appearing brain regions. Brain MRI imaging was performed using a Philips Gyroscan Intera 1.5 T Nova Dual scanner (Philips, Best, the Netherlands). The imaging protocol included axial T1 weighted, axial T2 weighted, coronal T2 weighted FLAIR, axial DTI with 16 directions and axial Gadolinium-enhanced 3DT1 weighted sequences. The conventional sequences (T1, T2, FLAIR and 3DT1 with Gadolinium) were used for the routine neuroradiological analyses.

4.2.1 Volumetric Analyses and Evaluation of MS Lesions

In studies **I, III and IV**, the total lesion load of T2 hyperintense MS lesions in WM was determined from coronal FLAIR sequences using a semiautomated thresholding technique, described in earlier MS-study (Virta et al. 2011), using GE AW1.0 software (GE Medical Imaging Systems, Milwaukee, WI, USA). A signal intensity threshold of ≥ 200 was applied for every patient's lesion load evaluation. FLAIR sequences were preferred over T2 images for the lesion volume measurement due to the FLAIR sequences' convenience in assessing intensity limits for separating MS lesions with a high signal when compared to normal appearing brain tissue, and especially since there is no hyperintense CSF signal in the FLAIR sequence as opposed to T2.

The measurement of the total brain, white matter and gray matter volumes in studies I and III and IV was performed with SIENAX (structural image evaluation, using normalization, of atrophy - v2.6, part of FSL) (Smith et al. 2002). The preprocessing of 3DT1 images for the regional analyses of PET image data was performed with Voxel-Based Morphometry, version 8 (VBM8, Structural Brain Mapping Group, University of Jena, Germany)(Gaser 2012) toolbox in Statistical Parametric Mapping, version 8 (SPM8, Wellcome Trust Center for Neuroimaging, London, UK) running on MatLab 2011 (The MathWorks, Natick, MA, USA). After segmenting the 3DT1 images into white and gray matter images according to standard VBM procedures (Good et al. 2001), normalization of the segmented images into MNI space was carried out by using DARTEL (Ashburner 2007), an SPM8 toolbox extension for accurate diffeomorphic registration yielding improved anatomic precision.

4.2.2 DTI analyses

The analyses of the DTI data were performed with the Functional Magnetic Resonance Imaging of the Brain (FMRIB) software and the FMRIB Software Library (FSL, Version 4.1.8; The Oxford Centre for Functional Magnetic Resonance Imaging of the Brain, Oxford, United Kingdom) (Smith et al. 2004). In order to analyse the NAWM, an inclusive mask image was created from the T2 images. The extracranial tissue was extracted from the T2 images with Brain Extraction Tool (BET) (Smith 2002) Thereafter, the resulting T2 brain images were segmented into four classes using FMRIB's Automated Segmentation Tool (FAST) in order to exclude CSF, GM and MS lesions from NAWM. In the segmentation with FAST, four iterations for bias field removal and 20 mm Full-Width Half-Maximum (FMWH) value for bias field smoothing were used. For the confirmation of the exclusion of the MS lesions, each slice of the resulting NAWM images were visually checked. Some small central white matter areas with obviously normal signal intensities were excluded from the NAWM class by the automatic procedure. Those areas were manually added back to the NAWM images with the FSL View tool.

After the NAWM masking procedure, the raw diffusion data was pre-aligned to correct for head motion and for the effects of gradient coil eddy currents. Then, the fractional anisotropy (FA) and mean diffusivity (MD) images were acquired with FMRIB's Diffusion Toolbox (FDT), with the extracranial tissue being extracted from the FA and MD images using BET. The FA and MD images were linearly co-registered to the respective T2 images with FMRIB's Linear Image Registration Tool (FLIRT), and then NAWM FA and MD maps were created with the above described T2-derived NAWM masks. Histograms with 170 bins were acquired from these maps by FSLmaths procedures. After normalising each histogram by the total number of the voxels contributing to the histogram, mean FA and MD values and histogram peak heights were derived from the histograms.

The voxel-wise statistical analysis of the FA data was conducted by using Tract-Based Spatial Statistics (TBSS) (Smith et al. 2006). The FA data of each subject was first aligned into common space with the nonlinear registration tool, FMRIB's Nonlinear Image Registration Tool (FNIRT). Then, a mean FA image was created, which was thinned in order to create a mean FA skeleton that represented the centres of all tracts common to the group. The aligned FA data of each subject was thereafter projected onto this skeleton, and the resulting data was fed into voxel-wise cross-subject statistics. The FA derived skeleton projection was also applied to MD images in the corresponding voxel-wise MD data analysis.

4.3 PET imaging

4.3.1 Radiochemical synthesis of [^{11}C]TMSX

[^{11}C]TMSX ([7-*N*-methyl- ^{11}C]-(*E*)-8-(3,4,5-trimethoxystyryl)-1,3,7-tri-methyl-xanthine) (Figure 7.) was synthesised from its des-methyl precursor using an adaption of the previously published methods (Ishiwata et al. 2003, Kawamura and Ishiwata 2004). Firstly, *in situ* produced [^{11}C]methane was converted into the labelling agent [^{11}C]methyl triflate, which was then trapped into a solution containing 0.4 mg of precursor and 10 mg of caesium carbonate in 200 μl of *N,N*-dimethylformamide. Consequently, 0.6 ml of high performance liquid chromatography (HPLC) mobile phase (acetonitrile/0.01 M phosphoric acid, 41:59) was added, after which the reaction solution was purified in a C18 column. Aliquots of 150 μl of ascorbic acid (100 mg/ml) and 0.5 ml of propylene glycol/ethanol (7:3) were added into the collected fraction and the mobile phase was evaporated. The residue was formulated in 0.1 M phosphoric acid buffer containing propylene glycol/ethanol/ascorbic acid (83:15:2) and sterile filtered through Pall Corp. Acrodisc 0.2 μm HT Tuffryn membrane. In study I, the mean radiochemical purity of [^{11}C]TMSX was 97.4% (SD 0.8) and the mean specific radioactivity was 342.6 MBq/nmol (SD 119,3) at the time of injection. Correspondingly, in study II the mean radiochemical purity was 97.6% (SD 0.7), and the mean specific radioactivity was 425.2 MBq/nmol (SD 160.2).

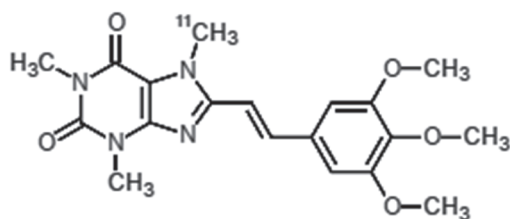


Figure 7. The chemical structure of [^{11}C]TMSX

4.3.2 Radiochemical synthesis of [^{11}C](R)-PK11195

The radiochemical synthesis of [^{11}C](R)-PK11195 ((R)-[N-methyl- ^{11}C]-1-(2-chlorophenyl)-N-(1-methylpropyl)-3-isoquinolinecarboxamide) (Figure 8), was performed according to previously published methods (Camsonne et al. 1984, Debruyne et al. 2003) with some modifications. Briefly, ^{11}C -carbon dioxide was converted into ^{11}C -methyl iodide, after which it was trapped into a solution containing 1.0 mg of desmethyl-(R)-PK11195 and 3.0 μl of 1.0 molar tetrabutylammonium hydroxide in 150 μl of dimethyl sulfoxide (150). The resulting reaction mixture was heated at 80 $^{\circ}\text{C}$ for 3 minutes. Subsequently, the tracer was purified with semi-preparative HPLC. Then, 0.5 ml of propylene glycol / ethanol (7:3) was added into the collected fraction, and the fraction was evaporated. The residue was formulated in 0.1 M phosphate buffer (pH 7.4) containing propyleneglycol / ethanol (8:2) and sterile filtered through Pall Corp. Acrodisc 0.2 μm HT Tuffryn membrane. In study III, the mean radiochemical purity of [^{11}C](R)-PK11195 was >99.9% and the mean specific radioactivity was 42.0 MBq/nmol (SD 10.6) at the time of the injection of the ligand and there were no statistically significant differences between the subgroups of healthy controls and SPMS patients. In addition, in the RRMS group in study IV, the mean radiochemical purity was >99.8% (SD 0.1) and specific radioactivity 53.4 MBq/nmol (SD 17.1).

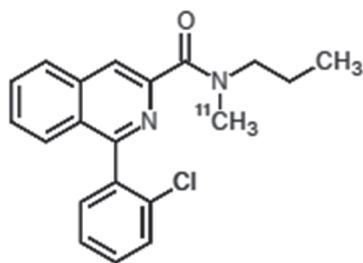


Figure 8. The chemical structure of [^{11}C](R)-PK11195

4.3.3 PET Image Acquisition

PET imaging was performed according to the same protocol for both [^{11}C]TMSX and [^{11}C](R)-PK11195 radioligands using the brain-dedicated high resolution ECAT HRRT scanner (CTI / Siemens, Knoxville, TN, USA) (Heiss et al. 2004). HRRT is a dual-layer, crystal-detector scanner that allows a depth-of-interaction measurement for the coincident photons providing isotropic 2.5-mm intrinsic spatial resolution. The spatial resolution of the reconstructed images varies from approximately 2.5 to 3 mm in radial and tangential directions and from 2.5 to 3.5 mm in axial directions in the 10 cm field of view covering the majority of the brain (de Jong et al. 2007).

The study subjects were instructed to abstain from caffeinated beverages for 12 hours prior to the imaging due to caffeine's antagonistic properties at adenosine receptors. In addition, PD patients were imaged in the off-phase with respect to dopaminergic medication, i.e. a minimum break of 12 hours for short lasting, and 24 hours for long lasting (depot) dopaminergic medications was required before the PET-imaging because of the possible reciprocal interaction within the dopamine D_2 – adenosine A_{2A} – heteromere receptor complex. After placing the subjects in a supine position on the scanner table, an individually shaped polymer face mask was donned in order to minimise spontaneous head movements during the scan. In addition, a Polaris Vicra (Northern Digital Inc., Waterloo, Ontario, Canada) motion detection device was used to record the head movements for quality control. Thereafter, a 6 minutes' transmission scan utilising the ^{137}Cs point source of the HRRT scanner was performed for attenuation correction. Then, the 60 minutes' dynamic imaging was initiated simultaneously with the administration of a smooth, <10 seconds' intravenous bolus of the radioligand. An arterial blood sampling system (ABSS) (Allogg AMSS, Allogg AB, Mariefred, Sweden) connected to the arterial cannula was used for the first 300 seconds of the dynamic scan in order to provide continuous arterial blood radioactivity measurements. Thereafter, manual arterial blood samples were drawn at time points of 5, 10, 15, 20, 30, 40, 50 and 60 minutes to allow the metabolite and radioactivity analyses of the ligands.

4.3.4 Blood radioactivity and metabolite analyses

Plasma protein binding for the [^{11}C]TMSX blood analyses were determined from six subjects using an ultrafiltration method of Microcon YM-30 units with 30000 molecular weight cut-off filter (Millipore/Amicon, Bedford, USA) (Montgomery et al. 2007). [^{11}C]TMSX was highly bound to plasma proteins, the mean percentage being 90.9% (SD 0.4). Consequently, the mean free fraction of [^{11}C]TMSX in plasma was 9.1% (SD 0.4).

The total radioactivity concentrations and the fractions of the non-metabolised [^{11}C]TMSX were evaluated from the arterial plasma samples (studies I and II). The radioactivity analyses were performed with an automatic gamma counter (1480

Wizard 3"; EG&G Wallac, Turku, Finland), and the metabolite fractions were determined using radio-HPLC. The radio-HPLC system consisted of LaChrom Instruments (Hitachi; Merck, Darmstadt, Germany): pump L-7100, UV-detector L-7400 and Interface D-7000, of an on-line radioactivity detector (Radiomatic 150TR, Flow Scintillation Analyzer; Packard, Meriden, CT, USA) and a computerised data acquisition system. The radio-HPLC separations were carried out on a μ -Bondapak® C-18 column (125Å, 10 μ m, 7.8 \times 300 mm; Waters, Milford, MA, USA) at a flow rate of 6.0 mL/min and a gradient of acetonitrile (A) and of phosphoric acid, 50 mmol/L (B) as follows: 0-2 min of 25% A and 75% B, 6-8 min of 80% A and 20% B, and 8.5-10 min of 25% A and 75% B. The radioactivity peaks were integrated with plasma concentration, after which the fraction of the intact radiotracer was calculated. The non-metabolised [11 C]TMSX was identified by comparing the retention time of the "cold" TMSX at 351 nm wavelength. All the procedures for blood sampling and analyses, as well as the dosing and injection of the ligand, were carried out under dimmed light in order to prevent the photoisomerisation of the ligand.

The first five minutes' continuous radioactivity sampling with ABSS corresponds to the whole blood radioactivity. Thus, the plasma radioactivity of this initial phase was estimated by multiplying the whole blood radioactivity with the plasma / whole blood ratio acquired from population-based, tracer-dependent, mean haematocrit value of 0.40. For combining the ABSS and the manual sampling data, an in-house developed software was utilised for the calculation of arterial plasma input curve of the parent (non-metabolised) [11 C]TMSX radioactivity as a function of time, also corrected for physical decay of the radioligand and the time delay between the peripheral injection and the availability of the ligand in brain circulation as detected by the PET scanner.

For [11 C](R)-PK11195, the arterial blood sampling, and the radioactivity and metabolite analyses were performed according to a similarly timed protocol as applied with [11 C]TMSX. The resulting [11 C](R)-PK11195 plasma input data was available from 8 healthy controls and 9 SPMS patients, and was utilised in defining the kinetic classes for the supervised clustering of gray matter reference using SuperPK software (Imperial College, London, United Kingdom)(Turkheimer et al. 2007) explained in more detail in chapter 2.3.2.4.

4.3.5 Preprocessing of MRI and PET image data

The dynamic PET images were corrected for attenuation, scattering, random events, scanner dead time and detector normalisation, and were subsequently calibrated into kBq/mL with decay correction. Prompt and random events, attenuation, and scatter correction and normalisation factors were processed in a 3D sinogram mode, and an axial compression of span 9 and a maximum ring difference of 67 was used, resulting in 2,209 sinograms in 16 segments. Tissue attenuation maps were reconstructed using the maximum a posteriori for transmission data (MAP-TR) algorithm with standard human brain priors for air,

bone, noise, water, or soft tissue (Nuyts et al. 1999). The 3D attenuation correction sinograms were acquired by forward projection of the tissue attenuation maps. Scattered events were estimated by using the single scatter simulation algorithm (Watson 2000), and randoms were estimated from the block singles using a variance reduction algorithm (Byars et al. 2005). Finally, the dynamic data was smoothed with a Gaussian 2,5 mm post reconstruction filter (Hinz et al. 2008).

In the reconstruction of [^{11}C]TMSX images, a total of 27 time frames (6x10, 3x30, 5x60, 5x150 and 8x300 seconds; total of 3600 seconds) were used. The [^{11}C](R)-PK11195 PET images were reconstructed with 17 frames (2x15, 3x30, 3x60, 7x300 and 2x600 seconds; total of 3600 seconds). Possible displacements between the frames were corrected using mutual information realignment in SPM8. The frame-by-frame realignment parameters affirmed the external motion trackings, and thus, co-registration of the attenuation map images and image reconstruction were deemed unnecessary.

Static summed PET images were formed for both radioligands from the dynamic images by summing all the frames (frames 1–27 for [^{11}C]TMSX and 11–17 for [^{11}C](R)-PK11195) in SPM8. Then both the summed and dynamic PET images were co-registered with the 3DT1, T2 and FLAIR MR images in SPM8 for the individual manual region of interest assessment (see next chapter). Pre-processing of the 3DT1, T2 and FLAIR MR images for the atlas-based ROI analyses and the parametric PET image analysis was performed with the VBM8 toolbox in SPM8: after segmenting the 3DT1 images into white and gray matter images according to the standard VBM procedures (Good et al. 2001), the acquired segmented images were normalised into MNI space using DARTEL (Ashburner 2007), which is an SPM8 toolbox extension providing accurate diffeomorphic registration and yielding improved anatomic precision.

4.3.6 Definition of Regions of Interest (ROI)

In study I, individual regions of interest (ROI) were defined manually on the 3DT1 MR images co-registered with a sum image (frames 12–27) of the dynamic [^{11}C]TMSX images using in-house developed Imadeus software (version 1.20, Forima inc., Turku, Finland). Bilateral ROIs were placed on anterior cingulate gyri, medial temporal, lateral temporal, lateral frontal, occipital, and parietal cortices, and striatum, thalami, periventricular NAWM and supraventricular NAWM (centrum semiovale), and cerebellar cortex. Unilateral ROIs were delineated on anterior and posterior parts of corpus callosum (genu and splenium, respectively), pons and the inferior part of the sinus sagittalis superior. In addition, ROIs on active MS lesion with gadolinium enhancement on 3DT1 were defined. The NAWM ROIs were positioned in the above mentioned WM areas appearing normal in the reference MRI's FLAIR and 3DT1 sequences also avoiding the immediate subcortical WM in order to avoid a partial volume effect from GM.

In studies II–IV, a semiautomated segmentation based method for the acquisition of ROIs from global normal appearing gray matter (NAGM), NAWM and pathological WM was introduced in addition to the manual delineation of ROIs. For the formation of global cerebral cortical NAGM (segmented neocortex) ROI, a mask image of the cortical GM regions in the Automated Anatomical Labeling (AAL) template (Tzourio-Mazoyer et al. 2002) was created and warped to match the individual dynamic PET images using in-house developed software mapping integer values from a template image to subject space by applying the inverse deformation fields resulting from VBM8 segmentation. The warped cortical GM mask images were then multiplied by the VBM8 segmented GM (thresholded using a value of 0.5). Global cortical cerebellar ROIs were also created with AAL with a similar methodology.

For the identification of pathological WM with T2 hyperintense lesions in Study III, the Lesion Segmentation Tool (LST) (Schmidt et al. 2012) was used; this is a toolbox running within SPM8. Firstly, the initial threshold for the lesion growing algorithm was set to a value of 0.3. The resulting lesion probability maps were transformed into binary masks consisting of voxels having a value >0.9 , and these binary LST masks were used as the pathological WM ROIs. The global NAWM ROIs, devoid of T2 hyperintense lesions, were created by subtracting the segmented WM mask images with 1) LST mask and 2) with gray matter mask created with AAL and containing areas of deep gray matter structures, temporomedial regions and cerebellum in order to clean the WM segment from remaining gray matter voxels. Due to software upgrade related improvements, the manual ROI's previously drawn with Imadeus, were transferred into Carimas (Carimas 2.4, Turku PET Centre, Turku, Finland) for TAC acquisition.

In order to create more comprehensive deep gray matter ROIs in Study IV, manually delineated bilateral ROIs of thalamus and striatum were combined with the corresponding AAL ROIs in subject space. In study IV, mask images for NAWM ROIs were created by subtracting the T1 hypointense lesion mask image, perilesional mask images, and striatum and thalamus masks from the segmented WM. Thus, the NAWM ROIs in study IV were defined slightly differently from those used in Study III.

In study IV, T1 hypointense lesions (black holes) and a perilesional area with a 6 mm radius surrounding the black holes, were determined also with a semiautomated approach. Firstly, the T2 hyperintense white matter MS lesions were identified with LST as described above. Subsequently, mask images of T1 the hypointense lesions were derived from LST's T1 lesion filling feature. The T1 hypointense lesion masks were visually checked slice by slice and manually corrected if needed. Next, the masks were segregated into two groups for gadolinium negative and gadolinium positive T1 hypointense lesions, being correspondingly used for the evaluation of intralesional white matter, and as a core for the perilesional white matter. For each lesion mask, a surrounding mask with the 6 mm radius was created by filtering the mask with 3 mm FWHM

Gaussian 3D filter, then thresholding the resulting image with a value of 0.01, and by finally repeating the procedure. Overlapping regions between the perilesional areas of gadolinium negative and positive masks were removed from both of the resulting masks. An example image of the resulting T1-lesional and perilesional white matter masks is shown in the publication of study IV (Figure 1.). The T1 hypointense lesion masks were also utilised for the T1 lesion load assessment, the lesion load volumes being derived from the respective mask volumes.

4.3.7 Modelling of [¹¹C]TMSX and [¹¹C](R)-PK11195 image data

4.3.7.1 ROI analyses

For the modelling of reversible binding of both [¹¹C]TMSX and [¹¹C](R)-PK11195 radioligands, the Logan plot (Logan et al. 1990, Logan et al. 1996, Logan 2000) was used.

In studies I and II, the ROI-specific V_T (total distribution volume) of [¹¹C]TMSX was evaluated with the Logan plot using the ROI TACs derived from the dynamic PET images and the metabolite corrected plasma input obtained from arterial blood sampling. The Logan plot was calculated for the time interval from 10 to 40 in study I. However, in study II with a larger study population, the time range of 10 to 60 minutes was selected, because, on average, it yielded the best linear fitting of the tested time intervals in thalamus; for each subject, the initial equilibrating time that gave the smallest variation co-efficient for the V_T estimate was selected, after which the median of the resulting time ranges was adapted.

In study III, the ROI specific binding of [¹¹C](R)-PK11195 was evaluated as distribution volume ratios (DVR) using the graphical reference Logan. A non-invasive reference region input was acquired with the supervised cluster algorithm (SVCA) with four predefined kinetic tissue classes (SuperPK software, SVCA4 classification) (Turkheimer et al. 2007, Yaqub et al. 2012). The kinetic classes representing the radioligand binding in GM, WM and vasculature were defined using the available arterial metabolite corrected plasma input and the corresponding ROI specific TACs of healthy controls (n=8). The HSB was defined using thalamus ROI data from SPMS patients (n=9), respectively. The rationales for using thalamic binding of SPMS patients in the HSB class formation were that [¹¹C](R)-PK11195 binding in thalami 1) increases with age (Schuitemaker et al. 2007) and 2) that it is increased in MS patients when compared to controls (Banati et al. 2000). A time range of 5–60 minutes was selected for the Logan equation based on the inspection of Logan plot regression lines. The mean k_2 value in reference region ($k_2=0.145$) was calculated using the parameter estimates acquired from SRTM with metabolite-corrected arterial input in thalamus with SVCA4 gray reference region. Finally, the non-invasive reference Logan method was applied to the target region specific TACs using the SVCA4 gray reference input for regional DVR estimation. The same methodology was applied in study IV with the following updates to the algorithm: The metabolite

corrected [^{11}C](R)-PK11195 time activity curves acquired from arterial sampling of the above mentioned healthy controls and SPMS patients were normalised by the group average in a leave-one-out procedure similar to the methodology for [^{11}C]TMSX SVCA by excluding the specific subject from the group average before the normalisation in order to exclude that specific subject's effect on the group average. When predefining the kinetic tissue classes, the normal gray matter maps of healthy controls were cleaned of gray matter voxels in thalamus and striatum using an AAL template based mask resulting in a cortical gray matter reference cluster, from which the average normal gray matter kinetic time activity curve was derived. In addition, the clustered gray matter reference coefficient map was thresholded to include only voxels with a coefficient value <0.25 in order to acquire a reference cluster more representative of typical gray matter voxels.

4.3.7.2 Parametric image analyses

Parametric PET images were used for the statistical evaluation of voxel-wise group differences. In parametric images, the signal intensity of each voxel represents the amplitude of the ligand binding in the voxel. The parametric images for both [^{11}C]TMSX and [^{11}C](R)-PK11195 were produced using an in-house developed algorithm with the implementation of the Logan plot with the same time intervals as used for the ROI specific V_T and DVR assessments.

In study I, the parametric images were calculated for [^{11}C]TMSX V_T , and in study III for [^{11}C](R)-PK11195 DVR using the SVCA4 gray reference input. Subsequently, the parametric images were normalized to MNI (Montreal Neurological Institute) space with VBM8 using DARTEL normalisation with subject-specific transformation parameters, which were acquired from the pre-processing phase of the 3DT1 MR images. For [^{11}C](R)-PK11195, the voxel-wise DVR values were limited to range $[-1 \ 10]$. Before the statistical analyses in SPM8, the parametric [^{11}C]TMSX V_T images were smoothed with an 8 mm FWHM Gaussian kernel for noise reduction. An additional procedure was carried out for [^{11}C](R)-PK11195 in order to prevent the spill-over effect from the ligand binding in the vasculature and soft tissue (mainly meninges) surrounding the cortical gray matter: the parametric [^{11}C](R)-PK11195 DVR images were multiplied with an average binary mask image obtained from the segmented GM and WM images of both control and SPMS patients using Masking toolbox in SPM8. Thereafter, the masked parametric DVR images were smoothed with an in-house developed edge-preserving 8 mm full width half maximum (FWHM) Gaussian 3D filter.

4.3.7.3 Visual evaluation of [^{11}C](R)-PK11195 binding in T1-lesions

In addition to the LST based evaluation of the T2 hyperintense lesions, a visual qualitative assessment of the perilesional [^{11}C](R)-PK11195 binding of the T1 hypointense lesions was carried out in study III. The evaluation was performed on

parametric [^{11}C](R)-PK11195 images overlaid with gadolinium enhanced 3DT1 end FLAIR images using Carimas. A T1 hypointense lesion which showed as T2 hyperintense in FLAIR was regarded positive for perilesional [^{11}C](R)-PK11195 uptake if the [^{11}C](R)-PK11195 DVR signal was higher in more than half of the lesion's circumference in all axial slices than in the adjacent or contralateral NAWM.

4.4 Developing non-invasive input functions for [^{11}C]TMSX analyses

4.4.1 Population based input function

In order to replace arterial blood sampling for future [^{11}C]TMSX brain PET studies, a population-based plasma input function (PBIF) was created using all of the available [^{11}C]TMSX arterial input data consisting of a total of 28 study subjects from the subgroups of healthy volunteers ($n=7$), MS patients ($n=12$; of which 4 RRMS patients and 8 SPMS patients) and PD patients ($n=9$). Firstly, each metabolite corrected plasma TAC was standardised by the dose of injected activity and the subject's body surface area (BSA) by implementing the Mosteller formula (Mosteller 1987). The standardised curves were then interpolated to the same time points, shifted to average peak time, and lastly, normalised by the group average in a leave-one-out procedure by excluding the specific subject from the group average for before the normalisation. Despite the subtle variation of the arterial data between different cohorts, differences could be noted in the peak heights of the group specific average PBIFs, illustrated in supplementary figure 1. in the publication of study II. Therefore, the subgroup specific average PBIFs were regarded as being more optimal than a single shared PBIF for all subjects. The resulting subgroup specific average PBIFs were individually scaled to their original levels with two alternative methods: 1) with BSA (non-invasive individually scaled PBIF; PBIF_{nis}) and 2) with an average of two metabolite corrected arterial blood samples at 9 and 23 minutes that were tested to give the best correlation with plasma AUC in this cohort (invasive individually scaled PBIF; PBIF_{is}) (Takikawa et al. 1993).

4.4.2 Clustered Reference Region Acquisition

An automated reference region extraction method for dynamic brain [^{11}C]TMSX images was developed in order to provide a user independent creation of a gray reference region with low specific binding based on the supervised clustering algorithm implemented for [^{11}C](R)-PK11195 brain PET image analyses (SuperPK software; Imperial College, London, UK)(Turkheimer et al. 2007). Four different kinetic tissue class TACs were defined, representing average binding in average GM, WM, vasculature and in areas of high specific binding (HSB). Firstly, the segmented GM and WM MRI images of the healthy controls were transformed into

binary masks (thresholded using a value of 0.9). The WM and GM mask images were then used as ROIs for the extraction of corresponding TACs from the dynamic [^{11}C]TMSX images. The TACs representing vasculature and high specific binding were acquired from the PET images using the manually delineated venous sinus ROIs from the healthy controls and thalamus ROIs from SPMS patients, respectively. For comparison, an alternative HSB class delineated on anterior putamen of PD patients was formed. The resulting PD HSB TACs yielded similar results with no statistically significant differences when compared to the MS HSB class (data not shown). Consequently, only the results acquired with the MS HSB classification are reported here. Finally, an individual set of kinetic class TACs were created for each subject. At first, all the class TACs were standardised to match the above mentioned standardised PET data, after which the average standardised TAC for each class was calculated in a similar leave-one-out manner than described in the previous chapter (4.4).

In order to reduce the possible effect of misclassification in the clustering step, the following strategy was implemented. Firstly, a ratio of the gray coefficient to the sum of all the weight coefficients was calculated for all the gray map voxels. Secondly, the gray coefficient map was thresholded to contain only values >0.25 in the gray ratio map (Ikoma et al. 2013). In addition, those voxels of the gray coefficient that had also HSB and vascular binding coefficients <0 were excluded from the gray coefficient map. Finally, the remaining gray map coefficients were used for the calculation of a weighted average of the dynamic PET image, thus forming the supervised clustering derived gray matter (SCgm) reference region TAC.

4.5 Post-mortem [^{11}C](R)-PK11195 autoradiography and immunohistochemistry of progressive MS brain samples

The autopsy brain samples were obtained as 5 μm thin cryosections ($-80\text{ }^{\circ}\text{C}$), that were mounted on glass slides. Two of the samples were from the brain stem, the rest from either hemisphere. Serial tissue sections were utilised for ex-vivo and immunohistochemistry. In autoradiography, the tissue sections were defrosted at room temperature, after which they were incubated for an hour in TRIS (50 mM) buffer at room temperature. The sections were incubated with [^{11}C](R)-PK11195 (24.8 kBq, $\sim 50\text{ pM}$) for 30 minutes, and were then washed (2 x 5 minutes) in ice cold TRIS buffer, dried and placed in an imaging cassette and exposed to a phosphor imaging plate (Fuji Imaging Plate BAS-TR2025, Fuji Photo Film Co., Ltd., Japan) for 40 minutes (corresponding to a period of two half-lives of the radioligand). Finally, the plates were read in a phosphor imaging plate reader (BAS-5000, Fuji, Japan; 25 mm² resolution).

In the histological and immunohistochemical studies, monoclonal anti-CD68 antibody (clone PG-M1, Dako, Glostrup, Denmark) was used for the detection of activated microglia/macrophages, and anti-GFAP antibody (clone EP672Y, Ventana Medical Systems, Strasbourg, France) was utilised for the identification of astrocytes. LFB staining was used for the evaluation of myelin density. In LFB staining, the tissue sections were first fixed for 20 minutes in formalin, and then rinsed with aqua. In the immunohistochemistry, the sections were first fixed for 5 minutes in cold acetone, after which they were allowed to dry in a laminar-flow cabinet. The tissue sections were incubated with the monoclonal anti-CD68 and anti-GFAP antibodies. The stainings were carried out using a BenchMark XT Autostainer (Ventana) with the *ultraVIEW* Universal DAB Detection Kit (Ventana). Finally, the tissue sections were then examined visually for the co-localisation of [¹¹C](R)-PK11195 binding and expression of CD68, GFAP and myelin in WM lesions, perilesional and NAWM.

In the analyses of immunohistochemical data, white matter lesions were identified according to demyelinated areas devoid of LFB staining. In order to characterize the microglial/macrophage and astrocytic cell quantity and distribution, GFAP-positive astrocytes and CD68 positive microglia/macrophages were quantified in three areas: the non-demyelinated white matter, in the core of the demyelinated area, and at the edge of demyelination. In this assessment, three representative areas in each location were evaluated using high power (x400) microscopy and the mean number of positively stained cells was counted from these representative fields. The number of positive cells outside the lesion was set as a reference level in each sample. The relative increase/decrease of positive cells at the edge and core of lesions was calculated. An increase of over 100% was regarded as significant, and a decrease of more than 50% was set as a threshold for reporting cell loss.

In the evaluation of the autoradiography results, the LFB and CD68 stainings in the adjacent sections were utilised for the localisation of the white matter lesions. The autoradiography signal intensity in the core and at the border of the lesion was visually evaluated with respect to the surrounding white matter. PK11195 binding was regarded as being increased if the signal was of higher intensity than in the adjacent white matter, and decreased if the intensity appeared to be lower when compared to the surrounding white matter.

4.6 Statistical methods

Based on the reports of previous brain [¹¹C]TMSX (Mishina et al. 2007, Mishina et al. 2011, Naganawa et al. 2007) and [¹¹C](R)-PK11195 studies (Debruyne et al. 2003, Edison et al. 2008, Turkheimer et al. 2007), it was estimated that ten subjects per study group would suffice to reveal a 15% difference in the radioligand uptake between groups with 90 percent power at the level of $p < 0.05$.

The statistical analyses of the individual clinical, MRI and PET variables were performed with SPSS (IBM SPSS Statistics, version 19 in study I and version 21 in studies II–IV). The normality of distribution of the variables was checked using the Shapiro-Wilk test. The group characteristics have been reported as mean and standard deviation (SD) values if the distribution of the variables was normal, otherwise median and interquartile range (IQR) or coefficient of variation percentage ($CV = \text{median}/\text{IQR} * 100$) was used. Independent samples T-test with Levene's test of variance equality was used in the group comparisons with normal distributions. The non-parametric Mann-Whitney's U-test was used to estimate group differences with non-normally distributed variables. The evaluation of possible correlations between non-dependent different variables of interest was performed with Pearson's test and Spearman's non-parametric test for linear and non-linear associations, respectively. In the comparisons of dependent variables within groups, the paired sample Wilcoxon signed rank test was used. In addition, Bland-Altman's method was applied in Study II to evaluate the agreement of the V_T estimates between the original arterial input and population based input function methods.

The voxel-wise statistical analyses of the group differences of the parametric PET images were performed using SPM8. In study I, before the evaluation of group differences in the parametric [^{11}C]TMSX V_T images, proportional scaling for global normalisation of the parametric images was performed in SPM8. Prior to the proportional scaling, the requirements for implementing the methodology were checked according to previous publications (Friston et al. 1990, Okazawa et al. 2000), and the relation of global to regional V_T s was not additive but proportional (for illustration see supplementary figure 1 in the publication of study I), thus it was decided to opt for the proportional scaling instead of analysis of covariance in the global normalization. In the normalisation using image specific global values, the grand mean scaling value was set to 1. In order to use the mean V_T of brain parenchymal voxels only for the global normalisation, the parametric V_T -images, and inclusive mask of the WM and GM segments were applied. The statistical analyses of the possible voxel-wise group differences of the parametric [^{11}C]TMSX V_T images in study I and [^{11}C](R)-PK11195 DVR images in study III were performed in SPM8 with independent samples T-Test. The group differences were regarded as statistically significant at the voxel level if $p < 0.001$ (uncorrected), and at the cluster level if $p < 0.05$ (corrected for multiple comparisons; family-wise error, FWE).

5. RESULTS

Altogether, the results have originated from the clinical and imaging data from 8 healthy controls, 10 SPMS patients, 10 RRMS patients and 9 PD patients.

In study I, conventional MRI, DTI and [^{11}C]TMSX PET data from 7 healthy controls and 8 SPMS patients were included in the final analyses and are reported here.

In study II, [^{11}C]TMSX-PET data from the same 7 healthy controls and 8 SPMS patients as in study I in addition to 4 RRMS and 9 PD patients were included in the validation of non-invasive input function methods for [^{11}C]TMSX PET.

In study III, conventional MRI and [^{11}C](R)-PK11195 PET imaging data from 8 healthy controls and 10 SPMS patients were included in the final analyses and are reported here.

In study IV, conventional MRI, DTI and [^{11}C](R)-PK11195 PET imaging data of the same 8 healthy controls and 10 SPMS patients as in study III in addition to 10 RRMS patients, and supplemented with post mortem [^{11}C](R)-PK11195 PET autoradiography and immunohistochemistry data from 13 samples were used, and are presented here.

For clarity, the results of the clinical parameters, MRI and DTI imaging of all study subjects are reported first, followed by the results from the *in vivo* [^{11}C]TMSX and [^{11}C](R)-PK11195 PET imaging with the correlations to the clinical, MRI and DTI parameters, and finally, the *ex vivo* [^{11}C](R)-PK11195 PET autoradiography and immunohistochemistry results are presented.

5.1 Demographics and clinical characteristics

The RRMS patients were significantly younger than the SPMS patients and the controls which were age matched for the SPMS patients ($p < 0.001$ for both comparisons). When compared to the RRMS patients, as expected, the SPMS patients had significantly longer disease duration ($p < 0.001$), EDSS ($p < 0.001$) and MSSS ($p = 0.003$) (Table 5). The median (IQR) age of PD patients (4 men, 5 women) was 66 (59–72) years.

5.2 MRI and DTI in healthy controls and MS patients

5.2.1 Increased atrophy, lesion load and DTI abnormalities in SPMS

The SPMS patients displayed considerable brain atrophy when compared to the healthy controls and RRMS patients (Table 4). There was a statistically significant reduction in the GM volumes in SPMS versus RRMS ($p = 0.002$) and control ($p = 0.001$)

groups. Furthermore, the WM volumes were significantly lower in the SPMS patients than in the RRMS patients ($p=0.029$) and the healthy controls ($p=0.006$).

The lesion load was markedly higher in the SPMS patients as opposed to their RRMS counterparts (Table 5), with both the total T2 lesion volume and total T1 lesion volume being higher in the SPMS than in the RRMS group ($p<0.001$ and $p=0.001$, respectively)

Table 5. Demographical, clinical MRI and DTI parameters of RRMS patients, SPMS patients and healthy controls expressed as median (IQR) values by group. Modified from Study IV.

	<i>RRMS (n=10)</i>	<i>SPMS (n=10)</i>	<i>Controls (n=8)</i>
Male / Female (n)	3/7	4/6	2/6
Age (years)	27.0 (25.0–29.8)	49.5 (42.0–57.8)	47.5 (43.5–55.0)
Disease duration (years)	0.7 (0.5–1.8)	13.5 (9.0–15.8)	<i>na</i>
EDSS	1.5 (1.5–1.9)	6.5 (6.0–8.0)	<i>na</i>
MDSS	4.12 (3.23–4.62)	7.57 (7.02–8.66)	<i>na</i>
WM volume (cm ³)	762 (741–770)	718 (695–729)	788 (763–812)
GM volume (cm ³)	834 (789–863)	756 (711–780)	825 (807–853)
T2 lesion lesion load (cm ³)	3.7 (2.7–8.4)	50.0 (103.0–132.0)	<i>na</i>
T1 Gd- lesion load (cm ³)	1.1 (0.5–2.3)	9.4 (3.1–17.3)	<i>na</i>
T1 Gd+ lesion load (cm ³)	0.5 (0.3–0.7)	0.5 (0.5–0.7)	<i>na</i>
T1 total lesion load (cm ³)	1.4 (0.6–2.6)	9.6 cm (3.1–17.4)	<i>na</i>
Mean FA in NAWM	0.370 (0.356–0.379)	0.301 (0.299–0.304)*	0.336 (0.331–0.338)
Mean MD in NAWM	797 (790–816)	833 (797–849)*	792 (782–801)

* DTI data available for 9 of 10 SPMS patients

RRMS = relapsing remitting multiple sclerosis; SPMS secondary progressive multiple sclerosis; EDSS = expanded disability status scale; MSSS = multiple sclerosis severity scale; WM = white matter; GM = gray matter; Gd- = gadolinium negative; Gd = gadolinium positive; FA = fractional anisotropy; NAWM = normal appearing white matter; MD = mean diffusivity; DTI = diffusion tensor imaging

In the DTI analyses, the SPMS patients had significantly reduced structural integrity in the NAWM when compared to the RRMS patients and the healthy controls (Table 5). The mean FA in NAWM among the SPMS patients was significantly reduced in comparison to controls ($p<0.001$) and the RRMS patients ($p<0.001$). The mean MD was significantly higher in SPMS vs. controls ($p=0.036$), whereas only a trend without any statistical significance for higher MD in SPMS vs. RRMS group was noted ($p=0.113$) was noted.

Although the mean FA values were significantly higher in RRMS when compared to control group, no significant group differences were found in the mean MD

values ($p=0.360$). The voxel-wise TBSS analyses of 7 healthy controls and 8 SPMS patients in Study I revealed widespread localisation of the structural damage both in the periventricular and subcortical white matter and in corpus callosum among the SPMS patients when compared to the healthy controls (Figure 9).

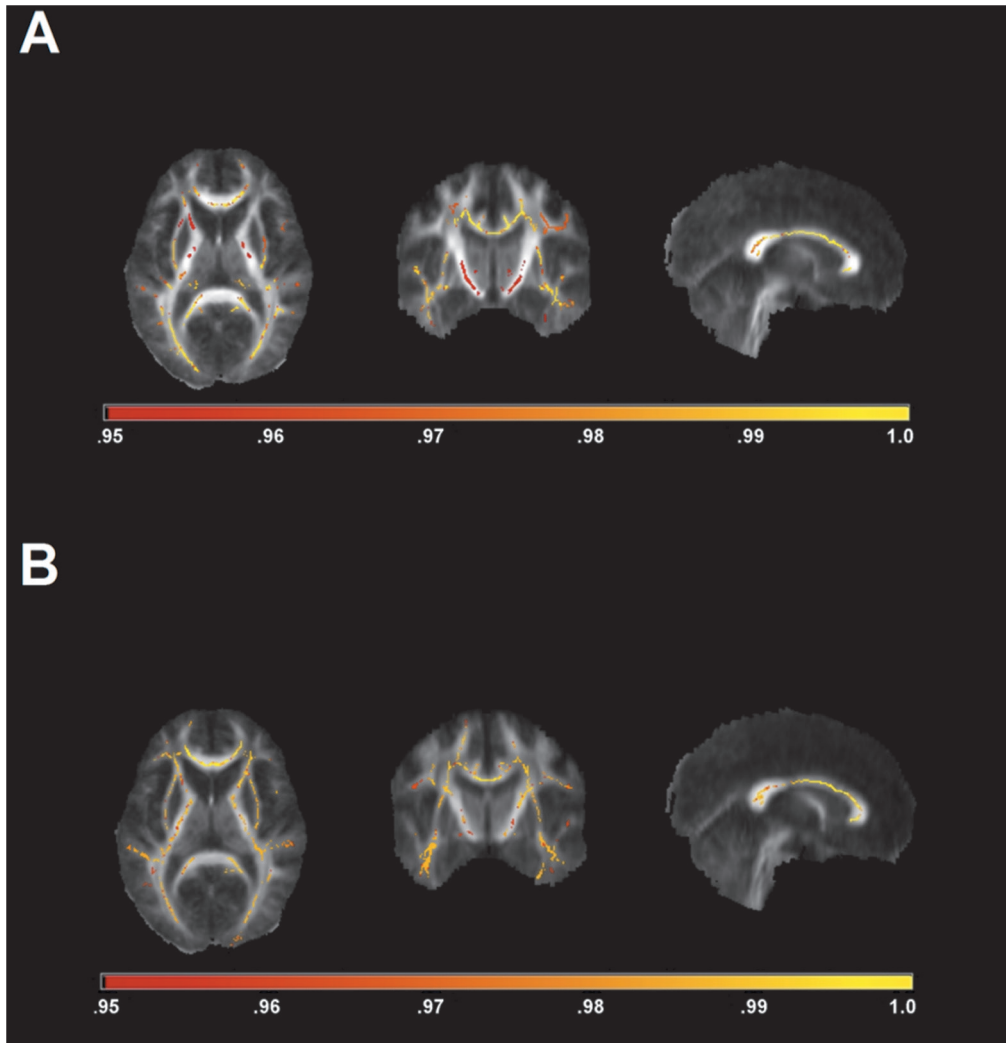


Figure 9. TBSS analysis of DTI from 8 SPMS patients and 7 healthy controls visualised as voxel-wise group differences in FA **(A)** and MD **(B)** data overlaid on mean FA images. Areas of statistically significantly reduced FA and increased MD indicated according to the horizontal coloured bar scale with values corresponding to 1-p. Reprinted with permission from Study I.

5.2.2 Association of brain atrophy and reduced FA to disability and age

In the correlational analyses of the MS patients (Table 6; RRMS and SPMS patients pooled into one group), several associations were found between the clinical, MRI and DTI parameters. The increases in GM and WM atrophy correlated positively

with higher EDSS. A longer disease duration was associated with more notable GM atrophy, whereas in WM, the correlation did not reach statistical significance. The higher total T2 lesion load correlated positively with higher EDSS and MSSS. Despite the significant group differences between RRMS and SPMS, no significant correlation were found between T1 hypointense lesion loads and disease duration or severity measured as EDSS and MSSS. The lower mean FA in NAWM correlated with higher age, longer disease duration, higher EDSS, and higher MSSS, whereas for MD, no corresponding correlations of statistical significance were found. The correlations of EDSS and age to reduced mean FA in NAWM are also visualized as scatterplots in Figure 3 (C-D) in the publication of study IV.

Table 6. Correlations of MRI and DTI parameters to the clinical characteristics in all MS patients (n=20; SPMS n=10, RRMS n=10). The correlations are expressed as Spearman's rho values and the respective p-values (modified from study IV).

MRI and DTI parameters	Age	Disease duration	EDSS	MSSS
	Spearman (p)	Spearman (p)	Spearman (p)	Spearman (p)
T1 lesion load [#]	0.353 (0.127)	0.281 (0.230)	0.338 (0.145)	0.286 (0.221)
T2 lesion load [§]	0.596 (0.007*)	0.442 (0.058)	0.617 (0.005*)	0.558 (0.013**)
Mean FA [§]	-0.642 (0.003*)	-0.534 (0.018**)	-0.671 (0.002*)	-0.573 (0.010**)
Mean MD [§]	0.319 (0.183)	0.149 (0.544)	0.141 (0.564)	0.128 (0.600)
GM volume	-0.661 (<0.002*)	-0.537 (0.015**)	-0.505 (0.023**)	-0.356 (0.123)
WM volume	-0.433 (0.056)	-0.311 (0.181)	-0.583 (0.007*)	-0.507 (0.022*)

[#] Gadolinium negative T1 lesions

[§] DTI and lesion load available from 9/10 SPMS and 10/10 RRMS patients

* Spearman correlation statistically significant at the level of $p < 0.01$

** Spearman correlation statistically significant at the level of $p < 0.05$

MRI = magnetic resonance imaging; DTI = diffusion tensor imaging; EDSS = expanded disability status scale; MSSS = multiple sclerosis severity scale; FA = fractional anisotropy; MD = mean diffusivity; GM = gray matter; WM = white matter

5.3 *In vivo* imaging of adenosine A_{2A} receptors with [¹¹C]TMSX

5.3.1 Increased [¹¹C]TMSX binding in NAWM of SPMS patients in comparison to healthy controls

In study I, the mean injected dose of [¹¹C]TMSX radioactivity was 476.9 (SD 33.2) MBq with no significant differences between groups [469.9 (SD 45.8) MBq in controls and 483.0 (17.7) MBq in SPMS group). According to the metabolite analyses of the arterial blood samples, [¹¹C]TMSX remained very stable with the non-metabolised fraction of the ligand being 90.5% (SD 9.7) at the 50 minutes' time point.

As a marker of increase adenosine A_{2A} receptor binding, [^{11}C]TMSX V_T was increased in NAWM in the SPMS patients when compared to the healthy controls. The group differences reached statistical significance in supraventricular (centrum semiovale) and total NAWM ($p=0.022$ and $p=0.036$, respectively) ROIs. In other ROIs, no significant differences were found, although a trend was observed towards higher mean V_T in thalami of SPMS patients than in controls ($p=0.094$). The ROI specific V_T results are shown in detail in Table 7.

Table 7. ROI specific [^{11}C]TMSX V_T estimates with Logan (10-40 minutes) in healthy controls ($n=7$) and SPMS patients ($n=8$) shown as group mean (SD) values in ml/cm^3 , group differences expressed in percentages of differences of means. Modified from study I.

<i>ROI</i>	<i>Controls</i>	<i>SPMS patients</i>	<i>Group difference</i>
Anterior cingulate cortex	0.69 (0.07)	0.72 (0.09)	+ 3.4
Medial temporal cortex	0.59 (0.07)	0.60 (0.09)	+ 2.7
Lateral temporal cortex	0.63 (0.07)	0.66 (0.10)	+ 3.7
Lateral frontal cortex	0.72 (0.07)	0.74 (0.09)	+ 3.0
Occipital cortex	0.70 (0.09)	0.73 (0.14)	+ 4.3
Parietal cortex	0.70 (0.09)	0.74 (0.17)	+ 6.7
Neocortex ¹	0.67 (0.08)	0.70 (0.10)	+ 3.5
Striatum	1.11 (0.12)	1.14 (0.19)	+ 3.5
Thalamus	0.80 (0.11)	0.92 (0.15)	+ 15.4
Pons	0.56 (0.07)	0.59 (0.12)	+ 5.1
Cerebellar cortex	0.70 (0.08)	0.74 (0.11)	+ 6.8
Venous sinus ²	0.45 (0.05)	0.46 (0.12)	+ 2.2
Periventricular NAWM	0.44 (0.05)	0.51 (0.07)	+ 15.0
Supraventricular NAWM	0.45 (0.06)	0.56 (0.10)	+ 24.8*
Total NAWM ³	0.45 (0.05)	0.55 (0.08)	+ 23.3*
Corpus callosum, splenium	0.38 (0.06)	0.41 (0.12)	+ 6.9
Corpus callosum, genu	0.42 (0.06)	0.44 (0.09)	+ 5.5
Active plaques ⁴	na	0.54 (0.10)	na

¹ Combined ROIs of lateral temporal and frontal, occipital, and parietal cortical ROIs

² Cross-sectional ROI from the inferior part of sinus sagittalis superior

³ Combined ROIs of bilateral periventricular and supraventricular NAWM ROIs

⁴ ROIs from active plaques with slightly increased gadolinium uptake from two patients

* Statistically significant difference with the level of $p<0.05$ (Independent samples T-Test)

ROI = region of interest; SPMS = secondary progressive multiple sclerosis; NAWM = normal appearing white matter

In the correlational analyses of the ROI specific results including all study subjects, increased [^{11}C]TMSX V_T in total NAWM ROI correlated to reduced FA in NAWM (Pearson's correlation -0.54, $p=0.038$). The increase in V_T in NAWM was also associated with the reduced WM volumes (Pearson's correlation -0.59, $p=0.028$). In addition, there was a positive correlation between increased

[¹¹C]TMSX V_T and higher EDSS (Pearson's correlation 0.56, $p=0.030$); however, the small group sizes did not permit a reliable estimation of the correlations within the SPMS group.

For the statistical analyses of voxel-wise group differences in the parametric [¹¹C]TMSX V_T analyses, global normalisation was performed as described in the methods. There were no significant group differences in the global TMSX V_T between the groups before the global normalisation [mean global V_T (SD) 0.64 (0.07) in controls vs. 0.67 (0.11) in SPMS group; $p=ns$]. In concordance with the results from manually delineated ROIs, the voxel-wise analyses of group differences in the parametric V_T [¹¹C]TMSX images revealed statistically significant increases of the radioligand binding in widespread areas of white matter in SPMS group in comparison to healthy controls (Figure 10).

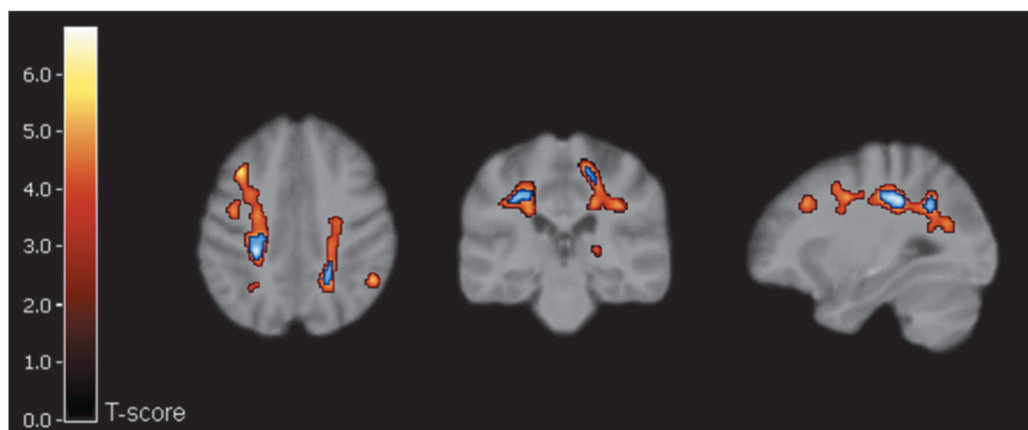


Figure 10. SPM analysis of parametric [¹¹C]TMSX V_T images in healthy controls ($n=7$) and SPMS patients ($n=8$) showing significantly increased V_T in SPMS compared to control group in voxel clusters overlain on the study subjects' averaged MRI template. T-scores (indicated in the red-yellow scaled colour bar) with values >3.8 correspond to uncorrected $p<0.001$. Blue areas indicate clusters with FWE-corrected $p<0.05$. Reprinted with permission from study I.

5.3.2 Automated reference region extraction and non-invasive input functions for [¹¹C]TMSX image analyses

In study II, [¹¹C]TMSX binding was estimated using both V_T and DVR for the validation of PBIF inputs as an alternative for arterial plasma input (OPIF), and cluster algorithm derived reference region (SCgm) as an option for ROI based cerebellum reference region. The mean (SD) injected dose of [¹¹C]TMSX was 469.2 (55.2) MBq, with no significant differences between the subgroups [469.9 (45.8) MBq for controls, 458.8 (74.7) MBq for MS and 482.6 (26.1) MBq for PD group. The metabolism of [¹¹C]TMSX was slow with the mean (SD) fraction of the intact ligand being 93.4% (4.7) at the 50 minutes' time point. No significant differences

between groups were observed, the mean (SD) percentages being 90.5% (6.7) in control, 92.7% (4.6) in MS and 95.5% (2.8) in the PD groups, despite the mean in PD group being 5 percentage points higher when compared to the control group.

5.3.2.1 Reference region extraction

The acquired TACs representing the four tissue classes for [^{11}C]TMSX SVCA reference region extraction are illustrated in the publication of study II (Figure 1). The distributions of the resulting coefficient maps of the clustered gray matter reference region (SCgm) appeared similar in all subgroups. The majority of the voxels contributing to the reference cluster were located in cerebral, and to a lesser extent, in cerebellar cortex (Figure 11). The SCgm TACs revealed slightly higher initial peak but lower uptake in the latter part of the curve in comparison to cerebellum (see Figure 3 in the publication of study II).

5.3.2.2 [^{11}C]TMSX distribution volumes in SCgm and cerebellum reference regions with OPIF and PBIFs

The [^{11}C]TMSX V_T estimates in SCgm and ROI based cerebellum reference region using the Logan plot with both the original plasma input (OPIF) and the noninvasive and invasive population based inputs (PBIFnis and PBIFis, respectively) in all subgroups are reported in detail in Table 8. Both PBIFs produced similar V_T results with no statistically significant differences between the methods, and with moderate-to-good correlations in the cerebellum and SCgm in comparison to the results acquired with OPIF. Pearson correlation of the results with PBIFnis to OPIF was 0.76 ($p < 0.001$) in cerebellum and 0.73 ($p < 0.001$) in SCgm, whereas for PBIFis, the corresponding correlations were 0.97 ($p < 0.001$) in cerebellum and 0.97 ($p < 0.001$) in SCgm when evaluated for all study subjects pooled together. The correlations in all of the study subjects are also visualised as a Bland-Altman plot and a scatterplot illustrated in the publication of study II (Figure 5).

In addition, when evaluating the bias of the PBIFs as a median V_T ratio to OPIF, V_T values estimated with PBIFis showed a slightly better concordance with OPIF than did PBIFnis in both cerebellum and SCgm (Table 8). The V_T values were generally lower in SCgm than in cerebellum reference region, the difference being statistically significant in the MS group ($p = 0.006$ in OPIF, PBIFnis and PBIFis) and in PD group being significant or borderline ($p = 0.04$ in PBIFnis and $p = 0.05$ in OPIF and PBIFnis). In addition, a trend, but without statistical significance, was noted in healthy controls ($p = 0.09$ in OPIF and PBIFnis, $p = 0.06$ in PBIFis) (Table 8).

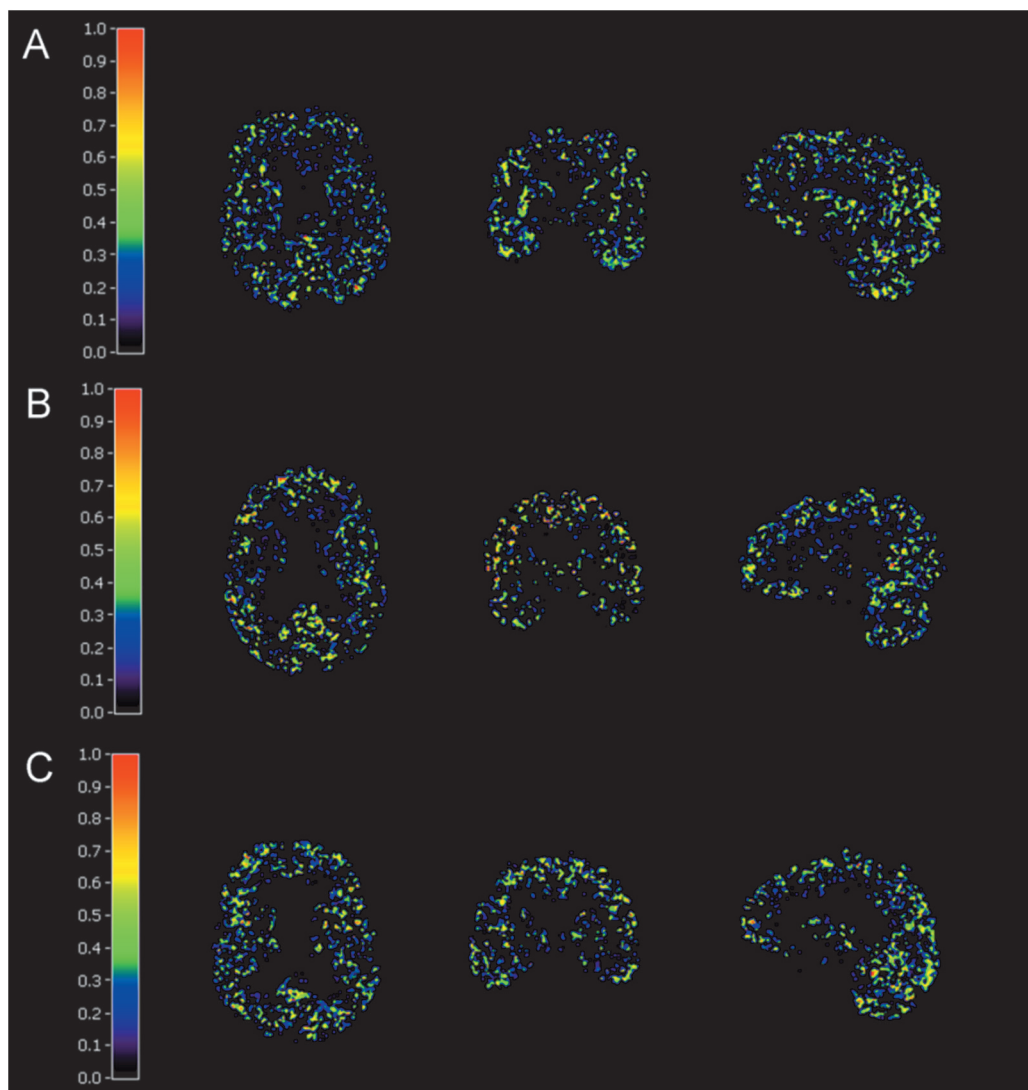


Figure 11. Example images of [^{11}C]TMSX SVSCgmCA gray matter weight coefficient maps in **A)** a healthy control (male, 61 years), **B)** SPMS patient (female, 39 years) and **C)** PD patient (male, 75 years). The scaled colour bars indicate the voxel-wise ratio of the gray coefficient value to the sum of all weight coefficients, calculated for each voxel. Reprinted with permission from study II.

In PD patients, the V_T s in the reference regions were overall lower than in healthy controls (Table 7). The difference was statistically significant in SCgm with all inputs ($p=0.023$ for OPIF, $p=0.023$ for PBIFnis and $p=0.032$ for PBIFis). In cerebellum, the difference was statistically significant for PBIFis ($p=0.042$), and a similar trend without statistical significance was observed also for OPIF ($p=0.91$) and PBIFnis (0.71). The comparison between healthy controls and MS patients, no

Table 8. Comparison of different input functions in the estimation of [^{11}C]TMSX V_T in cerebellum and SCgm reference regions in all study subjects and the subpopulations. V_T expressed in ml/cm^3 as group median (CV% calculated with Logan using OPIF, PBIFnis and PBIFis. Bias of the PBIFs reported as a V_T ratio (CV%) to OPIF. Modified from study II.

Group	Input function	Reference region	
		Cerebellum	SCgm
Healthy controls (n=7)	OPIF V_T (CV%)	0.69 (11.6)	0.65 (15.2)
	PBIFnis V_T (CV%)	0.74 (22.6)	0.69 (18.3)
	Bias	0.92 (0.2)	0.92 (0.2)
	PBIFis V_T (CV%)	0.70 (10.5)	0.66 (6.0)
	Bias	1.00 (0.1)	1.00 (0.1)
SPMS patients (n=8)	OPIF V_T (CV%)	0.69 (16.6)	0.67 (17.0)
	PBIFnis V_T (CV%)	0.73 (12.3)	0.70 (11.7)
	Bias	0.99 (0.1)	0.99 (0.1)
	PBIFis V_T (CV%)	0.72 (13.2)	0.68 (19.1)
	Bias	1.01 (0.1)	1.01 (0.10)
RRMS patients (n=4)	OPIF V_T (CV%)	0.59 (18.6)	0.54 (11.4)
	PBIFnis V_T (CV%)	0.59 (25.2)	0.55 (16.2)
	Bias	0.99 (5.7)	0.99 (5.6)
	PBIFis V_T (CV%)	0.58 (17.4)	0.54 (9.7)
	Bias	0.99 (8.1)	1.02 (7.7)
All MS patients (n=12)	OPIF V_T (CV%)	0.67 (18.7)	0.62 (21.4)
	PBIFnis V_T (CV%)	0.70 (21.8)	0.66 (25.9)
	Bias	0.99 (10.2)	0.99 (9.9)
	PBIFis V_T (CV%)	0.68 (20.41)	0.63 (21.0)
	Bias	0.98 (8.1)	0.98 (8.0)
PD patients (n=9)	OPIF V_T (CV%)	0.58 (37.0)	0.51 (31.8)
	PBIFnis	0.59 (21.2)	0.53 (25.6)
	Bias	1.03 (14.5)	1.03 (14.6)
	PBIFis V_T (CV%)	0.57 (35.4)	0.50 (31.0)
	Bias	0.98 (3.1)	0.98 (3.1)
All study subjects (n=28)	OPIF V_T (CV%)	0.65 (22.0)	0.60 (23.2)
	PBIFnis	0.64 (26.1)	0.63 (26.9)
	Bias	0.99 (15.3)	0.99 (15.4)
	PBIFis V_T (CV%)	0.64 (25.1)	0.61 (22.8)
	Bias	0.99 (7.15)	0.99 (7.0)

V_T = total distribution volume; CV% = coefficient of variation in percentages ($|IQR|/\text{median} \times 100$); SCgm = supervised clustering derived gray matter reference region; OPIF = original plasma input function; PBIFnis = population based input function, noninvasive, individually scaled; PBIFis = population based input function, invasive, individually scaled; MS = multiple sclerosis; SPMS = secondary progressive MS; RRMS = relapsing remitting MS; PD = Parkinson's disease

revealed no significant group differences. However, when analysing the MS subgroups separately, the V_T in SCgm with OPIF was significantly lower in RRMS vs. control group ($p=0.042$), but in SCgm with other inputs and in cerebellum with any of the inputs, no significant group differences were detected. Between the control and SPMS groups, no statistically significant differences were found in the reference region V_{TS} .

5.3.2.3 Performance of PBIFs and SCgm in the estimation of [^{11}C]TMSX binding in target regions

The performance of PBIFnis and PBIFis as input functions, and SCgm as a reference region in estimating [^{11}C]TMSX binding in target regions of interest (global cortical gray matter, segmented neocortex ROI; striatum, thalamus and global NAWM) was further evaluated in healthy controls and SPMS patients. Firstly, the V_T estimates in the cortical GM, deep GM and NAWM ROIs yielded with PBIFs compared well to the original V_T results obtained with OPIF (Table 9). However, when observing the median V_T estimates of both PBIFs, there was a small positive bias in comparison to OPIF, although when evaluating median V_T ratios to OPIF, the bias for PBIFnis appeared to be negative and negligibly positive for PBIFis. In NAWM, the group difference between SPMS patients and controls observed with OPIF was reproduced with PBIFnis but not with PBIFis, although the differences at the percentage level were alike (Table 9).

Secondly, for the evaluation of specific [^{11}C]TMSX binding, DVRs from plasma-input Logan (using OPIF, PBIFnis or PBIFis as an input) and reference-input Logan with cerebellum or SCgm as reference regions were calculated, and the group differences were evaluated with respect to the V_T results. The resulting DVR estimates with all of the above mentioned optional inputs and both reference regions revealed similar group differences between healthy controls and SPMS patients when they were compared to the original V_T values with OPIF (Table 10.). The significant group difference in NAWM noted with the original OPIF V_T was reproduced with all optional inputs in DVR estimation when using the SCgm reference, whereas with cerebellum as the reference, the group differences in NAWM DVR did not reach statistical significance with any of the inputs although there was a similar trend in the percentage differences. In thalamus ROI, the trend towards the higher [^{11}C]TMSX binding in SPMS patients than in the controls evaluated with OPIF V_T became more pronounced in the DVR estimation reaching statistical significance with all inputs and both reference regions.

Table 9. Comparison of different input functions in the estimation of [^{11}C]TMSX V_T in target regions in healthy controls and SPMS patients. V_T expressed in ml/cm^3 as group median (CV%) values, calculated with Logan and OPIF, PBIFnis and PBIFis. as input functions. Modified from study II.

ROI	Healthy controls (n=7)		SPMS patients (n=8)		Group differences, %	
	OPIF	PBIFnis PBIFis	OPIF	PBIFnis PBIFis	OPIF	PBIFnis PBIFis
Neocortex	0.68 (15.0)	0.70 (17.2) 0.92 (0.20)	0.69 (20.4)	0.71 (13.6) 0.99 (0.11)	2.2	2
<i>Bias#</i>				0.71 (21.8) 1.01 (0.10)		1.4
Striatum	1.03 (20.6)	1.11 (18.0) 0.92 (0.20)	1.09 (14.3)	1.14 (11.2) 0.99 (0.11)	5.9	2.8
<i>Bias#</i>				1.10 (16.5) 1.01 (0.10)		0.8
Thalamus	0.78 (13.3)	0.83 (12.5) 0.92 (0.20)	0.89 (22.2)	0.92 (15.9) 1.00 (0.11)	13.9	11.2
<i>Bias#</i>				0.92 (21.7) 1.01 (0.10)		17.8
NAWM	0.45 (14.2)	0.45 (14.6) 0.94 (0.23)	0.53 (19.4)	0.54 (9.8) 0.99 (0.09)	16.2*	22.2*
<i>Bias#</i>				0.53 (12.7) 1.02 (0.08)		18.8

V_T = total distribution volume; CV% = coefficient of variation in percentages (IQR/median*100); ROI = region of interest; OPIF = original plasma input function; PBIFnis = population based input function, noninvasive, individually scaled; PBIFis = population based input function, invasive, individually scaled; SPMS = secondary progressive multiple sclerosis; NAWM = normal appearing white matter

* Mann-Whitney U-test $p < 0.05$.

Bias of PBIFnis and PBIFis reported as a median (CV%) V_T -ratio to OPIF

Table 10. Comparison of different plasma inputs (OPIF, PBIFnis and PBIFis) and the reference Logan in the estimation of [¹¹C]TMSX DVR in target regions. DVR expressed as median (CV%) using cerebellum and SCgm reference regions in healthy controls and SPMS patients. Group differences are shown in percentages of the difference of medians. The correlations of DVR estimates yielded with PBIFnis, PBIFis and RefLog to OPIF are shown as Spearman's correlation coefficients (ρ). Modified from study II.

ROI	Healthy controls (n=7)				SPMS patients (n=8)				Group differences (%)			
	OPIF	PBIFnis	PBIFis	RefLog	OPIF	PBIFnis	PBIFis	RefLog	OPIF	PBIFnis	PBIFis	RefLog
Neocortex	0.96 (6.8)	0.97 (6.7)	0.97 (6.7)	0.96 (6.9)	0.98 (7.4)	0.98 (7.2)	0.98 (7.2)	0.98 (7.2)	2.0	1.7	1.7	1.8
ρ to OPIF (p-value)	1.00 (<0.001)#	1.00 (<0.001)#	1.00 (<0.001)#	1.00 (<0.001)#	1.00 (<0.001)#	1.00 (<0.001)#	1.00 (<0.001)#	1.00 (<0.001)#				
Striatum	1.49 (10.0)	1.49 (10.0)	1.49 (10.0)	1.49 (10.2)	1.59 (7.7)	1.59 (7.6)	1.59 (7.6)	1.59 (7.6)	6.3	6.5	6.5	6.5
ρ to OPIF (p-value)	1.00 (<0.001)#	1.00 (<0.001)#	1.00 (<0.001)#	1.00 (<0.001)#	1.00 (<0.001)#	1.00 (<0.001)#	1.00 (<0.001)#	1.00 (<0.001)#				
Thalamus	1.13 (7.3)	1.13 (7.6)	1.13 (7.6)	1.13 (7.6)	1.28 (9.2)	1.28 (9.3)	1.28 (9.3)	1.28 (9.3)	13.5*	13.6*	13.6*	13.6*
ρ to OPIF (p-value)	1.00 (<0.001)#	1.00 (<0.001)#	1.00 (<0.001)#	1.00 (<0.001)#	1.00 (<0.001)#	1.00 (<0.001)#	1.00 (<0.001)#	1.00 (<0.001)#				
NAWM	0.60 (17.1)	0.60 (18.3)	0.60 (18.3)	0.60 (17.6)	0.72 (9.1)	0.72 (6.8)	0.72 (6.8)	0.71 (7.1)	20.4	19.8	19.8	19.7
ρ to OPIF (p-value)	0.82 (0.02)#	0.82 (<0.001)#	0.82 (<0.001)#	0.75 (0.05)	0.99 (<0.001)#	0.99 (<0.001)#	0.99 (<0.001)#	0.80 (0.017)#				

Cerebellum reference region

Table 10. continued.

ROI	Healthy controls (n=7)				SPMS patients (n=8)				Group differences (%)			
	OPIF	PBIFnis	PBIFis	RefLog	OPIF	PBIFnis	PBIFis	RefLog	OPIF	PBIFnis	PBIFis	RefLog
Neocortex	1.02 (4.7)	1.02 (4.7)	1.02 (4.7)	1.02 (4.7)	1.03 (3.2)	1.03 (3.3)	1.03 (3.3)	1.03 (3.3)	0.8	0.8	0.8	0.8
ρ to OPIF (p-value)	$(<0.001)^{\#}$ ($<0.001)^{\#}$ ($<0.001)^{\#}$ ($<0.001)^{\#}$)				$(<0.001)^{\#}$ ($<0.001)^{\#}$ ($<0.001)^{\#}$ ($<0.001)^{\#}$)				$(<0.001)^{\#}$ ($<0.001)^{\#}$ ($<0.001)^{\#}$ ($<0.001)^{\#}$)			
Striatum	1.67 (6.3)	1.67 (6.6)	1.67 (6.6)	1.67 (6.5)	1.66 (10.6)	1.66 (10.9)	1.66 (10.9)	1.66 (10.7)	-0.4	-0.4	-0.3	-0.25
ρ to OPIF (p-value)	$(<0.001)^{\#}$ ($<0.001)^{\#}$ ($<0.001)^{\#}$ ($<0.001)^{\#}$)				$(<0.001)^{\#}$ ($<0.001)^{\#}$ ($<0.001)^{\#}$ ($<0.001)^{\#}$)				$(<0.001)^{\#}$ ($<0.001)^{\#}$ ($<0.001)^{\#}$ ($<0.001)^{\#}$)			
Thalamus	1.2 (5.0)	1.2 (5.0)	1.19 (5.0)	1.19 (4.7)	1.33 (3.7)	1.33 (4.0)	1.33 (3.9)	1.33 (3.9)	11.1**	11.1**	11.1**	11.2**
ρ to OPIF (p-value)	$(<0.001)^{\#}$ ($<0.001)^{\#}$ ($<0.001)^{\#}$ ($<0.001)^{\#}$)				$(<0.001)^{\#}$ ($<0.001)^{\#}$ ($<0.001)^{\#}$ ($<0.001)^{\#}$)				$(<0.001)^{\#}$ ($<0.001)^{\#}$ ($<0.001)^{\#}$ ($<0.001)^{\#}$)			
NAWM	0.65 (10.2)	0.68 (8.5)	0.68 (8.5)	0.66 (9.8)	0.75 (12.4)	0.76 (10.4)	0.76 (10.4)	0.77 (8.7)	15.7**	12.4**	12.4**	15.7**
ρ to OPIF (p-value)	$(0.003)^{\#}$ ($0.003)^{\#}$ ($0.003)^{\#}$ ($0.003)^{\#}$)				$(0.007)^{\#}$ ($0.007)^{\#}$ ($0.007)^{\#}$ ($0.002)^{\#}$)				$(0.002)^{\#}$ ($0.002)^{\#}$ ($0.002)^{\#}$ ($0.002)^{\#}$)			

V_T = total distribution volume; CV% = coefficient of variation in percentages (IQR/median*100); ROI = region of interest; OPIF = original plasma input function; PBIFnis = population based input function, noninvasive, individually scaled; PBIFis = population based input function, invasive, individually scaled; RefLog = reference Logan; SPMS = secondary progressive multiple sclerosis; NAWM = normal appearing white matter

Spearman correlation statistically significant at the level of $p < 0.05$ * Mann-Whitney U-test, $p < 0.05$ ** Mann-Whitney U-test, $p < 0.001$

The correlations of the DVR estimates yielded with PBIFnis, PBIFis and the reference Logan (RefLog) to the DVR values provided with OPIF were highly significant for both the control and SPMS groups and with both cerebellum and SCgm reference regions in neocortex, striatum and thalamus ROIs (Table 10). In NAWM ROI, all correlations to OPIF in the SPMS group were statistically significant, whereas in the control group, the correlations were significant in all other comparisons, except for a borderline finding for RefLog with the cerebellum reference (Table 10).

5.4 *In vivo* imaging of activated microglia with [¹¹C](R)-PK11195

5.4.1 Increased [¹¹C](R)-PK11195 binding in NAWM and thalami of SPMS patients in comparison to healthy controls

In study III, the mean (SD) injected radioactivity of [¹¹C](R)-PK11195 was 480.3 (17.8) MBq. There were no significant group differences in the injected doses between healthy controls and SPMS patients [mean (SD) of 481.7 (18.8) in SPMS vs. 478.6 (17.7) in control group, $p=ns$].

The results of the ROI specific [¹¹C](R)-PK11195 DVR values in 10 SPMS patients and 8 healthy controls by group are summarised in Table 11. As a marker of microglial activation, [¹¹C](R)-PK11195 DVR was significantly higher in the manually derived NAWM ROI of SPMS patients when compared to healthy controls ($p=0.016$). In addition, in the thalamus ROI, the SPMS patients had higher [¹¹C](R)-PK11195 binding than the controls, $p=0.027$. No significant group differences were observed in other manual ROIs.

With the segmentational ROI approach, similar results were obtained when compared to the manual ROIs: [¹¹C](R)-PK11195 binding within the segmented global NAWM ROI was significantly higher in SPMS patients than in the healthy controls $p<0.001$. Binding in the pathological WM (T2 lesional area derived from LST) of SPMS patients was significantly lower than in the segmented global NAWM (related samples Wilcoxon's signed rank test, $p=0.008$). No statistically significant differences were found between the groups in radioligand binding within the segmented cortical NAGM ROI. The ROI based results are also illustrated as boxplots in the publication of study III.

Corroborating the results from the ROI based approach, the voxel-wise analyses of parametric [¹¹C](R)-PK11195 DVR images showed significantly increased [¹¹C](R)-PK11195 binding in widespread locations in periventricular and subcortical WM in SPMS patients when compared to healthy controls (Figure 12).

Table 11. [^{14}C](R)-PK11195 binding in healthy controls and SPMS patients shown as median DVR (CV) values, and group differences reported as difference of medians in percentages between the groups. ROIs acquired with manual delineation and segmentation marked with (m) and (s), correspondingly.

ROI	CTRL (n=8)	SPMS (n=10)	SPMS vs. CTRL
NAWM (m)	0.86 (6.4)	0.96 (11.5)	+11.6%*
NAWM (s)	0.92 (1.4)	0.96 (3.9)	+3.9%**
T2lesion (s)	<i>na</i>	0.88 (7.6)	<i>na</i>
Neocortex (m)	0.98 (2.5)	0.99 (3.7)	+0.1%
Neocortex (s)	0.98 (1.6)	0.96 (3.4)	-2.1%
Thalamus (m)	1.10 (4.8)	1.19 (8.2)	+ 8.0%*
Striatum (m)	1.00 (4.6)	1.01 (5.1)	+0.5%
Cingulum ant (m)	0.98 (2.4)	0.97 (6.4)	-0.8%
Pons (m)	0.98 (6.1)	0.92 (17.0)	-5.6%
Cerebellum (m)	0.84 (7.1)	0.86 (4.9)	+1.8%
Venous sinus (m)	0.90 (15.8)	0.94 (27.1)	+4.0%

ROI = region of interest; CTRL = healthy control; SPMS = secondary progressive multiple sclerosis; NAWM = normal appearing white matter; m = manually delineated ROI; s = segmented ROI; ant = anterior; na = not applicable

* Mann-Whitney U-test, $p < 0.05$

** Mann-Whitney U-test, $p < 0.001$

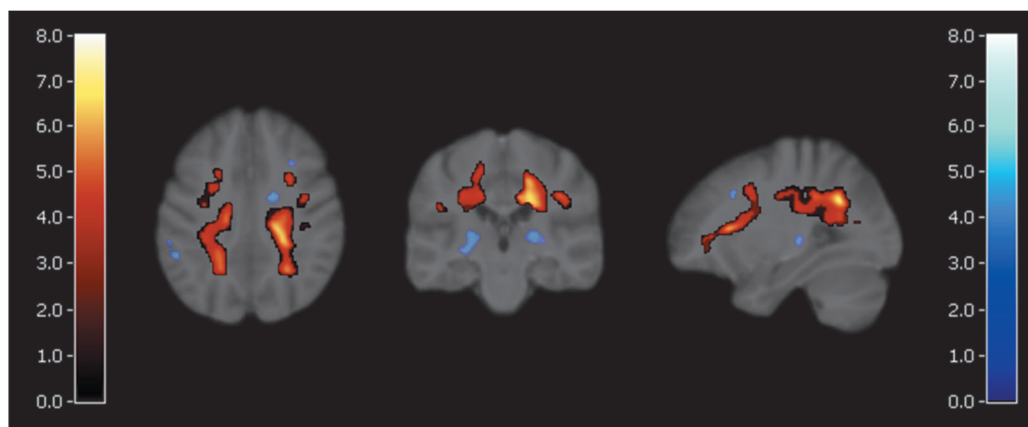


Figure 12. Results from SPM analysis of the parametric [^{14}C](R)-PK11195 DVR images in healthy controls (n=8) and SPMS patients (n=10). Voxel clusters of significantly increased DVR in SPMS compared to control group, rendered on study subjects' average 3D T1 MRI template, with levels of significance indicated according to coloured bar scales (T-score > 3.8 corresponding to $p < 0.001$; independent samples T-test with FWE-correction for multiple comparisons). In addition, areas statistically significant in voxel peak level but not significant after multiple comparisons are shown in blue (T-score > 3.7 corresponding to $p < 0.001$; uncorrected). Reprinted with permission from study III.

In the visual analyses of the parametric [^{11}C](R)-PK11195 images fused with 3DT1 and FLAIR images, a pattern of increased TSPO binding was observed in the perilesional area of T1 hypointense WM lesions (illustrated in Figure 3 in the publication of study III), and upon quantification, increased periplaque binding was observed in an average of 57% of the chronic T1 lesions (Table 12). All but one patient (Case 5 in Table 12) had chronic lesions both with and without increased periplaque binding. In active plaques with Gd-enhancement, increased binding was observed in the core of the lesions but not in the area surrounding them. Additionally, focal areas with increased PK-binding were found in the NAWM (Figure 13).

Table 12. Patient specific clinical, MRI volumetric and lesion characterisation of the SPMS patients (n=10). Modified from study III

Case	Age (y), gender	Disease duration (y)	EDSS	GM vol (cm ³)	WM vol (cm ³)	T2 lesion load (cm ³)	T1 lesions (n)	PK11195+ T1 lesions * (n (%))
1	51, f	9	6,0	742	721	22	3	3 (100)
2	39, f	15	8,0	782	697	102	19	11 (58)
3	61, m	16	6,5	775	757	50	19	13 (68)
4	51, m	21	3,5	714	721	41	22	11 (50)
5	48, f	23	7,5	711	759	22	1	0 (0)
6	33, f	9	6,5	783	731	20	11	6 (55)
7	60, f	15	7,5	770	716	33	8	5 (63)
8	48, f	6	7,5	794	655	132	33	20 (61)
9	66, f	12	6,0	609	694	58	17	9 (53)
10	40, m	7	4,0	623	673	128	31	22 (71)

y = years; EDSS = expanded disability status scale; GM = gray matter; WM = white matter; vol = volume

* Number of chronic T1-lesions with increased perilesional [^{11}C]PK11195 uptake, and the percentage of [^{11}C]PK11195 positive lesions of all T1-hypointense lesions.

5.4.2 [^{11}C](R)-PK11195 PET in determining clinical severity and disease type in RRMS and SPMS

In study IV, updated methodology of the reference region extraction from [^{11}C](R)-PK11195 PET images using SVCA (SuperPK) was applied, and the semiautomated method for the intra- and perilesional segmentation of T1 hypointense lesion was introduced and utilised in the imaging data of the same 10 SPMS patients and 8 healthy controls than in study III in addition to the 10 RRMS patients.

5.4.2.1 ROI specific [^{11}C](R)-PK11195 binding

The detailed ROI specific [^{11}C](R)-PK11195 DVR estimates subdivided by group and comparisons between groups with the corresponding statistical significances are presented in Table 13. The DVR was significantly increased in the NAWM of SPMS patients when compared to RRMS patients and healthy controls. In the perilesional

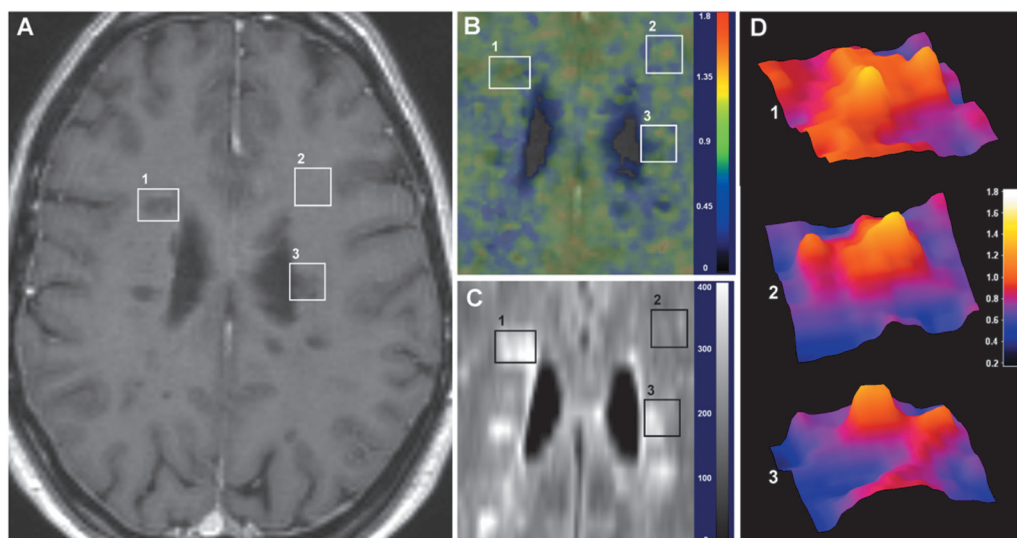


Figure 13. Example of $[^{11}\text{C}](\text{R})\text{-PK11195}$ binding patterns in respect to MRI pathology in a 39 year old female with SPMS (EDSS 8.0, disease duration 15 years) Axial views of **A)** Gadolinium-enhanced 3DT1, **B)** parametric $[^{11}\text{C}](\text{R})\text{-PK11195}$ DVR and **C)** FLAIR images, and **D)** surface plots from the $[^{11}\text{C}](\text{R})\text{-PK11195}$ DVR image in areas of 1) a slightly Gd-enhancing active plaque with increased DVR inside the plaque 2) NAWM with increased DVR 3) a chronic T1 hypointense lesion with increased DVR in the perilesional area, but not inside the lesion, illustrated in panels D1–D3. The scales in panels B) and D) represent DVR values, and in C) the FLAIR signal intensity. Reprinted with permission from study III.

ROI of Gd-negative T1 hypointense lesions, the $[^{11}\text{C}](\text{R})\text{-PK11195}$ binding was also significantly higher in SPMS than in RRMS patients, whereas no significant group differences were observed within the Gd-negative T1 hypointense lesions. Moreover, the radioligand binding was generally low within the T1 lesions, and the perilesional binding was significantly higher than within the T1 hypointense lesions in SPMS patients ($p=0.005$), but not among the RRMS patients ($p=0.878$). Gadolinium enhancing lesions were found in 4 SPMS and 4 RRMS patients. Within the Gd-positive T1-hypointense lesions, and in their perilesional area, $[^{11}\text{C}](\text{R})\text{-PK11195}$ binding was generally high with no significant differences between the intralesional and perilesional ROIs in either MS group. The binding in thalamus of SPMS patients was slightly higher when compared to the RRMS and control groups, but these differences were not statistically significant. In other gray matter ROIs, no group differences were observed.

5.4.2.2 Correlations of $[^{11}\text{C}](\text{R})\text{-PK11195}$ binding to clinical and MRI parameters in all MS patients

Several correlations between $[^{11}\text{C}](\text{R})\text{-PK11195}$ binding and the clinical characteristics of the patients were found. The increased $[^{11}\text{C}](\text{R})\text{-PK11195}$ DVR in NAWM correlated positively with the higher EDSS, and a similar

Table 13. ROI specific [¹¹C](R)-PK11195 binding expressed as median (CV%) DVR values in healthy controls, SPMS patients and RRMS patients. The group differences are shown in differences of medians and corresponding p-values with Mann-Whitney U-test.

ROI	Median (CV%) DVR within groups		Group differences, % (p-value)			
	CTRL (n=8)	SPMS (n=10)	RRMS (n=10)	SPMS vs. CTRL	RRMS vs. CTRL	SPMS vs. RRMS
Neocortex	1.05 (3.3)	1.04 (4.6)	1.06 (1.8)	-0.7 (0.897)	+0.4 (0.696)	+1.1 (0.315)
Thalamus	1.09 (6.1)	1.12 (10.0)	1.07 (3.6)	+3.3 (0.237)	-1.1 (0.829)	+4.4 (0.165)
Striatum	0.95 (3.3)	0.96 (4.8)	0.95 (3.9)	+0.7 (0.315)	-0.1 (0.897)	+0.8 (0.353)
Cerebellum	0.94 (3.5)	0.91 (5.3)	0.94 (2.2)	-2.4 (0.573)	-0.2 (0.897)	+2.2 (0.315)
NAWM	0.98 (2.1)	1.05 (2.2)	1.00 (3.0)	+6.8 (<0.001*)	+1.5 (0.315)	+5.2 (<0.001*)
T2lesion	<i>na</i>	0.95 (4.0)	0.93 (11.2)	<i>na</i>	<i>na</i>	+2.2 (0.796)
Gd- T1 lesion	<i>na</i>	0.93 (4.3)	0.91 (14.6)	<i>na</i>	<i>na</i>	+2.2 (1.000)
Gd- T1 perilesion	<i>na</i>	1.00 (4.6)	0.93 (11.9)	<i>na</i>	<i>na</i>	+7.0 (0.011*)
Gd+ T1 lesion [§]	<i>na</i>	1.17 (3.9)	0.99 (30.7)	<i>na</i>	<i>na</i>	+19.0 (0.343)
Gd+ T1 perilesion [§]	<i>na</i>	1.11 (2.2)	1.08 (9.8)	<i>na</i>	<i>na</i>	+2.7 (0.486)

ROI = region of interest; CV% = coefficient of variation in percentages (IQR/median*100); CTRL = healthy controls; SPMS = secondary progressive multiple sclerosis; RRMS = relapsing remitting multiple sclerosis; Gd- = gadolinium-negative; Gd+ = gadolinium-positive

* Statistically significant at the level of p<0.05

§ Gadolinium enhancing lesions in 4 SPMS and 4 RRMS patients

but a weaker association was noted in the perilesional ROI of Gd-negative T1 hypointense lesions (Table 14). When using a cut-off value of DVR=1.02 in [¹¹C](R)-PK11195 DVR in NAWM, the MS patients could be divided into two separate groups corresponding to the original RRMS vs. SPMS classification of the patients except for one RRMS patient with a borderline DVR of 1.023 (Figure 14). Significant correlations of higher age, longer disease duration and higher MSSS to increased [¹¹C](R)-PK11195 DVR in NAWM were also found (Table 14). In control subjects, a trend for higher [¹¹C](R)-PK11195 binding with increasing age was also observed, although no statistically significant correlation was detected (Spearman's rho 0.297, p=0.474). By assuming a linear correlation between NAWM DVR and EDSS in the MS patients, the cut-off value of DVR 1.02 corresponded to EDSS 4.2 and the age of 40 years in this data (95% confidence interval 1.01–1.03). The correlations are further visualized as scatterplots in Figure 13.

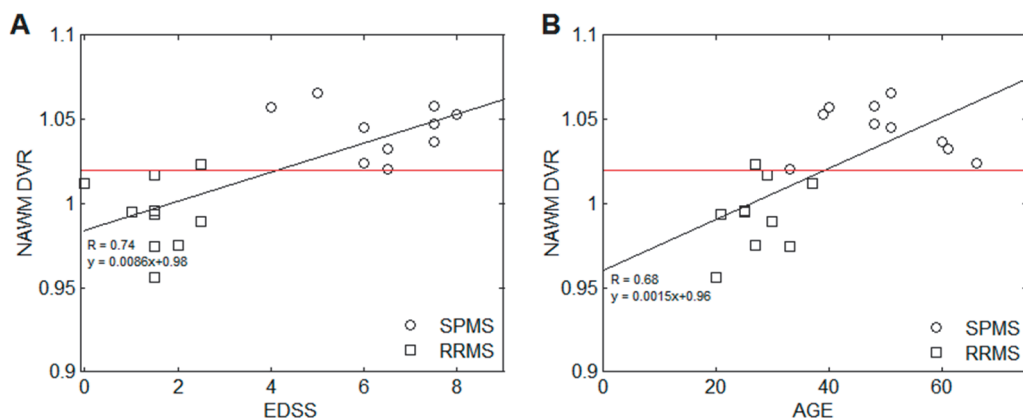


Figure 14. Scatter plot of [¹¹C](R)-PK11195 DVR in NAWM in respect to A) EDSS and B) age in SPMS (n=10) and RRMS (n=10) patients. Red line signifies DVR cut-off value of 1.02.

Several statistically significant correlations were observed also between the ROI specific [¹¹C](R)-PK11195 DVR values and the MRI parameters (Table 15). The increased radioligand binding in both NAWM and in the perilesional ROI of Gd-negative black holes correlated with the reduced global FA in NAWM, whereas the global MD in NAWM correlated only with higher [¹¹C](R)-PK11195 binding in the perilesional ROI. Higher [¹¹C](R)-PK11195 uptake in NAWM was also associated to increased atrophy in both gray and white matter. There was also a significant correlation of the increased radioligand binding in NAWM and perilesional ROIs to higher total T1 and T2 lesion volumes as opposed to the negative correlation between the lower [¹¹C](R)-PK11195 uptake in cortical GM to the higher T1 and T2 lesion loads.

Table 14. Correlations of ROI-specific [¹¹C](R)-PK11195 DVR to the clinical patient characteristics in all MS patients (n=20; SPMS n=10, RRMS n=10) expressed as Spearman's rho and the corresponding p-values. Modified from study IV

[¹¹ C](R)-PK11195 DVR in ROI	Age		Disease Duration		EDSS		MSSS	
	Spearman	p-value	Spearman	p-value	Spearman	p-value	Spearman	p-value
NAWM	0.734	<0.001*	0.663	0.001*	0.733	<0.001*	0.524	0.018**
T1 perilesional#	0.331	0.153	0.328	0.158	0.426 [‡]	0.061 [‡]	0.383	0.096
T1 black hole#	-0.126	0.597	-0.044	0.853	-0.040	0.866	-0.003	0.990
T2 lesion	-0.021	0.930	0.005	0.985	0.076	0.750	0.120	0.613
Thalamus	0.242	0.304	0.224	0.342	0.324	0.163	0.303	0.195
Striatum	0.053	0.823	0.188	0.427	0.055	0.816	0.000	1.000
Cortical GM	-0.106	0.656	-0.139	0.558	-0.043	0.859	-0.001	0.997

DVR = distribution volume ratio; ROI = region of interest; EDSS = expanded disability status scale; MSSS = multiple sclerosis severity scale; NAWM = normal appearing white matter

Gadolinium negative T1 perilesional and black hole ROIs

* Spearman correlation statistically significant at the level of p<0.01

** Spearman correlation statistically significant at the level of p<0.05

‡ Corresponding Pearson correlation 0.479, p=0.033, significant at the level of p<0.05

Table 15. Correlations of ROI specific [¹¹C](R)-PK11195 DVR to MRI and DTI findings in all MS patients (n=20; SPMS n=10, RRMS n=10) expressed as Spearman's rho and the corresponding p-values. Modified from study IV.

[¹¹ C]PK11195 DVR (ROI)	T1 lesion load [#]		T2 lesion load [§]		Mean FA [§]		Mean MD [§]		GM volume		WM volume	
	Spearman	p-value	Spearman	p-value	Spearman	p-value	Spearman	p-value	Spearman	p-value	Spearman	p-value
NAWM	0.573	0.008*	0.761	<0.001*	-0.766	<0.001*	0.398	0.092	-0.701	0.001*	-0.523	0.018**
T1 perilesional [#]	0.782	<0.001*	0.795	<0.001	-0.661	0.002*	0.510	0.026**	-0.258	0.272	-0.296	0.206
T1 black hole [#]	0.377	0.101	0.259	0.285	-0.103	0.676	0.289	0.230	0.152	0.523	0.096	0.689
T2 lesion [§]	0.457	0.043**	0.341	0.154	-0.200	0.339	0.339	0.156	0.226	0.337	-0.053	0.825
Thalamus	0.248	0.292	0.278	0.249	-0.429	0.067	0.109	0.657	0.197	0.405	-0.141	0.554
Striatum	0.215	0.363	0.048	0.844	-0.216	0.374	0.121	0.621	0.185	0.435	0.296	0.205
Cortical GM	-0.721	<0.001*	-0.473	0.041**	0.457	0.049**	-0.513	0.025**	0.188	0.427	0.174	0.462

DVR = distribution volume ratio; ROI = region of interest; FA = fractional anisotropy; MD = mean diffusivity; GM = gray matter; WM white matter; NAWM = normal appearing white matter

[#] Gadolinium negative T1 perilesional and black hole ROIs

* Spearman correlation statistically significant at the level of p<0.01

** Spearman correlation statistically significant at the level of p<0.05

[§] DTI and lesion load data available from 9/10 SPMS and 10/10 RRMS patients

5.5 Post-mortem [¹¹C](R)-PK11195 autoradiography and immunohistochemistry of progressive MS brain samples

According to the clinical characteristics provided by the UK Multiple Sclerosis Tissue Bank, of the 15 samples all but two included white matter lesions. Altogether 5 WM lesions from 5 different MS patients (4 SPMS, 1 PPMS) were identifiable from both the [¹¹C](R)-PK11195 autoradiography images and photomicroscopy of the immunohistochemical stainings. The clinical characteristics and the results of lesion analyses are shown in Table 16.

Table 16. Results of post-mortem [¹¹C](R)-PK11195 autoradiography and immunohistochemistry analyses of WM lesions in patients with progressive MS. Lesion evaluations of autoradiography and immunohistochemistry performed qualitatively (+/-) in the core and rim of the lesions. Additionally, the ratio of the number of positively staining cells compared to WM are shown in parentheses. Modified from study IV.

Case	Sex/Age	Disease type	Disease duration	[¹¹ C](R)-PK11195		CD68		GFAP	
				Core	Rim	Core	Rim	Core	Rim
1	46/m	SPMS	8	-	+	-(1.0)	+(8.3)	-(1.8)	+(3.0)
2	49/f	SPMS	21	+	+	+(2.0)	+(3.0)	+(2.9)	+(2.9)
3	51/m	SPMS	10	-	+	-(0.9)	+(2.4)	-(0.7)	-(0.9)
4	73/m	PPMS	52	-	+*	-(1.1)	+(4.3)	-(0.8)	-(1.0)
5	53/m	SPMS	11	-	-	-(0.7)	-(1.8)	-(0.5)	-(0.5)

CD68 = cluster of differentiation 68, GFAP = glial fibrillary acidic protein; m = male; f = female; SPMS = secondary progressive multiple sclerosis; RRMS = relapsing remitting multiple sclerosis; + = increased binding / staining compared to adjacent white matter; - = binding / staining not increased or decreased in the area of interest compared to white matter

In addition, representative cases are illustrated in Figure 14. In a sample with a chronic active white matter lesion (Figure 15A), a notable loss of myelin and increased gliosis with astrocytosis was detected within the lesion with both the LFB and GFAP stainings. However, astrocytosis was more notable in the perilesional than in the intralesional area according to the results of the GFAP staining. In the perilesional area of the lesion, a dense rim of activated microglia/macrophages was detected in the CD68 staining, whereas within the lesion, CD68 expression was clearly lower. Accordingly, the [¹¹C](R)-PK11195 signal in the autoradiography image was higher around the lesion when compared to the intralesional or more distant adjacent WM. In contrast, Figure 15B demonstrates a late active lesion characterised with increased microglial/macrophage activity and astrocytosis within and around the lesion in the CD68 and GFAP stainings. Correspondingly, an increased [¹¹C](R)-PK11195

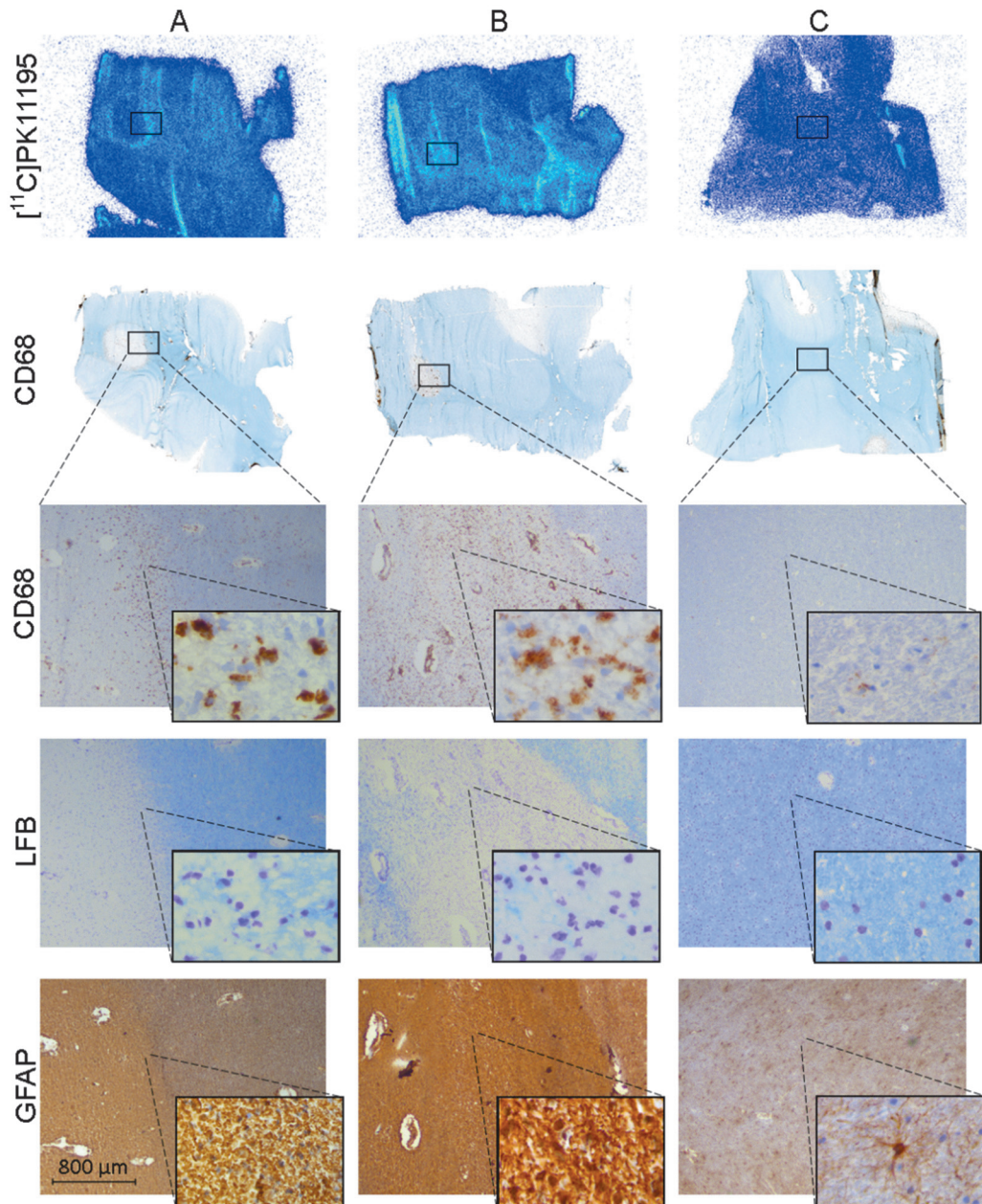


Figure 15. [^{11}C](R)-PK1195 autoradiography and respective CD68, LFB and GFAP immunohistochemistry (IHC) images of serial autopsy sample cryosections from SPMS-patients. A) 46-year-old male, disease duration 8 years (case 1 in Table 16) B) 49-year-old female, disease duration 21 years (case 2 in Table 16) C) 51-year-old male, disease duration 10 years. The enlarged (x25 and x630) IHC images demonstrate the border of a chronic active (A) and the core of late active (B) plaques and normal WM (C).

signal was seen within, but not around, the lesion. In addition, notable astrocytosis and gliosis was present within the lesion. In normal WM (Figure 15C) with a typical myelin density, there was normal amount of astrocytes and a low count of activated microglia/macrophages in the immunohistochemistry and the [¹¹C](R)-PK11195 signal in the corresponding autoradiography image was weak.

6. DISCUSSION

6.1 Summary of the main findings

In study I, [^{11}C]TMSX PET imaging was used for the first time to evaluate adenosine A_{2A} receptor binding in MS patients. A total of 7 healthy controls and 8 SPMS patients were examined in the study. A_{2A} receptor binding was increased in the NAWM of SPMS patients in comparison to healthy controls. There was also a trend without statistical significance for higher [^{11}C]TMSX uptake in the thalami of SPMS patients than in healthy controls. The increased [^{11}C]TMSX binding in NAWM was associated with increased WM atrophy and reduced FA in NAWM as a sign of structural damage in the SPMS patients.

In study II, non-invasive input function methods were developed and validated for the evaluation of brain [^{11}C]TMSX binding by using arterial blood sampling and [^{11}C]TMSX image data from 7 healthy controls, 8 SPMS patients, 4 RRMS patients and 9 PD patients. Supervised clustering for the extraction of the GM reference region performed reliably in healthy controls and MS patients, and the V_T -values in the SCgm reference were generally lower than the corresponding values in the cerebellum reference. In the evaluation of DVR in SPMS patients and healthy controls, the reference Logan with the SCgm reference yielded reproducible results when they were compared with the original arterial input function, thus providing a non-invasive alternative for the evaluation of specific binding. However, in PD patients, the V_T s in both SCgm and cerebellum references were significantly lower than in healthy controls. V_T estimates with both population-based input functions (PBIFis with invasive and PBIFnis with non-invasive scaling) correlated well with the results yielded with the original arterial input function. Although the variance in the results was lower with PBIFis than PBIFnis, in the DVR estimation, both methods performed robustly when compared to OPIF.

Study III evaluated microglial activation in 10 SPMS patients and 10 healthy controls using TSPO binding radioligand [^{11}C](R)-PK11195. TSPO binding was significantly higher in the NAWM of SPMS patients than in the healthy controls. In addition, SPMS patients had higher [^{11}C](R)-PK11195 binding in the thalami when compared to the control group. The total TSPO binding within T2 hyperintense lesions was generally low. In the perilesional area of T1 black holes, TSPO binding pattern appeared to be heterogeneous with increased perilesional [^{11}C](R)-PK11195 uptake observed in 57% of the lesions in the visual qualitative assessment.

In study IV, the patterns of [^{11}C](R)-PK11195 binding were further evaluated in NAWM and T1 perilesional area of the same 10 SPMS patients and 10 healthy controls as examined in study III in addition to 10 RRMS patients receiving no immunomodulatory medication. Additionally, autoradiography with [^{11}C](R)-PK11195 and immunohistochemistry to study activated microglia, astrocytes and

myelin density in 8 post-mortem brain samples of progressive MS patients were performed. TSPO binding was significantly higher in NAWM and the total perilesional area of T1 hypointense lesions of SPMS patients when compared to RRMS patients. When all the MS patients were pooled together, the higher TSPO binding in NAWM correlated with longer disease duration and considerably more clinical disability measured with EDSS and MSSS. Furthermore, increased T1 perilesional binding had a borderline significant association to higher EDSS. By using a cut-off value of 1.02 for [^{11}C](R)-PK11195 DVR in NAWM, SPMS patients could be segregated from RRMS patients. Additionally, increased (R)-[^{11}C]PK11195 binding in NAWM and the T1 perilesional area correlated with more severe brain atrophy, reduced FA in NAWM and increased T1 and T2 lesion loads. In [^{11}C](R)-PK11195 autoradiography, the increased perilesional TSPO binding in chronic lesions was associated with a dense rim of amount of activated microglia around the lesions.

6.2 Methodological considerations

In order to overcome the challenges in defining a reference region for radioligands with widespread specific binding when conducting an evaluation of diseases with diffuse brain pathology, the application of a supervised cluster algorithm has been proven feasible not only with [^{11}C](R)-PK11195 (Turkheimer et al. 2007, Yaqub et al. 2012), but also with [^{11}C]PIB (Ikoma et al. 2013) and [^{18}F]FDG (Dukart et al. 2013). In addition, in the present studies (III and IV), supervised clustering for [^{11}C](R)-PK11195 was applied and it was found to provide robust DVR estimates. Importantly, when one has a reliable reference region (i.e. low specific and non-specific binding) available, it is possible to acquire DVR or BP_{ND} estimates, which are the measures of specific radioligand binding unlike V_{T} estimates, which can include both specific and unspecific binding components of the target region. Moreover, when using the reference Logan for the DVR estimation, there is no need for arterial sampling, thus making the imaging studies more comfortable for the study subjects. Additionally, the methodology for supervised clustering of the reference regions is independent of the time consuming drawing of ROIs, which in turn is also prone to operator bias.

In this study (II), it was also possible to implement successfully the gray matter reference region clustering for the first time for [^{11}C]TMSX. In healthy controls and MS patients, the performance of the SCgm reference region appeared robust with low and similar V_{T} -values across the groups. However, in PD patients, the V_{T} s were lower in both SCgm and cerebellum reference regions when compared to other groups. Even though [^{11}C]TMSX binding in the striatum does not change with age, the striatal binding of [^{11}C]MPDX to A_1 receptors has been reported to decline with age (Mishina et al. 2012). Moreover, no data exist on the effect of healthy aging in the A_{2A} receptor expression, or on the effect of dopaminergic medication in PD patients in distinct brain regions other than striatum. Thus, either of these factors could contribute to the low [^{11}C]TMSX binding in cerebellum and cortical gray matter detected in the PD patients. Consequently, the

supervised clustering of brain [^{11}C]TMSX PET images will need to be applied for aged healthy controls or for patients with other neurological diseases with caution until further studies have been conducted, even though in younger controls and MS patients the results were encouraging.

According to the results in study II, PBIFs provides a robust alternative to OPIF with fewer blood samples needed. In the V_T estimates, PBIFs appeared preferable to PBIFnis due to its better concordance with OPIF. On the other hand, in the DVR estimates, both PBIFnis and PBIFs compared excellently to OPIF. Thus, it is recommended that PBIFnis should be adopted in future studies because of its non-invasiveness. Population based input function as an alternative for arterial input function derived with blood sampling has also been utilised in brain PET studies with other radioligands, i.e. with [^{11}C]rolipram (Zanotti-Fregonara et al. 2012) and [^{18}F]FMPEP- d_2 (Zanotti-Fregonara et al. 2013). However, when compared to OPIF, PBIF may be less sensitive at the individual level, and consequently, might not detect subtle differences between groups as efficiently as OPIF. On the other hand, PBIF is not vulnerable to possible inaccuracies associated with manual sampling and analysis methods of the blood samples. In addition, a shared average PBIF for all study subjects regardless of possible disease statuses would likely contribute a bias in V_T estimates (Zanotti-Fregonara et al. 2013), and thus it is recommended that PBIFs should be acquired separately for healthy controls and different patient populations.

In study III, the perilesional [^{11}C](R)-PK11195 binding in the black holes was evaluated using a visual, qualitative assessment. These kinds of methods are very user dependent and prone to errors. Moreover, in patients with a progressive disease, the enlarging white matter lesions can become confluent with adjacent lesions, and in that situation, the assessment of individual lesions becomes challenging. Consequently, a semiautomated method was developed for the identification of the perilesional zone of the T1 hypointense lesions for the quantification of radioligand binding in study IV.

Until today, the methods for the modelling of dynamic brain [^{11}C](R)-PK11195 and [^{11}C]TMSX image data have been very variable in different studies due to the lack of harmonisation of protocols. For instance, reference regions used in [^{11}C](R)-PK11195 imaging have included cortical gray matter (Debruyne et al. 2003, Versijpt et al. 2005), whereas for [^{11}C]TMSX, centrum semiovale (Mishina et al. 2007, Naganawa et al. 2007), has been used in addition to cerebral cortex (Mishina et al. 2011, Mishina et al. 2012). However, it is not feasible to use either centrum semiovale or cerebral cortex as a reference region in MS, since this is a disease with widespread pathology and also increased ligand binding as reviewed here. Nevertheless, according to recent studies with [^{11}C](R)-PK11195 studies, the use of a clustered reference region appears to have established its position in the estimation of specific ligand binding (Giannetti et al. 2014a, Giannetti et al. 2014b, Politis et al. 2012). In addition, it appears likely that reference region clustering could be developed also for 2nd generation TSPO ligands in future studies investigating neuroinflammatory and neurodegenerative brain diseases.

Nonetheless, subtle differences in the results between study groups may arise from differences in image reconstruction protocols and PET scanner features, as well as due to the different methods used for kinetic modelling and ROI acquisition and also for calculating the parametric images as reviewed in the publications of substudies II and III. Thus, it would be a major advantage if the different study centres would agree to harmonise the protocols for image processing and specific binding estimation for future studies.

It is also necessary to acknowledge some limitations in the present study. The lack of age and sex matched controls for RRMS and PD groups hinders the comparison of the results in these groups to healthy controls. However, the main focus of this study was on the patients with a progressive disease, to which the control subjects group were matched. Naturally, the SPMS patients were older than RRMS patients due to the course of the disease, but in turn this made it possible to conduct an evaluation of MS patients as a continuum of the disease process. Finally, the low number of study subjects per group sets its limits on the interpretation and generalisation of these results. On the other hand, according to the general ethical principles of good clinical practice, the number of participants in PET imaging studies should be kept as low as possible in order to limit the radiation exposure to the study subjects.

6.3 Adenosine A_{2A} receptors in progressive MS

It does seem that the [¹¹C]TMSX PET imaging in studies I and II are the first ones to have been published in patients with MS. The results of the increased [¹¹C]TMSX binding in the NAWM of SPMS patients compared to controls suggest that A_{2A} receptors might be involved in modifying the widespread pathological processes in the brain of SPMS patients. As reviewed in study II, the striatal A_{2A} receptors which are linked to the modulation of dopaminergic transmission are regarded as the classical or typical A_{2A} receptors, whereas those in other locations (cerebral cortex, cerebellum and thalami) are called atypical A_{2A} receptors. Taking into account the role of A_{2A} receptors in modulating the function of astrocytes (Matos et al. 2013) and microglia (Orr et al. 2009), it can be hypothesised that the increased A_{2A} binding in normal appearing brain structures in SPMS might be linked to the activation of microglia and astrocytes representing the widespread neuroinflammation in the disease and possibly also contributing to neurodegeneration.

It is not possible to deduce from the present human *in vivo* study whether the increased A_{2A} receptor binding in SPMS patients represents a beneficial, endogenous attempt to limit neuroinflammation, or whether it is a neuroinflammation and neurodegeneration propelling phenomenon *per se*. However, the evidence from *in vivo* animal experiments and *in vitro* studies on the neuroinflammatory capacity of A_{2A} antagonism in neuroinflammatory conditions, and upregulation of A_{2A} receptors in microglia (reviewed in chapter 2.2.2 and in (Santiago et al. 2014)) indicates that A_{2A} overexpression might be harmful in

neuroinflammatory diseases causing neurodegeneration, including MS. More support for this theory is provided by the findings from animal models of PD, where A_{2A} receptor antagonism reduced the activation of microglia in striatum and substantia nigra in addition to the effect on striatal functions mediated by dopamine D_2 receptors (Pierri et al. 2005). Thus compounds targeting these modifying adenosine A_{2A} receptors might represent an alternative pathway for drug development aiming at reducing neuroinflammation and disease progression also in MS.

The challenge in understanding the mechanisms of adenosine and A_{2A} receptors in MS is in its complexity since it involves immune cells in both the periphery and CNS. Additionally, little is known of these phenomena in living humans, since the hypotheses have been mainly derived from evidence emerging from *in vitro* experiments and *in vivo* animal studies. Based on the results from animal studies mimicking MS disease, it appears that treatment with an A_{2A} antagonist may be able to protect the animals against EAE development even though genetically A_{2A} deficient animals are prone to develop more severe EAE (Mills et al. 2008, Mills et al. 2012, Yao et al. 2012). Accordingly, it has been proposed that adenosine receptors on other cell types may also be involved in attenuating or boosting the pro-inflammatory capacity of lymphocytes and in susceptibility of CNS to disease progression and lymphocyte infiltration in MS (Volonte 2013).

More studies will be needed to clarify the role of adenosine A_{2A} receptors in progressive MS. Comparison of A_{2A} binding characteristics between relapsing and progressive subtypes of MS with *in vivo* PET imaging would be informative with respect to disease progression. If one conducted post-mortem A_{2A} receptor autoradiography in conjunction with immunohistochemistry then it might be possible to identify the cell types expressing A_{2A} receptors in MS lesions and normal appearing brain structures. Furthermore, with regard to the reported regulatory function of A_{2A} receptors in microglia, PET studies evaluating the possible co-localisation of increased A_{2A} receptor and TSPO binding in MS patients could provide more evidence on this connection *in vivo*. Finally, studies with A_{2A} antagonists in EAE models mimicking chronic lesions could help clarify the putative effect of A_{2A} antagonism in neuroinflammation in progressive MS.

6.4 TSPO and activated microglia in progressive MS

The present results of the increased *in vivo* [^{11}C](R)-PK11195 binding in the NAWM of MS patients, and increasingly so in SPMS when compared to RRMS patients, are in line with previous studies (Banati et al. 2000, Debruyne et al. 2003, Politis et al. 2012). Furthermore, the borderline finding of the increased TSPO binding in the thalami of SPMS patients in respect to healthy controls is corroborated by the comparable observation in the report of Banati et al. (Banati et al. 2000). In the study by Politis and colleagues (Politis et al. 2012a), increased cortical [^{11}C](R)-PK11195 binding was also reported for SPMS and RRMS patients, a finding which was not confirmed in the present work.

In the recent *in vivo* PET studies, cumulative evidence has emerged that TSPO binding can serve as a potential marker of disease progression. Politis and colleagues (Politis et al. 2012) have shown that increased cortical TSPO binding correlated with clinical disability, and that the correlation was more evident in patients with SPMS than with RRMS. However, no similar correlations were found for WM. Nevertheless, in another study, the total TSPO binding in NAWM predicted the conversion of CIS to RRMS (Giannetti et al. 2014b). This is also in concordance with the present results i.e. the correlation between more severe disability and the increased radioligand binding in NAWM when analysing the RRMS and SPMS patients together as a progressive continuum of the disease process. In addition, TSPO binding in T2 lesions of RRMS patients (Colasanti et al. 2014), and in T1 black holes of progressive patients (Giannetti et al. 2014a) has been shown to correlate with the clinical disability. The level of total TSPO binding in the black holes of the progressive patients was also shown to be predictive of disease progression (Giannetti et al. 2014a). However, black holes with smaller volumes were shown to have higher TSPO binding compared to larger lesions in RRMS patients, which could also be explained by partial volume effect, since it was demonstrated here that the radioligand binding was negligible within chronic lesions, but was higher in the perilesional area. Interestingly, the [¹¹C](R)-PK11195 DVR threshold of 1.02 in NAWM dividing the SPMS patients from RRMS patients corresponding to the disability level of EDSS 4.2, whereas EDSS >3 has been considered to be the turning point of irreversible accumulating disability (Andersen 2010, Leray et al. 2010). Clinically, it is challenging to identify patients on the verge of progressive disease, where EDSS measurements and conventional MRI are of limited value. It could be hypothesized that evaluating TSPO binding in NAWM with PET imaging might aid in predicting the development of progressive disease, as it can be regarded as an indicator of the increasing global inflammatory burden associated with irreversible tissue damage. Thus, TSPO PET imaging could possibly be adopted as an imaging biomarker for disease progression before clinically measurable signs of permanent disability have emerged.

Interestingly, the onset of progression in MS has been shown to be heavily dependent on age, on average corresponding to the age of 45 years irrespective of the disease subtype (Tutuncu et al. 2013). Based on animal studies, it has been postulated that the process of remyelination and the efficiency of macrophages/microglia changes with age: the increases in the numbers of macrophage/microglia associated with the early stages of remyelination becomes slower with ageing resulting in changes in the kinetics of the cytokine and chemokine profiles, whereas there is a concomitant delay in the clearing of myelin debris (Miron and Franklin 2014). In addition, in general the slowly expanding lesions in progressive multiple sclerosis show very little oligodendrocyte progenitor cell recruitment and remyelination (Kutzelnigg and Lassmann 2014). Thus, it appears that in aging brain, the pro-regenerative capacity of macrophages/microglia becomes reduced and more inefficient, leading to the need to recruit more macrophages/microglia, but even this might not be sufficient

to promote effective repair and remyelination. The demonstration of the clear correlations found here between higher age with increased TSPO binding and decreased mean FA in NAWM as markers of microglial/macrophage activation and disintegrity of the myelinated white matter tracts also fits well with this hypothesis.

Until today, only a few studies with 2nd generation TSPO ligands have been performed in MS patients *in vivo*. The inability of [¹¹C]PBR28 to reveal differences in the TSPO binding in WM or GM between healthy controls and MS patients in the study by Oh and colleagues (Oh et al. 2011) is most likely explained by the high variation in the specific binding caused by the TSPO gene polymorphism, since the role of this genetic variation in TSPO binding was not established until 2012 (Owen et al. 2012). However, that same study claimed that the ratio of WM to GM uptake of [¹¹C]PBR28 was increased in RRMS in comparison to healthy controls, which is in line with the findings of increased [¹¹C](R)-PK11195 binding in the WM in this present work as well as that reported by others as reviewed in chapter 2.2.1. Similarly to the situation with [¹¹C](R)-PK11195, the [¹¹C]PBR28 binding was also increased in gadolinium-enhancing active plaques. Interestingly, in some lesions, a focal increase in [¹¹C]PBR28 binding preceded the appearance of gadolinium enhancement, pointing to a role for early glial activation in MS lesion development (Oh et al. 2011). Another pilot study with 4 RRMS patients detected similar patterns of TSPO binding with the 2nd generation TSPO ligand [¹¹C]vinpocetine when compared to [¹¹C](R)-PK11195, but with higher binding potentials and a better signal-to-noise ratio (Vas et al. 2008). Now that the stratification of the study subjects according to the TSPO binding phenotype has become feasible with simple PCR testing (Owen et al. 2012), it is probable that the 2nd generation TSPO ligands will be utilised increasingly in human studies on neuroinflammation, such as MS studies.

In view of the number of neuroinflammation PET studies conducted with [¹¹C](R)-PK11195 over the years, it seems somewhat surprising, that only one treatment study has evaluated the effect of disease modifying therapies on microglial activation (Ratchford et al. 2011). As reviewed earlier, that study found a significant reduction of microglial activation in RRMS patients after one year of treatment with glatiramer acetate. Interestingly, glatiramer acetate has been proposed to exert also direct CNS effects by promoting the differentiation of monocytes and microglia into antigen-presenting cells (Kim et al. 2004, Ratchford et al. 2011). According to *in vitro* studies, another potent peripheral immunomodulator in MS, fingolimod, has been shown to exert direct effects in CNS by modulating microglial activation and promoting remyelination through interactions with microglia, oligodendrocytes, and astrocytes, which are all cells which can express the target receptors of fingolimod (sphingosine 1-phosphate receptors) (Groves et al. 2013, Jackson et al. 2011). When considering the proposed theory on compartmentalised inflammation and the putative role of microglia in neuronal damage in progressive MS (Lassmann et al. 2012), the above mentioned direct CNS effects of fingolimod appear especially intriguing. Moreover, a recent study conducted by Airas and colleagues (Airas et al. 2015) on

a rat EAE model with chronic focal MS-like lesions revealed that treatment with fingolimod achieved a significant reduction in the perilesional microglial activity as confirmed with *in vivo* [^{18}F]GE180 PET imaging and *ex vivo* autoradiography and immunohistochemistry.

According to the present [^{11}C](R)-PK11195 autoradiography and immunohistochemistry results, and the findings from previous *in vitro* and animal studies with TSPO radioligands (reviewed in chapter 2.3.2.3), it appears probable that the increased TSPO binding in MS tissues *in vivo* is also partly attributable to the activated astrocytes in addition to the activated microglia. However, considering the co-localisation of [^{11}C](R)-PK11195 uptake with both CD68 and GFAP positivity at the plaque edge of chronic active lesions but not in the centre of the plaque with low CD68 staining and notable GFAP staining, it is plausible that the perilesional binding of [^{11}C](R)-PK11195 *in vivo* represents mainly the microglial activation in chronic active, “smouldering”, plaques, which have also been proposed to be one of the contributors to the disease progression (Lassmann et al. 2012).

It is not entirely known whether the microglial activation in progressive MS represents the beneficial, debris cleaning and inflammatory damage limiting function as a reaction to the pathological disease process, or whether it is an uncontrolled, prolonged overactivation contributing to chronic inflammation and further tissue damage (Biber et al. 2014). Whichever is the case, microglial activation can be regarded as a sign of disease progression, probably associated with neuronal damage, and TSPO PET imaging could therefore be utilised as a surrogate marker of disease progression. This is especially important when striving to develop disease modifying therapies in progressive MS, where conventional imaging markers are known to correlate inadequately with the clinical phenotype and the prognosis of the disease (Bakshi et al. 2008, Miki et al. 1999, Nijeholt et al. 1998).

In summary, the present results corroborate the proposed correlation between neuroinflammation and neurodegeneration in progressive MS: increasing atrophy, higher age, higher lesion load and more severe structural disintegrity in NAWM were associated with increased microglial activity in the perilesional white matter and NAWM with increasing clinical disability. According to these findings and the results from earlier TSPO PET and neuropathology studies, it is probable that increased TSPO binding in MS reflects microglial activation related to myelin degradation, gliosis and inflammation in the perilesional area, and to diffuse inflammation in NAWM. Accordingly, it appears reasonable to propose that TSPO PET imaging could be used to assess the inflammatory burden in MS, and that it may help in identifying of – or even in predicting the conversion to – progressive disease. Moreover, TSPO PET imaging could possibly be used as a surrogate biomarker for clinical treatment studies, especially in progressive MS.

6.5 MRI and DTI abnormalities in progressive MS

The present findings of the higher T1 and T2 lesion load, more severe WM and GM atrophy and reduced FA in NAWM as a sign of structural damage in SPMS in comparison to RRMS patients and healthy controls are in line with previous studies (reviewed in chapter 2.3.1). However, these studies appear to be the first which have compared DTI abnormalities with adenosine A_{2A} and TSPO binding *in vivo*. The findings of the correlation of reduced FA in NAWM to increased TSPO binding in NAWM and perilesional WM are in line with earlier neuropathology and post-mortem studies, also reviewed in this thesis (chapter 2.3.1.3). Clarifying the role of adenosine A_{2A} receptors in WM tract pathology will need further investigation, but the link may be mediated through the activated microglia as discussed above (chapter 6.3).

Future studies will reveal whether DTI measurements of axonal disintegrity in NAWM will be validated as a direct indicator or predictor of neurodegeneration in MS. The advantage of DTI in comparison to PET imaging is that it is more widely available, because the short-lived radioligands used in these studies demand the proximity of specialised facilities and expert personnel involved in isotope production and radiochemical syntheses. However, DTI along with other advanced MRI techniques are more unspecific than PET imaging, which can reveal specific pathological alterations at the molecular and cellular levels.

7. CONCLUSIONS

The purpose of this thesis was to investigate the role of adenosine A_{2A} receptors and activated microglia in progressive MS using *in vivo* PET imaging with [^{11}C]TMSX and [^{11}C](R)-PK11195 radioligands, respectively. It was also intended to investigate associations of PET imaging parameters with pathological imaging findings in DTI and conventional MRI and to clinical measurements of disability. Another aim was to develop non-invasive input function methods for the analyses of brain [^{11}C]TMSX PET imaging. Finally, the histopathological correlates of [^{11}C](R)-PK11195 binding were investigated in post-mortem samples of MS brain using autoradiography and immunohistochemistry. Based on the results presented in this thesis, the following conclusions can be drawn:

- I [^{11}C]TMSX PET imaging can be used to evaluate adenosine A_{2A} receptor binding in the brain of SPMS patients. A_{2A} receptor binding is increased in the NAWM of SPMS patients and this correlates with the increased WM atrophy and structural damage in NAWM measured as reduced FA. [^{11}C]TMSX PET represents a new approach for investigating neuroinflammation in progressive MS.
- II Supervised clustering appears to be a feasible method for GM reference region extraction from brain [^{11}C]TMSX PET images in healthy controls and MS patients, and with the reference Logan, it provides a non-invasive way to evaluate DVR. The adoption of a population-based input function for the estimation of brain [^{11}C]TMSX V_T and DVR provides a robust alternative for arterial input function and may make it possible to omit arterial blood sampling in future studies.
- III Microglial activation measured with [^{11}C](R)-PK11195 PET is increased in the NAWM of SPMS patients in comparison to healthy controls. Total [^{11}C](R)-PK11195 binding within T2 hyperintense lesions is generally low. In the perilesional area of T1 black holes, the microglial activation pattern is heterogeneous, with increased perilesional [^{11}C](R)-PK11195 uptake being detected in more than half of the lesions.
- IV [^{11}C](R)-PK11195 uptake is increased in NAWM and total perilesional area of T1 hypointense lesions of SPMS patients in comparison to RRMS patients; furthermore, the extent of this increase correlates with the severity of the disability. By using [^{11}C](R)-PK11195 DVR in NAWM as a predictive marker, SPMS patients may be differentiated from RRMS patients. The increased [^{11}C](R)-PK11195 binding in NAWM correlates with the brain atrophy, reduced FA in NAWM and increased lesion volume. In [^{11}C](R)-PK11195 autoradiography, increased perilesional radioligand uptake associates with the increased numbers of activated microglia as identified by CD68 expression.

8. ACKNOWLEDGEMENTS

This study was conducted in the Turku PET Centre and Division of Clinical Neurosciences in the University of Turku and Turku University Hospital during the years 2008 – 2015. This work was financially supported by scholarships from the Finnish MS Foundation, the Finnish Parkinson Foundation, Instrumentarium Science Foundation, and Turku University Hospital research funds.

I wish to express my sincere thanks to Professor Risto O. Roine and Professor Emeritus Reijo Marttila at the Division of Clinical Neurosciences and Professor Juhani Knuuti in the Turku PET Centre for providing the invaluable opportunity and excellent facilities for conducting this research and for the possibility to combine clinical work with this project during these years.

Most importantly, I would like to express my gratitude to my supervisors, Docent Laura Airas and Professor Juha O. Rinne. Laura's broad knowledge of neuroimmunology combined with her creative mind and enthusiasm for research, and Juha's vast experience and practical know-how in clinical neuroimaging and neurological research have been of irreplaceable value and have been tremendously inspiring, thus motivating me to push forward with this work. It would never have been possible to carry this study through to fruition without my supervisors' kind guidance and unwavering dedication to neuroscience.

I am sincerely grateful to Docent Hanna Kuusisto and Senior Lecturer Alexander Gerhard for their constructive and valuable comments during the revision process of this thesis. I would also like to thank Dr. Ewen MacDonald for the careful and prompt English revision of this thesis.

I would like to express my gratitude to all my co-authors Jere Virta, Jouni Tuisku, Teemu Paavilainen, Riitta Parkkola, Pauliina Luoto, Jarkko Johansson, Vesa Oikonen, Semi Helin, Johanna Rokka, Eveliina Arponen, Marcus Sucksdorff, Alex Dickens and Maria Gardberg. It has been a pleasure and privilege working with such an intelligent group of scientists from whom I have learned so much about PET and neuroscience. I wish to especially thank Alex, Jouni and Marcus for all the good times also outside office hours and beyond the realm of neuroscience.

The expert staff at Turku PET Centre also deserves my sincerest gratitude. The radiographers Minna Aatsinki, Heidi Betlehem, Anne-Mari Jokinen, Tarja Keskitalo, Leena Lehtimäki, Hannele Lehtinen, Kaleva Mölsä, Tiina Santakivi, Johanna Siivonen and Marjo Tähti, and the laboratory technicians Heidi Partanen, Emilia Puhakka, Eija Salo, Sanna Suominen, Minna Tuominen, Tiina Tuominen and Leena Tokoi are thanked for their skilled work in this project and for making the atmosphere so pleasant. The Radiochemistry Department is also gratefully acknowledged for their excellent work in producing the radiotracers. I would also like to thank Mika Teräs, Tuula Tolvanen, Virva Saunavaara and Hannu Sipilä for their professional consultations in all technical issues, and Marko Tättäläinen and Rami Mikkola for their IT-expertise in numerous problems.

I am greatly indebted to all my fellow-researchers in the Turku PET Centre for their friendship and support. In particular, I would like to mention Kati Alakurtti, Juho Joutsa, Pekka Jokinen, Anna Brück, Nina Kemppainen, Elina Rauhala, Timo Suotunen, Noora Scheinin, Terhi Tuokkola and Susanne Vainio from the neuro group, and Minna Yli-Karjanmaa, Lauri Tuominen, Henry Karlsson, Jetro Tuulari, Jarmo Teuho and Jani Linden along with everybody else in the extended brain researcher ensemble; thank you for your vivid and stimulating company at work as well as in the extracurricular activities. The merry members of the “house band” Pets and Boys also deserve a special acknowledgement; thank you for the music and fun moments on stage.

I wish to warmly thank all the former and present colleagues, with whom I have had the pleasure to enjoy the clinical work at the Neurology Department in Turku University Hospital. Especially, I would like to thank Dr. Markku Päivärinta for his invaluable mentorship and Dr. Jaana Korpela for being such a reliable colleague and friend in our expeditions into the world of neurology. I would also like to thank all my good friends and colleagues in the non-neurological fields, especially Jakke and JJ for the supportive and relaxing moments outside office hours, and Mika for all our inspirational discussions as well as our unforgettable trips overseas and beyond. They have always provided a fresh perspective on life and science.

I owe my special gratitude to my “Riekkohauta brothers” Timo, Ville, Jarmo and Mikko and their families, and especially my wonderful godchildren Kaapo, Helmi and Saana. Thank you all for your friendship and for the memorable experiences we have had along the way. They have helped me remember the really important things in life. You can take the man out of Iisalmi, but you cannot take Iisalmi out of the man.

I wish to express my loving thanks to my family and closest relatives. I am most deeply grateful to my dear parents Kaarina and Kalevi for their everlasting love, support and understanding, and to my dear brother Tapio; you were the one to teach me the art of reading and exploring, and look how far that has taken me!

I would like to express my heartfelt gratitude to Hanna-Riikka for being the one to rely on all these years. Your support and motivation has been the strongest force to keep me moving forward even when being in dire straits.

Finally, I am grateful to my four-legged friends Eetu and his late brother Urho for their unreserved affection and never-ending bewilderment on the everyday miracles of nature. Thank you for forcing me to go out regularly and explore these miracles with you.

Turku, April 2015

Eero Rissanen

9. REFERENCES

- Abourbeh G, Theze B, Maroy R, Dubois A, Brulon V, Fontyn Y, et al. Imaging microglial/macrophage activation in spinal cords of experimental autoimmune encephalomyelitis rats by positron emission tomography using the mitochondrial 18 kDa translocator protein radioligand [(1)(8)F]DPA-714. *J Neurosci* 2012;32:5728-5736.
- Airas L, Niemela J, Yegutkin G, Jalkanen S. Mechanism of action of IFN-beta in the treatment of multiple sclerosis: a special reference to CD73 and adenosine. *Ann NY Acad Sci* 2007;1110:641-648.
- Airas L, Dickens A, Elo P, Marjamaki PM, Johansson J, Eskola O, et al. In vivo Positron Emission Tomography Imaging Demonstrates Diminished Microglial Activation after Fingolimod Treatment in an Animal Model of Multiple Sclerosis. *J Nucl Med* 2015;56:305-310.
- Alexander AL, Lee JE, Lazar M, Field AS. Diffusion tensor imaging of the brain. *Neurotherapeutics : the journal of the American Society for Experimental NeuroTherapeutics* 2007;4:316-329.
- Allen IV, McKeown SR. A histological, histochemical and biochemical study of the macroscopically normal white matter in multiple sclerosis. *J Neurol Sci* 1979;41:81-91.
- Almohmeed YH, Avenell A, Aucott L, Vickers MA. Systematic review and meta-analysis of the sero-epidemiological association between Epstein Barr virus and multiple sclerosis. *PLoS One* 2013;8:e61110.
- Andersen O. Predicting a window of therapeutic opportunity in multiple sclerosis. *Brain* 2010;133:1863-1865.
- Ashburner J. A fast diffeomorphic image registration algorithm. *Neuroimage* 2007;38:95-113.
- Babbe H, Roers A, Waisman A, Lassmann H, Goebels N, Hohlfeld R, et al. Clonal expansions of CD8(+) T cells dominate the T cell infiltrate in active multiple sclerosis lesions as shown by micromanipulation and single cell polymerase chain reaction. *J Exp Med* 2000;192:393-404.
- Bakshi R, Thompson AJ, Rocca MA, Pelletier D, Dousset V, Barkhof F, et al. MRI in multiple sclerosis: current status and future prospects. *Lancet Neurol* 2008;7:615-625.
- Banati RB, Myers R, Kreutzberg GW. PK ('peripheral benzodiazepine')-binding sites in the CNS indicate early and discrete brain lesions: microautoradiographic detection of [3H]PK11195 binding to activated microglia. *J Neurocytol* 1997;26:77-82.
- Banati RB, Goerres GW, Myers R, Gunn RN, Turkheimer FE, Kreutzberg GW, et al. [11C](R)-PK11195 positron emission tomography imaging of activated microglia in vivo in Rasmussen's encephalitis. *Neurology* 1999;53:2199-2203.
- Banati RB, Newcombe J, Gunn RN, Cagnin A, Turkheimer F, Heppner F, et al. The peripheral benzodiazepine binding site in the brain in multiple sclerosis: quantitative in vivo imaging of microglia as a measure of disease activity. *Brain* 2000;123:2321-2337.
- Banati RB, Middleton RJ, Chan R, Hatty CR, Wai-Ying Kam W, Quin C, et al. Positron emission tomography and functional characterization of a complete PBR/TSPO knockout. *Nat Commun* 2014;5:5452.
- Barkhof F, Filippi M, Miller DH, Scheltens P, Campi A, Polman CH, et al. Comparison of MRI criteria at first presentation to predict conversion to clinically definite multiple sclerosis. *Brain* 1997;120:2059-2069.
- Barkhof F. MRI in multiple sclerosis: correlation with expanded disability status scale (EDSS). *Mult Scler* 1999;5:283-286.
- Barkhof F. The clinico-radiological paradox in multiple sclerosis revisited. *Curr Opin Neurol* 2002;15:239-245.
- Basser PJ, Pierpaoli C. Microstructural and physiological features of tissues elucidated by quantitative-diffusion-tensor MRI. *J Magn Reson B* 1996;111:209-219.
- Bauer A, Holschbach MH, Meyer PT, Boy C, Herzog H, Olsson RA, et al. In vivo imaging of adenosine A1 receptors in the human brain with [18F]CPFPX and positron emission tomography. *Neuroimage* 2003;19:1760-1769.
- Bhattacharjee AK, Lang L, Jacobson O, Shinkre B, Ma Y, Niu G, et al. Striatal adenosine A(2A) receptor-mediated positron emission tomographic imaging in 6-hydroxydopamine-lesioned rats using [(18)F]-MRS5425. *Nucl Med Biol* 2011;38:897-906.
- Biber K, Owens T, Boddeke E. What is microglia neurotoxicity (Not)? *Glia* 2014;62:841-854.
- Black KL, Ikezaki K, Santori E, Becker DP, Vinters HV. Specific high-affinity binding of peripheral benzodiazepine receptor ligands to brain tumors in rat and man. *Cancer* 1990;65:93-97.
- Blackburn MR, Vance CO, Morschl E, Wilson CN. Adenosine receptors and inflammation. *Handb Exp Pharmacol* 2009;193:215-269.

- Boutin H, Chauveau F, Thominiaux C, Kuhnast B, Gregoire MC, Jan S, et al. In vivo imaging of brain lesions with [(11)C]CLINME, a new PET radioligand of peripheral benzodiazepine receptors. *Glia* 2007;55:1459-1468.
- Boutin H, Prenant C, Maroy R, Galea J, Greenhalgh AD, Smigova A, et al. [18F]DPA-714: direct comparison with [11C]PK11195 in a model of cerebral ischemia in rats. *PLoS One* 2013;8:e56441.
- Boutin H, Murray K, Pradillo J, Maroy R, Smigova A, Gerhard A, et al. F-GE-180: a novel TSPO radiotracer compared to C-R-PK11195 in a preclinical model of stroke. *Eur J Nucl Med Mol Imaging* 2014;42:503-511.
- Boy C, Meyer PT, Kircheis G, Holschbach MH, Herzog H, Elmenhorst D, et al. Cerebral A1 adenosine receptors (A1AR) in liver cirrhosis. *Eur J Nucl Med Mol Imaging* 2008;35:589-597.
- Breij EC, Brink BP, Veerhuis R, van den Berg C, Vloet R, Yan R, et al. Homogeneity of active demyelinating lesions in established multiple sclerosis. *Ann Neurol* 2008;63:16-25.
- Brex PA, Ciccarelli O, O'Riordan JI, Sailer M, Thompson AJ, Miller DH. A longitudinal study of abnormalities on MRI and disability from multiple sclerosis. *N Engl J Med* 2002;346:158-164.
- Bricker AO, Jones SE. Magnetic Resonance Imaging in Multiple Sclerosis. In: Rae-Grant AD, Fox RJ, Bethoux F, editors. *Multiple Sclerosis and Related Disorders Clinical Guide to Diagnosis, Medical Management and Rehabilitation*. New York, USA. Demos Medical, 2013: 59-69.
- Broaddus WC, Bennett JP, Jr. Peripheral-type benzodiazepine receptors in human glioblastomas: pharmacologic characterization and photoaffinity labeling of ligand recognition site. *Brain Res* 1990;518:199-208.
- Brooks DJ, Papapetropoulos S, Vandenhende F, Tomic D, He P, Coppell A, et al. An open-label, positron emission tomography study to assess adenosine A2A brain receptor occupancy of vipadenant (BIIB014) at steady-state levels in healthy male volunteers. *Clin Neuropharmacol* 2010;33:55-60.
- Bruck W, Porada P, Poser S, Rieckmann P, Hanefeld F, Kretzschmar HA, et al. Monocyte/macrophage differentiation in early multiple sclerosis lesions. *Ann Neurol* 1995;38:788-796.
- Byars LG, Sibomana M, Burbar Z, Jones J, Panin V, Barker WC, et al. Variance reduction on randoms from coincidence histograms for the HRRT. *IEEE Nucl Sci Conf R* 2005;5:2622-2626.
- Cagnin A, Brooks DJ, Kennedy AM, Gunn RN, Myers R, Turkheimer FE, et al. In-vivo measurement of activated microglia in dementia. *Lancet* 2001;358:461-467.
- Camsonne R, Crouzel C, Comar D, Mazière M, Prenant C, Sastre J, et al. Synthesis of N-(¹¹C) methyl, N-(methyl-1 propyl), (chloro-2 phenyl)-1 isquinoline carboxamide-3 (PK 11195): A new ligand for peripheral benzodiazepine receptors. *J Labelled Comp Radiopharm* 1984;21:985-991.
- Cannella B, Raine CS. The adhesion molecule and cytokine profile of multiple sclerosis lesions. *Ann Neurol* 1995;37:424-435.
- Casellas P, Galiegue S, Basile AS. Peripheral benzodiazepine receptors and mitochondrial function. *Neurochem Int* 2002;40:475-486.
- Chauveau F, Van Camp N, Dolle F, Kuhnast B, Hinnen F, Damont A, et al. Comparative evaluation of the translocator protein radioligands 11C-DPA-713, 18F-DPA-714, and 11C-PK11195 in a rat model of acute neuroinflammation. *J Nucl Med* 2009;50:468-476.
- Chen JF, Lee CF, Chern Y. Adenosine receptor neurobiology: overview. *Int Rev Neurobiol* 2014;119:1-49.
- Ching AS, Kuhnast B, Damont A, Roeda D, Tavitian B, Dolle F. Current paradigm of the 18-kDa translocator protein (TSPO) as a molecular target for PET imaging in neuroinflammation and neurodegenerative diseases. *Insights Imaging* 2012;3:111-119.
- Ciruela F, Casado V, Rodrigues RJ, Lujan R, Burgueno J, Canals M, et al. Presynaptic control of striatal glutamatergic neurotransmission by adenosine A1-A2A receptor heteromers. *J Neurosci* 2006;26:2080-2087.
- Colasanti A, Guo Q, Muhlert N, Giannetti P, Onega M, Newbould RD, et al. In Vivo Assessment of Brain White Matter Inflammation in Multiple Sclerosis with 18F-PBR111 PET. *J Nucl Med* 2014;55:1112-1118.
- Coles AJ. Alemtuzumab treatment of multiple sclerosis. *Semin Neurol* 2013;33:66-73.
- Compston A. Genetic epidemiology of multiple sclerosis. *J Neurol Neurosurg Psychiatry* 1997;62:553-561.
- Compston A, Coles A. Multiple sclerosis. *Lancet* 2002;359:1221-1231.
- Compston A, Coles A. Multiple sclerosis. *Lancet* 2008;372:1502-1517.
- Confavreux C, Vukusic S. Age at disability milestones in multiple sclerosis. *Brain* 2006;129:595-605.
- Cosenza-Nashat M, Zhao ML, Suh HS, Morgan J, Natividad R, Morgello S, et al. Expression of the translocator protein of 18 kDa by microglia, macrophages and astrocytes based on immunohistochemical localization in abnormal human brain. *Neuropathol Appl Neurobiol* 2009;35:306-328.

- Costello K, Halper J, Kalb R, Skutnik S, Rapp R. The Use of Disease-Modifying Therapies in Multiple Sclerosis. Principles and Current Evidence. A Consensus Paper by the Multiple Sclerosis Coalition. Available at: http://www.nationalmssociety.org/getmedia/5ca284d3-fc7c-4ba5-b005-ab537d495c3c/DMT_Consensus_MS_Coalition_color. Accessed Dec 15th 2014.
- de Jong HW, van Velden FH, Kloet RW, Buijs FL, Boellaard R, Lammertsma AA. Performance evaluation of the ECAT HRRT: an LSO-LYSO double layer high resolution, high sensitivity scanner. *Physics in medicine and biology* 2007;52:1505-1526.
- de Paula Faria D, de Vries EF, Sijbesma JW, Dierckx RA, Buchpiguel CA, Copray S. PET imaging of demyelination and remyelination in the cuprizone mouse model for multiple sclerosis: a comparison between [11C]CIC and [11C]MeDAS. *Neuroimage* 2014;87:395-402.
- Debruyne JC, Van Laere KJ, Versijpt J, De Vos F, Eng JK, Strijckmans K, et al. Semiquantification of the peripheral-type benzodiazepine ligand [11C]PK11195 in normal human brain and application in multiple sclerosis patients. *Acta Neurol Belg* 2002;102:127-135.
- Debruyne JC, Versijpt J, Van Laere KJ, De Vos F, Keppens J, Strijckmans K, et al. PET visualization of microglia in multiple sclerosis patients using [11C]PK11195. *Eur J Neurol* 2003;10:257-264.
- Dickens AM, Vainio S, Marjamaki P, Johansson J, Lehtiniemi P, Rokka J, et al. Detection of microglial activation in an acute model of neuroinflammation using PET and radiotracers 11C-(R)-PK11195 and 18F-GE-180. *J Nucl Med* 2014;55:466-472.
- Doble A, Malgouris C, Daniel M, Daniel N, Imbault F, Basbaum A, et al. Labelling of peripheral-type benzodiazepine binding sites in human brain with [3H]PK 11195: anatomical and subcellular distribution. *Brain Res Bull* 1987;18:49-61.
- Doorduyn J, Klein HC, Dierckx RA, James M, Kassiou M, de Vries EF. [11C]-DPA-713 and [18F]-DPA-714 as new PET tracers for TSP0: a comparison with [11C]-(R)-PK11195 in a rat model of herpes encephalitis. *Mol Imaging Biol* 2009;11:386-398.
- Duan S, Lv Z, Fan X, Wang L, Han F, Wang H, et al. Vitamin D status and the risk of multiple sclerosis: a systematic review and meta-analysis. *Neurosci Lett* 2014;570:108-113.
- Dukart J, Pernecky R, Forster S, Barthel H, Diehl-Schmid J, Draganski B, et al. Reference cluster normalization improves detection of frontotemporal lobar degeneration by means of FDG-PET. *PLoS One* 2013;8:e55415.
- Dunwiddie TV, Masino SA. The role and regulation of adenosine in the central nervous system. *Annu Rev Neurosci* 2001;24:31-55.
- Durelli L, Conti L, Clerico M, Boselli D, Contessa G, Ripellino P, et al. T-helper 17 cells expand in multiple sclerosis and are inhibited by interferon-beta. *Ann Neurol* 2009;65:499-509.
- Dyment DA, Herrera BM, Cader MZ, Willer CJ, Lincoln MR, Sadovnick AD, et al. Complex interactions among MHC haplotypes in multiple sclerosis: susceptibility and resistance. *Hum Mol Gen* 2005;14:2019-2026.
- Edison P, Archer HA, Gerhard A, Hinz R, Pavese N, Turkheimer FE, et al. Microglia, amyloid, and cognition in Alzheimer's disease: An [11C](R)PK11195-PET and [11C]PIB-PET study. *Neurobiol Dis* 2008;32:412-419.
- Elmenhorst D, Meyer PT, Winz OH, Matusch A, Ermert J, Coenen HH, et al. Sleep deprivation increases A1 adenosine receptor binding in the human brain: a positron emission tomography study. *J Neurosci* 2007;27:2410-2415.
- Esser PD. PET Physics and Instrumentation. In: Van Heertum RD, Tikofsky RS, Ichise M, editors. *Functional Cerebral SPECT and PET Imaging*. Philadelphia, USA. Lippincott Williams & Wilkins, 2010: 23-33.
- Evans C, Beland SG, Kulaga S, Wolfson C, Kingwell E, Marriott J, et al. Incidence and prevalence of multiple sclerosis in the Americas: a systematic review. *Neuroepidemiology* 2013;40:195-210.
- Fahn S, Elton RL. Unified Parkinson's disease rating scale. In: Fahn S, Marsden CD, Calne D, Goldstein M, editors. *Recent developments in Parkinson's disease*. Macmillan Health Care Information, Florham Park, NJ, USA, 1987: 153-164, 293-304.
- Fazekas F, Soelberg-Sorensen P, Comi G, Filippi M. MRI to monitor treatment efficacy in multiple sclerosis. *J Neuroimaging*: 2007;17 Suppl 1:50S-55S.
- Ferré S, Ciruela F, Canals M, Marcellino D, Burgueno J, Casadó V, et al. Adenosine A2A-dopamine D2 receptor-receptor heteromers. Targets for neuropsychiatric disorders. *Parkinsonism Relat Disord* 2004;10:265-271.
- Filippi M, Paty DW, Kappos L, Barkhof F, Compston DA, Thompson AJ, et al. Correlations between changes in disability and T2-weighted brain MRI activity in multiple sclerosis: a follow-up study. *Neurology* 1995;45:255-260.
- Filippi M, Rocca MA. Dirty-appearing white matter: a disregarded entity in multiple sclerosis. *Am J Neuroradiol* 2010;31:390-391.
- Fisniku LK, Brex PA, Altmann DR, Miszkil KA, Benton CE, Lanyon R, et al. Disability and T2 MRI lesions: a

- 20-year follow-up of patients with relapse onset of multiple sclerosis. *Brain* 2008;131:808-817.
- Fredholm BB, Abbracchio MP, Burnstock G, Daly JW, Harden TK, Jacobson KA, et al. Nomenclature and classification of purinoceptors. *Pharmacolo Rev* 1994;46:143-156.
- Freedman MS, Selchen D, Arnold DL, Prat A, Banwell B, Yeung M, et al. Treatment optimization in MS: Canadian MS Working Group updated recommendations. *Can J Neurosci* 2013;40:307-323.
- Frischer JM, Bramow S, Dal-Bianco A, Lucchinetti CF, Rauschka H, Schmidbauer M, et al. The relation between inflammation and neurodegeneration in multiple sclerosis brains. *Brain* 2009;132:1175-1189.
- Friston KJ, Frith CD, Liddle PF, Dolan RJ, Lammertsma AA, Frackowiak RS. The relationship between global and local changes in PET scans. *J Cereb Blood Flow Metab* 1990;10:458-466.
- Fukumitsu N, Ishii K, Kimura Y, Oda K, Sasaki T, Mori Y, et al. Imaging of adenosine A1 receptors in the human brain by positron emission tomography with [¹¹C]MPDX. *Ann Nucl Med* 2003;17:511-515.
- Fukumitsu N, Ishii K, Kimura Y, Oda K, Sasaki T, Mori Y, et al. Adenosine A1 receptor mapping of the human brain by PET with 8-dicyclopropylmethyl-1-¹¹C-methyl-3-propylxanthine. *J Nucl Med* 2005;46:32-37.
- Fukumitsu N, Ishii K, Kimura Y, Oda K, Hashimoto M, Suzuki M, et al. Adenosine A(1) receptors using 8-dicyclopropylmethyl-1-[[¹¹C]methyl-3-propylxanthine PET in Alzheimer's disease. *Ann Nucl Med* 2008;22:841-847.
- Färber K, Kettenmann H. Purinergic signaling and microglia. *Pflugers Arch* 2006;452:615-621.
- Gao HM, Hong JS. Why neurodegenerative diseases are progressive: uncontrolled inflammation drives disease progression. *Trends in immunology* 2008;29:357-365.
- Gao Z, Tsirka SE. Animal Models of MS Reveal Multiple Roles of Microglia in Disease Pathogenesis. *Neurol Res Int* 2011;2011:383087.
- Gaser C. Structural Brain Mapping Group: 2012 VBM8 [online]. Available at: <http://dbm.neuro.uni-jena.de/vbm/>. Accessed Jan 13th 2015.
- Gehrmann J, Matsumoto Y, Kreutzberg GW. Microglia: intrinsic immunoeffector cell of the brain. *Brain Res Brain Res Rev* 1995;20:269-287.
- Gerhard A, Schwarz J, Myers R, Wise R, Banati RB. Evolution of microglial activation in patients after ischemic stroke: a [¹¹C](R)-PK11195 PET study. *Neuroimage* 2005;24:591-595.
- Gerhard A, Pavese N, Hotton G, Turkheimer F, Es M, Hammers A, et al. In vivo imaging of microglial activation with [¹¹C](R)-PK11195 PET in idiopathic Parkinson's disease. *Neurobiol Dis* 2006;21:404-412.
- Giannetti P, Politis M, Su P, Turkheimer F, Malik O, Keihaninejad S, et al. Microglia activation in multiple sclerosis black holes predicts outcome in progressive patients: an in vivo [(11)C](R)-PK11195-PET pilot study. *Neurobiol of Dis* 2014a;65:203-210.
- Giannetti P, Politis M, Su P, Turkheimer FE, Malik O, Keihaninejad S, et al. Increased PK11195-PET binding in normal-appearing white matter in clinically isolated syndrome. *Brain* 2014b; 138:110-119.
- Good CD, Johnsrude IS, Ashburner J, Henson RN, Friston KJ, Frackowiak RS. A voxel-based morphometric study of ageing in 465 normal adult human brains. *Neuroimage* 2001;14:21-36.
- Gourraud PA, Harbo HF, Hauser SL, Baranzini SE. The genetics of multiple sclerosis: an up-to-date review. *Immunol Rev* 2012;248:87-103.
- Graeber MB, Streit WJ. Microglia: biology and pathology. *Acta Neuropathol* 2010;119:89-105.
- Groves A, Kihara Y, Chun J. Fingolimod: direct CNS effects of sphingosine 1-phosphate (S1P) receptor modulation and implications in multiple sclerosis therapy. *J Neurol Sci* 2013;328:9-18.
- Gulyas B, Vas A, Toth M, Takano A, Varrone A, Cselenyi Z, et al. Age and disease related changes in the translocator protein (TSPO) system in the human brain: positron emission tomography measurements with [¹¹C]vinpocetine. *Neuroimage* 2011;56:1111-1121.
- Gulyas B, Toth M, Schain M, Airaksinen A, Vas A, Kostulas K, et al. Evolution of microglial activation in ischaemic core and peri-infarct regions after stroke: a PET study with the TSPO molecular imaging biomarker [[(11)C]vinpocetine. *J Neurol Sci* 2012a;320:110-117.
- Gulyas B, Toth M, Vas A, Shchukin E, Kostulas K, Hillert J, et al. Visualising neuroinflammation in post-stroke patients: a comparative PET study with the TSPO molecular imaging biomarkers [¹¹C]PK11195 and [¹¹C]vinpocetine. *Curr Radiopharm* 2012b;5:19-28.
- Gunn RN, Lammertsma AA, Hume SP, Cunningham VJ. Parametric imaging of ligand-receptor binding in PET using a simplified reference region model. *Neuroimage* 1997;6:279-287.
- Guo Q, Owen DR, Rabiner EA, Turkheimer FE, Gunn RN. Identifying improved TSPO PET imaging probes through biomathematics: the impact of multiple TSPO binding sites in vivo. *Neuroimage* 2012;60:902-910.

- Harhausen D, Sudmann V, Khojasteh U, Muller J, Zille M, Graham K, et al. Specific imaging of inflammation with the 18 kDa translocator protein ligand DPA-714 in animal models of epilepsy and stroke. *PLoS One* 2013;8:e69529.
- Hauser SL, Oksenberg JR. The neurobiology of multiple sclerosis: genes, inflammation, and neurodegeneration. *Neuron* 2006;52:61-76.
- Hawkes CH. Smoking is a risk factor for multiple sclerosis: a metaanalysis. *Mult Scler* 2007;13:610-615.
- Headrick JP, Lasley RD. Adenosine receptors and reperfusion injury of the heart. *Handb Exp Pharmacol* 2009;189-214.
- Heiss WD, Habedank B, Klein JC, Herholz K, Wienhard K, Lenox M, et al. Metabolic rates in small brain nuclei determined by high-resolution PET. *J Nucl Med* 2004;45:1811-1815.
- Hendee WR, Morgan CJ. Magnetic resonance imaging. Part I--physical principles. *West J Med* 1984a;141:491-500.
- Hendee WR, Morgan CJ. Magnetic resonance imaging. Part II--Clinical applications. *West J Med* 1984b;141:638-648.
- Hickman SJ, Brierley CM, Silver NC, Moseley IF, Scolding NJ, Compston DA, et al. Infratentorial hypointense lesion volume on T1-weighted magnetic resonance imaging correlates with disability in patients with chronic cerebellar ataxia due to multiple sclerosis. *J Neurol Sci* 2001;187:35-39.
- Hinz R, Jones M, Bloomfield P, Boellaard R, Turkheimer FE, PJ T. Reference tissue kinetics extraction from [11C]-(R)-PK11195 scans on the High Resolution Research Tomograph (HRRT). *Neuroimage* 2008; 41 (Suppl 2): T65.
- Hochmeister S, Grundtner R, Bauer J, Engelhardt B, Lyck R, Gordon G, et al. Dysferlin is a new marker for leaky brain blood vessels in multiple sclerosis. *J Neuropathol Exp Neurol* 2006;65:855-865.
- Horti AG, Gao Y, Ravert HT, Finley P, Valentine H, Wong DF, et al. Synthesis and biodistribution of [11C]A-836339, a new potential radioligand for PET imaging of cannabinoid type 2 receptors (CB2). *Bioorg Med Chem* 2010;18:5202-5207.
- Howell OW, Rundle JL, Garg A, Komada M, Brophy PJ, Reynolds R. Activated microglia mediate axonal disruption that contributes to axonal injury in multiple sclerosis. *Journal of neuropathology and experimental neurology* 2010;69:1017-1033.
- Iannaccone S, Cerami C, Alessio M, Garibotto V, Panzacchi A, Olivieri S, et al. In vivo microglia activation in very early dementia with Lewy bodies, comparison with Parkinson's disease. *Parkinsonism Relat Disord* 2013;19:47-52.
- Ikoma Y, Edison P, Ramlackhansingh A, Brooks DJ, Turkheimer FE. Reference region automatic extraction in dynamic [(11)C]PIB. *J Cereb Blood Flow Metab* 2013;33:1725-1731.
- Imaizumi M, Kim HJ, Zoghbi SS, Briard E, Hong J, Musachio JL, et al. PET imaging with [11C]PBR28 can localize and quantify upregulated peripheral benzodiazepine receptors associated with cerebral ischemia in rat. *Neurosci Lett* 2007;411:200-205.
- Ishiwata K, Noguchi J, Toyama H, Sakiyama Y, Koike N, Ishii S, et al. Synthesis and preliminary evaluation of [11C]KF17837, a selective adenosine A2A antagonist. *Appl Rad Isot* 1996;47:507-511.
- Ishiwata K, Wang WF, Kimura Y, Kawamura K, Ishii K. Preclinical studies on [11C]TMSX for mapping adenosine A2A receptors by positron emission tomography. *Ann Nucl Med* 2003;17:205-211.
- Ishiwata K, Mishina M, Kimura Y, Oda K, Sasaki T, Ishii K. First visualization of adenosine A(2A) receptors in the human brain by positron emission tomography with [11C]TMSX. *Synapse* 2005;55:133-136.
- Jackson SJ, Giovannoni G, Baker D. Fingolimod modulates microglial activation to augment markers of remyelination. *J Neuroinflammation* 2011;8:76.
- Jacobsen CO, Farbu E. MRI evaluation of grey matter atrophy and disease course in multiple sclerosis: an overview of current knowledge. *Acta Neurol Scand Suppl* 2014:32-36.
- Jellison BJ, Field AS, Medow J, Lazar M, Salamat MS, Alexander AL. Diffusion tensor imaging of cerebral white matter: a pictorial review of physics, fiber tract anatomy, and tumor imaging patterns. *Am J Neuroradiol* 2004;25:356-369.
- Ji B, Maeda J, Sawada M, Ono M, Okauchi T, Inaji M, et al. Imaging of peripheral benzodiazepine receptor expression as biomarkers of detrimental versus beneficial glial responses in mouse models of Alzheimer's and other CNS pathologies. *J Neurosci* 2008;28:12255-12267.
- Johnston JB, Silva C, Gonzalez G, Holden J, Warren KG, Metz LM, et al. Diminished adenosine A1 receptor expression on macrophages in brain and blood of patients with multiple sclerosis. *Ann Neurol* 2001;49:650-658.
- Juhász C, Nagy F, Watson C, da Silva EA, Muzik O, Chugani DC, et al. Glucose and [11C]flumazenil positron emission tomography abnormalities of thalamic nuclei in temporal lobe epilepsy. *Neurology* 1999;53:2037-2045.
- Junck L, Olson JM, Ciliax BJ, Koeppe RA, Watkins GL, Jewett DM, et al. PET imaging of human gliomas with ligands for the peripheral benzodiazepine binding site. *Ann Neurol* 1989;26:752-758.

- Kappos L, Moeri D, Radue EW, Schoetzau A, Schweikert K, Barkhof F, et al. Predictive value of gadolinium-enhanced magnetic resonance imaging for relapse rate and changes in disability or impairment in multiple sclerosis: a meta-analysis. *Gadolinium MRI Meta-analysis Group. Lancet* 1999;353:964-969.
- Kawamura K, Ishiwata K. Improved synthesis of [11C]SA4503, [11C]MPDX and [11C]TMSX by use of [11C]methyl triflate. *Ann Nucl Med* 2004;18:165-168.
- Khanapur S, Paul S, Shah A, Vatakuti S, Koole MJ, Zijlma R, et al. Development of [18F]-labeled pyrazolo[4,3-e]-1,2,4-triazolo[1,5-c]pyrimidine (SCH442416) analogs for the imaging of cerebral adenosine A2A receptors with positron emission tomography. *J Med Chem* 2014;57:6765-6780.
- Kim HJ, Biernacki K, Prat A, Antel JP, Bar-Or A. Inflammatory potential and migratory capacities across human brain endothelial cells of distinct glatiramer acetate-reactive T cells generated in treated multiple sclerosis patients. *Clin Immunol* 2004;111:38-46.
- Kobelt G, Berg J, Lindgren P, Fredrikson S, Jonsson B. Costs and quality of life of patients with multiple sclerosis in Europe. *J Neurol Neurosurg Psychiatry* 2006;77:918-926.
- Koch MW, Metz LM, Agrawal SM, Yong VW. Environmental factors and their regulation of immunity in multiple sclerosis. *J Neurol Sci* 2013;324:10-16.
- Kreisl WC, Jenko KJ, Hines CS, Hyoung Lyoo C, Corona W, Morse CL, et al. A genetic polymorphism for translocator protein 18 kDa affects both in vitro and in vivo radioligand binding in human brain to this putative biomarker of neuroinflammation. *J Cereb Blood Flow Metab* 2013;33:53-58.
- Kuhlmann AC, Guilarte TR. Cellular and subcellular localization of peripheral benzodiazepine receptors after trimethyltin neurotoxicity. *J Neurochem* 2000;74:1694-1704.
- Kurtzke JF. Rating neurologic impairment in multiple sclerosis: an expanded disability status scale (EDSS). *Neurology* 1983;33:1444-1452.
- Kutzelnigg A, Lucchinetti CF, Stadelmann C, Bruck W, Rauschka H, Bergmann M, et al. Cortical demyelination and diffuse white matter injury in multiple sclerosis. *Brain* 2005;128:2705-2712.
- Kutzelnigg A, Lassmann H. Pathology of multiple sclerosis and related inflammatory demyelinating diseases. *Handb Clin Neurol* 2014;122:15-58.
- Lammertsma AA, Hume SP. Simplified reference tissue model for PET receptor studies. *Neuroimage* 1996;4:153-158.
- Lampl Y, Lorberboym M, Blankenberg FG, Sadeh M, Gilad R, Annexin V. SPECT imaging of phosphatidylserine expression in patients with dementia. *Neurology* 2006;66:1253-1254.
- Lassmann H. New concepts on progressive multiple sclerosis. *Curr Neurol Neurosci Rep* 2007;7:239-244.
- Lassmann H, van Horsen J, Mahad D. Progressive multiple sclerosis: pathology and pathogenesis. *Nat Rev Neurol* 2012;8:647-656.
- Lavisse S, Guillermier M, Herard AS, Petit F, Delahaye M, Van Camp N, et al. Reactive astrocytes overexpress TSPO and are detected by TSPO positron emission tomography imaging. *J Neurosci* 2012;32:10809-10818.
- Le Bihan D, Mangin JF, Poupon C, Clark CA, Pappata S, Molko N, et al. Diffusion tensor imaging: concepts and applications. *J Magn Reson Imaging* 2001;13:534-546.
- Le Bihan D. Looking into the functional architecture of the brain with diffusion MRI. *Nat Rev Neurosci* 2003;4:469-480.
- Leray E, Yaouanq J, Le Page E, Coustans M, Laplaud D, Oger J, et al. Evidence for a two-stage disability progression in multiple sclerosis. *Brain* 2010;133:1900-1913.
- Logan J, Fowler JS, Volkow ND, Wolf AP, Dewey SL, Schlyer DJ, et al. Graphical analysis of reversible radioligand binding from time-activity measurements applied to [N-11C-methyl]-(-)-cocaine PET studies in human subjects. *J Cereb Blood Flow Metab* 1990;10:740-747.
- Logan J, Fowler JS, Volkow ND, Wang GJ, Ding YS, Alexoff DL. Distribution volume ratios without blood sampling from graphical analysis of PET data. *J Cereb Blood Flow Metab* 1996;16:834-840.
- Logan J. Graphical analysis of PET data applied to reversible and irreversible tracers. *Nucl Med Biol* 2000;27:661-670.
- Lorberboym M, Blankenberg FG, Sadeh M, Lampl Y. In vivo imaging of apoptosis in patients with acute stroke: correlation with blood-brain barrier permeability. *Brain Res* 2006;1103:13-19.
- Lubetzki C, Stankoff B. Demyelination in multiple sclerosis. *Handb Clin Neurol* 2014;122:89-99.
- Lublin FD, Reingold SC, Cohen JA, Cutter GR, Sorensen PS, Thompson AJ, et al. Defining the clinical course of multiple sclerosis: the 2013 revisions. *Neurology* 2014;83:278-286.
- Lucchinetti C, Bruck W, Parisi J, Scheithauer B, Rodriguez M, Lassmann H. Heterogeneity of multiple sclerosis lesions: implications for the pathogenesis of demyelination. *Ann Neurol* 2000;47:707-717.

- Lucchinetti CF, Bruck W, Rodriguez M, Lassmann H. Distinct patterns of multiple sclerosis pathology indicates heterogeneity on pathogenesis. *Brain Pathol* 1996;6:259-274.
- Magliozzi R, Howell OW, Reeves C, Roncaroli F, Nicholas R, Serafini B, et al. A Gradient of neuronal loss and meningeal inflammation in multiple sclerosis. *Ann Neurol* 2010;68:477-493.
- Mangia S, Carpenter AF, Tyan AE, Eberly LE, Garwood M, Michaeli S. Magnetization transfer and adiabatic T1rho MRI reveal abnormalities in normal-appearing white matter of subjects with multiple sclerosis. *Mult Scler* 2013;20:1066-1073.
- Martin A, Boisgard R, Theze B, Van Camp N, Kuhnast B, Damont A, et al. Evaluation of the PBR/TSP0 radioligand [(18)F]DPA-714 in a rat model of focal cerebral ischemia. *J Cereb Blood Flow Metab* 2010;30:230-241.
- Matos M, Augusto E, Agostinho P, Cunha RA, Chen JF. Antagonistic interaction between adenosine A2A receptors and Na⁺/K⁺-ATPase- α 2 controlling glutamate uptake in astrocytes. *J Neurosci* 2013;33:18492-18502.
- Mattner F, Staykova M, Berghofer P, Wong HJ, Fordham S, Callaghan P, et al. Central nervous system expression and PET imaging of the translocator protein in relapsing-remitting experimental autoimmune encephalomyelitis. *J Nucl Med* 2013;54:291-298.
- Mayne M, Shepel PN, Jiang Y, Geiger JD, Power C. Dysregulation of adenosine A1 receptor-mediated cytokine expression in peripheral blood mononuclear cells from multiple sclerosis patients. *Ann Neurol* 1999;45:633-639.
- McGeer PL, Itagaki S, Boyes BE, McGeer EG. Reactive microglia are positive for HLA-DR in the substantia nigra of Parkinson's and Alzheimer's disease brains. *Neurology* 1988;38:1285-1291.
- McMahon EJ, Bailey SL, Castenada CV, Waldner H, Miller SD. Epitope spreading initiates in the CNS in two mouse models of multiple sclerosis. *Nat Med* 2005;11:335-339.
- Meyer PT, Elmenhorst D, Matusch A, Winz O, Zilles K, Bauer A. A1 adenosine receptor PET using [18F]CPFPX: displacement studies in humans. *Neuroimage* 2006;32:1100-1105.
- Meyer PT, Elmenhorst D, Boy C, Winz O, Matusch A, Zilles K, et al. Effect of aging on cerebral A1 adenosine receptors: A [18F]CPFPX PET study in humans. *Neurobiol Aging* 2007;28:1914-1924.
- Miki Y, Grossman RI, Udupa JK, Wei L, Polansky M, Mannon LJ, et al. Relapsing-remitting multiple sclerosis: longitudinal analysis of MR images--lack of correlation between changes in T2 lesion volume and clinical findings. *Radiology* 1999;213:395-399.
- Miller PW, Long NJ, Vilar R, Gee AD. Synthesis of 11C, 18F, 15O, and 13N radiolabels for positron emission tomography. *Angew Chem Int Ed Engl* 2008;47:8998-9033.
- Mills JH, Thompson LF, Mueller C, Waickman AT, Jalkanen S, Niemela J, et al. CD73 is required for efficient entry of lymphocytes into the central nervous system during experimental autoimmune encephalomyelitis. *Proc Natl Acad Sci USA* 2008;105:9325-9330.
- Mills JH, Kim DG, Krenz A, Chen JF, Bynoe MS. A2A adenosine receptor signaling in lymphocytes and the central nervous system regulates inflammation during experimental autoimmune encephalomyelitis. *J Immunol* 2012;188:5713-5722.
- Milo R, Miller A. Revised diagnostic criteria of multiple sclerosis. *Autoimmun Rev* 2014;13:518-524.
- Minghetti L, Levi G. Microglia as effector cells in brain damage and repair: focus on prostanoids and nitric oxide. *Prog Neurobiol* 1998;54:99-125.
- Miron VE, Franklin RJ. Macrophages and CNS remyelination. *J Neurochem* 2014;130:165-171.
- Mishina M, Ishiwata K, Kimura Y, Naganawa M, Oda K, Kobayashi S, et al. Evaluation of distribution of adenosine A2A receptors in normal human brain measured with [11C]TMSX PET. *Synapse* 2007;61:778-784.
- Mishina M, Ishiwata K, Naganawa M, Kimura Y, Kitamura S, Suzuki M, et al. Adenosine A(2A) receptors measured with [C]TMSX PET in the striata of Parkinson's disease patients. *PLoS One* 2011;6:e17338.
- Mishina M, Kimura Y, Naganawa M, Ishii K, Oda K, Sakata M, et al. Differential effects of age on human striatal adenosine A(1) and A(2A) receptors. *Synapse* 2012;66:832-839.
- Mishina M, Ishiwata K. Adenosine receptor PET imaging in human brain. *Int Rev Neurobiol* 2014;119:51-69.
- Moll NM, Rietsch AM, Thomas S, Ransohoff AJ, Lee JC, Fox R, et al. Multiple sclerosis normal-appearing white matter: Pathology-imaging correlations. *Ann Neurol* 2011;70:764-773.
- Montgomery AJ, Asselin MC, Farde L, Grasby PM. Measurement of methylphenidate-induced change in extrastriatal dopamine concentration using [11C]FLB 457 PET. *J Cereb Blood Flow Metab* 2007;27:369-377.
- Mosteller RD. Simplified calculation of body-surface area. *N Engl J Med* 1987;317:1098.

- Mu L, Bieri D, Slavik R, Drandarov K, Muller A, Cermak S, et al. Radiolabeling and in vitro /in vivo evaluation of N-(1-adamantyl)-8-methoxy-4-oxo-1-phenyl-1,4-dihydroquinoline-3-carboxamide as a PET probe for imaging cannabinoid type 2 receptor. *J Neurochem* 2013;126:616-624.
- Munger KL, Zhang SM, O'Reilly E, Hernan MA, Olek MJ, Willett WC, et al. Vitamin D intake and incidence of multiple sclerosis. *Neurology* 2004;62:60-65.
- Munger KL, Levin LI, Hollis BW, Howard NS, Ascherio A. Serum 25-hydroxyvitamin D levels and risk of multiple sclerosis. *JAMA* 2006;296:2832-2838.
- Mustafa SJ, Morrison RR, Teng B, Pelleg A. Adenosine receptors and the heart: role in regulation of coronary blood flow and cardiac electrophysiology. *Handb Exp Pharmacol* 2009;161-188.
- Naganawa M, Kimura Y, Mishina M, Manabe Y, Chihara K, Oda K, et al. Quantification of adenosine A2A receptors in the human brain using [11C]TMSX and positron emission tomography. *Eur J Nucl Med Mol Imaging* 2007;34:679-687.
- Neuhaus O, Kieseier BC, Hartung HP. Immunosuppressive agents in multiple sclerosis. *Neurotherapeutics* 2007;4:654-660.
- Niemelä J, Ifergan I, Yegutkin GG, Jalkanen S, Prat A, Airas L. IFN-beta regulates CD73 and adenosine expression at the blood-brain barrier. *Eur J Immunol* 2008;38:2718-2726.
- Nijeholt GJ, van Walderveen MA, Castelijns JA, van Waesberghe JH, Polman C, Scheltens P, et al. Brain and spinal cord abnormalities in multiple sclerosis. Correlation between MRI parameters, clinical subtypes and symptoms. *Brain* 1998;121 (Pt 4):687-697.
- Nitz W. Principles of Magnetic Resonance Imaging and Magnetic Resonance Angiography. In Reimer P, Parizel PM, Stichnoth F-A, editors. *Clinical MR Imaging*, Springer, Berlin, Germany, 2003:2-52.
- Nuyts J, Dupont P, Stroobants S, Maes A, Mortelmans L, Suetens P. Evaluation of maximum-likelihood based attenuation correction in positron emission tomography. *IEEE Trans Nucl Sci* 1999;46:1136-1141.
- Obermeier B, Daneman R, Ransohoff RM. Development, maintenance and disruption of the blood-brain barrier. *Nature medicine* 2013;19:1584-1596.
- Oh U, Fujita M, Ikonomidou VN, Evangelou IE, Matsuura E, Harberts E, et al. Translocator protein PET imaging for glial activation in multiple sclerosis. *J Neuroimmune Pharmacol* 2011;6:354-361.
- Ohta A, Sitkovsky M. Role of G-protein-coupled adenosine receptors in downregulation of inflammation and protection from tissue damage. *Nature* 2001;414:916-920.
- Okazawa H, Leyton M, Benkelfat C, Mzengeza S, Diksic M. Statistical mapping analysis of serotonin synthesis images generated in healthy volunteers using positron-emission tomography and alpha-[11C]methyl-L-tryptophan. *J Psychiatry Neurosci* 2000;25:359-370.
- Okello A, Edison P, Archer HA, Turkheimer FE, Kennedy J, Bullock R, et al. Microglial activation and amyloid deposition in mild cognitive impairment: a PET study. *Neurology* 2009;72:56-62.
- Olerup O, Hillert J. HLA class II-associated genetic susceptibility in multiple sclerosis: a critical evaluation. *Tissue antigens* 1991;38:1-15.
- Orr AG, Orr AL, Li XJ, Gross RE, Traynelis SF. Adenosine A(2A) receptor mediates microglial process retraction. *Nat Neurosci* 2009;12:872-878.
- Orton SM, Herrera BM, Yee IM, Valdar W, Ramagopalan SV, Sadovnick AD, et al. Sex ratio of multiple sclerosis in Canada: a longitudinal study. *Lancet Neurol* 2006;5:932-936.
- Ouchi Y, Yoshikawa E, Sekine Y, Futatsubashi M, Kanno T, Ogusu T, et al. Microglial activation and dopamine terminal loss in early Parkinson's disease. *Ann Neurol* 2005;57:168-175.
- Owen DR, Yeo AJ, Gunn RN, Song K, Wadsworth G, Lewis A, et al. An 18-kDa translocator protein (TSPO) polymorphism explains differences in binding affinity of the PET radioligand PBR28. *J Cereb Blood Flow Metab* 2012;32:1-5.
- Paolicelli RC, Bolasco G, Pagani F, Maggi L, Scianni M, Panzanelli P, et al. Synaptic pruning by microglia is necessary for normal brain development. *Science* 2011;333:1456-1458.
- Papadopoulos V, Baraldi M, Guilarte TR, Knudsen TB, Lacapere JJ, Lindemann P, et al. Translocator protein (18kDa): new nomenclature for the peripheral-type benzodiazepine receptor based on its structure and molecular function. *Trends Pharmacol Sci* 2006;27:402-409.
- Pappata S, Levasseur M, Gunn RN, Myers R, Crouzel C, Syrota A, et al. Thalamic microglial activation in ischemic stroke detected in vivo by PET and [11C]PK1195. *Neurology* 2000;55:1052-1054.
- Pascual B, Prieto E, Arbizu J, Marti-Climent JM, Penuelas I, Quincoces G, et al. Decreased carbon-11-flumazenil binding in early Alzheimer's disease. *Brain* 2012;135:2817-2825.
- Pavese N, Gerhard A, Tai YF, Ho AK, Turkheimer F, Barker RA, et al. Microglial activation correlates with severity in Huntington disease: a clinical and PET study. *Neurology* 2006;66:1638-1643.

- Pierri M, Vaudano E, Sager T, Englund U. KW-6002 protects from MPTP induced dopaminergic toxicity in the mouse. *Neuropharmacology* 2005;48:517-524.
- Politis M, Pavese N, Tai YF, Kiferle L, Mason SL, Brooks DJ, et al. Microglial activation in regions related to cognitive function predicts disease onset in Huntington's disease: a multimodal imaging study. *Hum Brain Mapp* 2011;32:258-270.
- Politis M, Giannetti P, Su P, Turkheimer F, Keihaninejad S, Wu K, et al. Increased PK11195 PET binding in the cortex of patients with MS correlates with disability. *Neurology* 2012;79:523-530.
- Polman CH, O'Connor PW, Havrdova E, Hutchinson M, Kappos L, Miller DH, et al. A randomized, placebo-controlled trial of natalizumab for relapsing multiple sclerosis. *New Engl J Med* 2006;354:899-910.
- Polman CH, Reingold SC, Banwell B, Clanet M, Cohen JA, Filippi M, et al. Diagnostic criteria for multiple sclerosis: 2010 revisions to the McDonald criteria. *Ann Neurol* 2011;69:292-302.
- Preziosa P, Rocca MA, Mesaros S, Pagani E, Stosic-Opincal T, Kacar K, et al. Intrinsic damage to the major white matter tracts in patients with different clinical phenotypes of multiple sclerosis: a voxelwise diffusion-tensor MR study. *Radiology* 2011;260:541-550.
- Prineas JW, Kwon EE, Cho ES, Sharer LR, Barnett MH, Oleszak EL, et al. Immunopathology of secondary-progressive multiple sclerosis. *Ann Neurol* 2001;50:646-657.
- Qin W, Zhang M, Piao Y, Guo D, Zhu Z, Tian X, et al. Wallerian degeneration in central nervous system: dynamic associations between diffusion indices and their underlying pathology. *PLoS One* 2012;7:e41441.
- Ramagopalan SV, Dobson R, Meier UC, Giovannoni G. Multiple sclerosis: risk factors, prodromes, and potential causal pathways. *Lancet Neurol* 2010;9:727-739.
- Ramlackhansingh AF, Bose SK, Ahmed I, Turkheimer FE, Pavese N, Brooks DJ. Adenosine 2A receptor availability in dyskinetic and nondyskinetic patients with Parkinson disease. *Neurology* 2011;76:1811-1816.
- Ratchford JN, Endres CJ, Hammoud DA, Pomper MG, Shiee N, McGready J, et al. Decreased microglial activation in MS patients treated with glatiramer acetate. *J Neurol* 2011;259:1199-1205.
- Rebola N, Canas PM, Oliveira CR, Cunha RA. Different synaptic and subsynaptic localization of adenosine A2A receptors in the hippocampus and striatum of the rat. *Neuroscience* 2005;132:893-903.
- Rebola N, Simões AP, Canas PM, Tomé AR, Andrade GM, Barry CE, et al. Adenosine A2A receptors control neuroinflammation and consequent hippocampal neuronal dysfunction. *J Neurochem* 2011;117:100-111.
- Remes A, Airas L, Atula S, Färkkilä M, Hartikainen P, Koivisto K, et al. Multiple sclerosis. Current care guidelines by the working group appointed by the Finnish Medical Society Duodecim and the Finnish Neurological Society [online]. Available at: <http://www.kaypahoito.fi/web/kh/suosituksset/suositus?id=hoi36070>. Accessed Dec 10th 2014.
- Reshef A, Shirvan A, Waterhouse RN, Grimberg H, Levin G, Cohen A, et al. Molecular imaging of neurovascular cell death in experimental cerebral stroke by PET. *J Nucl Med* 2008;49:1520-1528.
- Rojas S, Martin A, Arranz MJ, Pareto D, Purroy J, Verdaguer E, et al. Imaging brain inflammation with [(11)C]PK11195 by PET and induction of the peripheral-type benzodiazepine receptor after transient focal ischemia in rats. *J Cereb Blood Flow Metab* 2007;27:1975-1986.
- Santiago AR, Baptista FI, Santos PF, Cristovao G, Ambrosio AF, Cunha RA, et al. Role of microglia adenosine A(2A) receptors in retinal and brain neurodegenerative diseases. *Mediators Inflamm* 2014;2014:465694.
- Saura J, Angulo E, Ejarque A, Casadó V, Tusell JM, Moratalla R, et al. Adenosine A2A receptor stimulation potentiates nitric oxide release by activated microglia. *J Neurochem* 2005;95:919-929.
- Sbardella E, Tona F, Petsas N, Pantano P. DTI Measurements in Multiple Sclerosis: Evaluation of Brain Damage and Clinical Implications. *Mult Scler Int* 2013;2013:671730.
- Schmidt P, Gaser C, Arsic M, Buck D, Forschler A, Berthele A, et al. An automated tool for detection of FLAIR-hyperintense white-matter lesions in Multiple Sclerosis. *Neuroimage* 2012;59:3774-3783.
- Schoemaker H, Morelli M, Deshmukh P, Yamamura HI. [3H]Ro5-4864 benzodiazepine binding in the kainate lesioned striatum and Huntington's diseased basal ganglia. *Brain Res* 1982;248:396-401.
- Schuitemaker A, van Berckel BN, Kropholler MA, Veltman DJ, Scheltens P, Jonker C, et al. SPM analysis of parametric (R)-[11C]PK11195 binding images: plasma input versus reference tissue parametric methods. *Neuroimage* 2007;35:1473-1479.
- Schweitzer PJ, Fallon BA, Mann JJ, Kumar JS. PET tracers for the peripheral benzodiazepine receptor and uses thereof. *Drug Discov Today* 2010;15:933-942.
- Sebastião AM, Ribeiro JA. Adenosine receptors and the central nervous system. In: *Handb Exp Pharmacol*, 2009: 471-534.

- Seewann A, Vrenken H, van der Valk P, Blezer EL, Knol DL, Castelijns JA, et al. Diffusely abnormal white matter in chronic multiple sclerosis: imaging and histopathologic analysis. *Arch Neurol* 2009;66:601-609.
- Shukuri M, Takashima-Hirano M, Tokuda K, Takashima T, Matsumura K, Inoue O, et al. In vivo expression of cyclooxygenase-1 in activated microglia and macrophages during neuroinflammation visualized by PET with 11C-ketoprofen methyl ester. *J Nucl Med* 2011;52:1094-1101.
- Sierra A, Encinas JM, Deudero JJ, Chancey JH, Enikolopov G, Overstreet-Wadiche LS, et al. Microglia shape adult hippocampal neurogenesis through apoptosis-coupled phagocytosis. *Cell stem cell* 2010;7:483-495.
- Simon JH, Li D, Traboulsee A, Coyle PK, Arnold DL, Barkhof F, et al. Standardized MR imaging protocol for multiple sclerosis: Consortium of MS Centers consensus guidelines. *Am J Neuroradiol* 2006;27:455-461.
- Simpson S, Jr., Blizzard L, Otahal P, Van der Mei I, Taylor B. Latitude is significantly associated with the prevalence of multiple sclerosis: a meta-analysis. *J Neurol Neurosurg Psychiatry* 2011;82:1132-1141.
- Smith SM. Fast robust automated brain extraction. *Hum Brain Mapp* 2002;17:143-155.
- Smith SM, Zhang Y, Jenkinson M, Chen J, Matthews PM, Federico A, et al. Accurate, robust, and automated longitudinal and cross-sectional brain change analysis. *Neuroimage* 2002;17:479-489.
- Smith SM, Jenkinson M, Woolrich MW, Beckmann CF, Behrens TE, Johansen-Berg H, et al. Advances in functional and structural MR image analysis and implementation as FSL. *Neuroimage* 2004;23 (Suppl 1):S208-S219.
- Smith SM, Jenkinson M, Johansen-Berg H, Rueckert D, Nichols TE, Mackay CE, et al. Tract-based spatial statistics: voxelwise analysis of multi-subject diffusion data. *Neuroimage* 2006;31:1487-1505.
- Sormani MP, Bonzano L, Roccatagliata L, Mancardi GL, Uccelli A, Bruzzi P. Surrogate endpoints for EDSS worsening in multiple sclerosis. A meta-analytic approach. *Neurology* 2010;75:302-309.
- Sormani MP, Li DK, Bruzzi P, Stubinski B, Cornelisse P, Rocak S, et al. Combined MRI lesions and relapses as a surrogate for disability in multiple sclerosis. *Neurology* 2011;77:1684-1690.
- Sospedra M, Martin R. Immunology of multiple sclerosis. *Annu Rev Immunol* 2005;23:683-747.
- Stankoff B, Wang Y, Bottlaender M, Aigrot MS, Dolle F, Wu C, et al. Imaging of CNS myelin by positron-emission tomography. *Proc Natl Acad Sci USA* 2006;103:9304-9309.
- Stankoff B, Freeman L, Aigrot MS, Chardain A, Dolle F, Williams A, et al. Imaging central nervous system myelin by positron emission tomography in multiple sclerosis using [methyl-(1)(1)C]-2-(4'-methylaminophenyl)-6-hydroxybenzothiazole. *Ann Neurol* 2011;69:673-680.
- Steenwijk MD, Daams M, Pouwels PJ, Balk LJ, Tewarie PK, Killestein J, et al. What explains gray matter atrophy in long-standing multiple sclerosis? *Radiology* 2014;272:832-842.
- Stephenson DT, Schober DA, Smalstig EB, Mincy RE, Gehlert DR, Clemens JA. Peripheral benzodiazepine receptors are colocalized with activated microglia following transient global forebrain ischemia in the rat. *J Neurosci* 1995;15:5263-5274.
- Stevens B, Porta S, Haak LL, Gallo V, Fields RD. Adenosine: a neuron-glia transmitter promoting myelination in the CNS in response to action potentials. *Neuron* 2002;36:855-868.
- Su Z, Roncaroli F, Durrenberger PF, Coope DJ, Karabatsou K, Hinz R, et al. The 18-kDa Mitochondrial Translocator Protein in Human Gliomas: A 11C-(R)PK11195 PET Imaging and Neuropathology Study. *J Nucl Med* 2015; Epub Feb 26. doi:10.2967/jnumed.114.151621
- Sumelahti ML, Tienari PJ, Wikstrom J, Palo J, Hakama M. Regional and temporal variation in the incidence of multiple sclerosis in Finland 1979-1993. *Neuroepidemiology* 2000;19:67-75.
- Sumelahti ML, Tienari PJ, Wikstrom J, Palo J, Hakama M. Increasing prevalence of multiple sclerosis in Finland. *Acta Neurol Scand* 2001;103:153-158.
- Suzuki Y, Nariai T, Kiyosawa M, Mochizuki M, Kimura Y, Oda K, et al. Increased adenosine A1 receptor levels in hemianopia patients after cerebral injury: an application of PET using 11C-8-dicyclopropylmethyl-1-methyl-3-propylxanthine. *Clin Nucl Med* 2012;37:1146-1151.
- Tai YF, Pavese N, Gerhard A, Tabrizi SJ, Barker RA, Brooks DJ, et al. Microglial activation in presymptomatic Huntington's disease gene carriers. *Brain* 2007;130:1759-1766.
- Takano A, Piehl F, Hillert J, Varrone A, Nag S, Gulyas B, et al. In vivo TSPO imaging in patients with multiple sclerosis: a brain PET study with [18F]FEDAA1106. *EJNMMI research* 2013;3:30.
- Takikawa S, Dhawan V, Spetsieris P, Robeson W, Chaly T, Dahl R, et al. Noninvasive quantitative fluorodeoxyglucose PET studies with an estimated input function derived from a population-based arterial blood curve. *Radiology* 1993;188:131-136.

- Tedeschi G, Lavorgna L, Russo P, Prinster A, Dinacci D, Savettieri G, et al. Brain atrophy and lesion load in a large population of patients with multiple sclerosis. *Neurology* 2005;65:280-285.
- Thiel A, Radlinska BA, Paquette C, Sidel M, Soucy JP, Schirmacher R, et al. The temporal dynamics of poststroke neuroinflammation: a longitudinal diffusion tensor imaging-guided PET study with ¹¹C-PK11195 in acute subcortical stroke. *J Nucl Med* 2010;51:1404-1412.
- Tienari PJ, Sumelahti ML, Rantamaki T, Wikstrom J. Multiple sclerosis in western Finland: evidence for a founder effect. *Clinical Neurol Neurosurg* 2004;106:175-179.
- Tintore M, Rovira A, Rio J, Nos C, Grive E, Tellez N, et al. Baseline MRI predicts future attacks and disability in clinically isolated syndromes. *Neurology* 2006;67:968-972.
- Todde S, Moresco RM, Simonelli P, Baraldi PG, Cacciari B, Spalluto G, et al. Design, radiosynthesis, and biodistribution of a new potent and selective ligand for in vivo imaging of the adenosine A_{2A} receptor system using positron emission tomography. *J Med Chem* 2000;43:4359-4362.
- Tomasi G, Edison P, Bertoldo A, Roncaroli F, Singh P, Gerhard A, et al. Novel reference region model reveals increased microglial and reduced vascular binding of ¹¹C-(R)-PK11195 in patients with Alzheimer's disease. *J Nucl Med* 2008;49:1249-1256.
- Trapp BD, Peterson J, Ransohoff RM, Rudick R, Mork S, Bo L. Axonal transection in the lesions of multiple sclerosis. *New Engl J Med* 1998;338:278-285.
- Trapp BD, Nave KA. Multiple sclerosis: an immune or neurodegenerative disorder? *Annu Rev Neurosci* 2008;31:247-269.
- Truyen L, van Waesberghe JH, van Walderveen MA, van Oosten BW, Polman CH, Hommes OR, et al. Accumulation of hypointense lesions ("black holes") on T1 spin-echo MRI correlates with disease progression in multiple sclerosis. *Neurology* 1996;47:1469-1476.
- Tsutsui S, Schnermann J, Noorbakhsh F, Henry S, Yong VW, Winston BW, et al. A1 adenosine receptor upregulation and activation attenuates neuroinflammation and demyelination in a model of multiple sclerosis. *J Neurosci* 2004;24:1521-1529.
- Turkheimer FE, Edison P, Pavese N, Roncaroli F, Anderson AN, Hammers A, et al. Reference and target region modeling of [¹¹C]-(R)-PK11195 brain studies. *J Nucl Med* 2007;48:158-167.
- Turkington TG. Introduction to PET instrumentation. *J Nucl Med Technol* 2001;29:4-11.
- Turner MR, Cagnin A, Turkheimer FE, Miller CC, Shaw CE, Brooks DJ, et al. Evidence of widespread cerebral microglial activation in amyotrophic lateral sclerosis: an [¹¹C]-(R)-PK11195 positron emission tomography study. *Neurobiol Dis* 2004;15:601-609.
- Tutuncu M, Tang J, Zeid NA, Kale N, Crusan DJ, Atkinson EJ, et al. Onset of progressive phase is an age-dependent clinical milestone in multiple sclerosis. *Mult Scler* 2013;19:188-198.
- Tzourio-Mazoyer N, Landeau B, Papathanassiou D, Crivello F, Etard O, Delcroix N, et al. Automated anatomical labeling of activations in SPM using a macroscopic anatomical parcellation of the MNI MRI single-subject brain. *Neuroimage* 2002;15:273-289.
- Van Camp N, Boisgard R, Kuhnast B, Theze B, Viel T, Gregoire MC, et al. In vivo imaging of neuroinflammation: a comparative study between [(18)F]PBR111, [(11)C]CLINME and [(11)C]PK11195 in an acute rodent model. *Eur J Nucl Med Mol Imaging* 2010;37:962-972.
- van Walderveen MA, Lycklama ANGJ, Ader HJ, Jongen PJ, Polman CH, Castelijns JA, et al. Hypointense lesions on T1-weighted spin-echo magnetic resonance imaging: relation to clinical characteristics in subgroups of patients with multiple sclerosis. *Arch Neurol* 2001;58:76-81.
- Vanderlugt CL, Miller SD. Epitope spreading in immune-mediated diseases: implications for immunotherapy. *Nature Rev Immunol* 2002;2:85-95.
- Wang WF, Ishiwata K, Nonaka H, Ishii S, Kiyosawa M, Shimada J, et al. Carbon-11-labeled KF21213: a highly selective ligand for mapping CNS adenosine A_{2A} receptors with positron emission tomography. *Nucl Med Biol* 2000;27:541-546.
- Wang Y, Wu C, Capriarello AV, Somoza E, Zhu W, Wang C, et al. In vivo quantification of myelin changes in the vertebrate nervous system. *J Neurosci* 2009;29:14663-14669.
- Wang Y, Yue X, Kiesewetter DO, Niu G, Teng G, Chen X. PET imaging of neuroinflammation in a rat traumatic brain injury model with radiolabeled TSPO ligand DPA-714. *Eur J Nucl Med Mol Imaging* 2014a;41:1440-1449.
- Wang Y, Yue X, Kiesewetter DO, Wang Z, Lu J, Niu G, et al. [(18)F]DPA-714 PET imaging of AMD3100 treatment in a mouse model of stroke. *Mol Pharm* 2014b;11:3463-3470.
- Varrone A, Mattsson P, Forsberg A, Takano A, Nag S, Gulyas B, et al. In vivo imaging of the 18-kDa translocator protein (TSPO) with [¹⁸F]FEDAA1106 and PET does not show increased binding in Alzheimer's disease patients. *Eur J Nucl Med Mol Imaging* 2013;40:921-931.

- Varrone A, Oikonen V, Forsberg A, Joutsa J, Takano A, Solin O, et al. Positron emission tomography imaging of the 18-kDa translocator protein (TSPO) with [¹⁸F]FEMPA in Alzheimer's disease patients and control subjects. *Eur J Nucl Med Mol Imaging* 2014;42:438-446.
- Vas A, Shchukin Y, Karrenbauer VD, Cselenyi Z, Kostulas K, Hillert J, et al. Functional neuroimaging in multiple sclerosis with radiolabelled glia markers: preliminary comparative PET studies with [¹¹C]vinpocetine and [¹¹C]PK11195 in patients. *J Neurol Sci* 2008;264:9-17.
- Watson CC. New, faster, image-based scatter correction for 3D PET. *IEEE Trans Nucl Sci* 2000;47:1587-1594.
- Weinshenker BG, Bass B, Rice GP, Noseworthy J, Carriere W, Baskerville J, et al. The natural history of multiple sclerosis: a geographically based study. I. Clinical course and disability. *Brain* 1989;112:133-146.
- Welton T, Kent D, Constantinescu CS, Auer DP, Dineen RA. Functionally Relevant White Matter Degradation in Multiple Sclerosis: A Tract-based Spatial Meta-Analysis. *Radiology* 2014:140925.
- Venneti S, Lopresti BJ, Wang G, Slagel SL, Mason NS, Mathis CA, et al. A comparison of the high-affinity peripheral benzodiazepine receptor ligands DAA1106 and (R)-PK11195 in rat models of neuroinflammation: implications for PET imaging of microglial activation. *J Neurochem* 2007a;102:2118-2131.
- Venneti S, Wagner AK, Wang G, Slagel SL, Chen X, Lopresti BJ, et al. The high affinity peripheral benzodiazepine receptor ligand DAA1106 binds specifically to microglia in a rat model of traumatic brain injury: implications for PET imaging. *Exp Neurol* 2007b;207:118-127.
- Versijpt J, Debruyne JC, Van Laere KJ, De Vos F, Keppens J, Strijckmans K, et al. Microglial imaging with positron emission tomography and atrophy measurements with magnetic resonance imaging in multiple sclerosis: a correlative study. *Mult Scler* 2005;11:127-134.
- Whitacre CC. Sex differences in autoimmune disease. *Nat Immunol* 2001;2:777-780.
- Viglietta V, Baecher-Allan C, Weiner HL, Hafler DA. Loss of functional suppression by CD4+CD25+ regulatory T cells in patients with multiple sclerosis. *J Exp Med* 2004;199:971-979.
- Willer CJ, Dyment DA, Sadovnick AD, Rothwell PM, Murray TJ, Ebers GC. Timing of birth and risk of multiple sclerosis: population based study. *BMJ* 2005;330:120-124.
- Vincenzi F, Corciulo C, Targa M, Merighi S, Gessi S, Casetta I, et al. Multiple sclerosis lymphocytes upregulate A2A adenosine receptors that are antiinflammatory when stimulated. *Eur J Immunol* 2013;43:2206-2216.
- Winkeler A, Boisgard R, Awde AR, Dubois A, Theze B, Zheng J, et al. The translocator protein ligand [(1)(8)F]DPA-714 images glioma and activated microglia in vivo. *Eur J Nucl Med Mol Imaging* 2012;39:811-823.
- Virta JR, Laatu S, Parkkola R, Oikonen V, Rinne JO, Ruutiainen J. Cerebral acetylcholinesterase activity is not decreased in MS patients with cognitive impairment. *Mult Scler* 2011;17:931-938.
- Vlodavsky E, Soustiel JF. Immunohistochemical expression of peripheral benzodiazepine receptors in human astrocytomas and its correlation with grade of malignancy, proliferation, apoptosis and survival. *J Neurooncol* 2007;81:1-7.
- Volonte C. Commentary: Never underestimate the power of adenosine in multiple sclerosis. *CNS Neurol Disord Drug Targets* 2013;12:895-896.
- Vos CM, Geurts JJ, Montagne L, van Haastert ES, Bo L, van der Valk P, et al. Blood-brain barrier alterations in both focal and diffuse abnormalities on postmortem MRI in multiple sclerosis. *Neurobiol Dis* 2005;20:953-960.
- Vowinckel E, Reutens D, Becher B, Verge G, Evans A, Owens T, et al. PK11195 binding to the peripheral benzodiazepine receptor as a marker of microglia activation in multiple sclerosis and experimental autoimmune encephalomyelitis. *J Neurosci Res* 1997;50:345-353.
- Vrenken H, Seewann A, Knol DL, Polman CH, Barkhof F, Geurts JJ. Diffusely abnormal white matter in progressive multiple sclerosis: in vivo quantitative MR imaging characterization and comparison between disease types. *Am J Neuroradiol* 2010;31:541-548.
- Wu C, Wang C, Popescu DC, Zhu W, Somoza EA, Zhu J, et al. A novel PET marker for in vivo quantification of myelination. *Bioorg Med Chem* 2010;18:8592-8599.
- Wu C, Zhu J, Baeslack J, Zaremba A, Hecker J, Kraso J, et al. Longitudinal PET imaging for monitoring myelin repair in the spinal cord. *Ann Neurol* 2013;74:688-698.
- Wu Y, Carson RE. Noise reduction in the simplified reference tissue model for neuroreceptor functional imaging. *J Cereb Blood Flow Metab* 2002;22:1440-1452.
- Yao SQ, Li ZZ, Huang QY, Li F, Wang ZW, Augusto E, et al. Genetic inactivation of the adenosine A(2A) receptor exacerbates brain damage in mice with

- experimental autoimmune encephalomyelitis. *J Neurochem* 2012;123:100-112.
- Yaqub M, van Berckel BN, Schuitemaker A, Hinz R, Turkheimer FE, Tomasi G, et al. Optimization of supervised cluster analysis for extracting reference tissue input curves in (R)-[¹¹C]PK11195 brain PET studies. *J Cereb Blood Flow Metab* 2012;32:1600-1608.
- Zanotti-Fregonara P, Hines CS, Zoghbi SS, Liow JS, Zhang Y, Pike VW, et al. Population-based input function and image-derived input function for [(1)(1)C](R)-rolipram PET imaging: methodology, validation and application to the study of major depressive disorder. *Neuroimage* 2012;63:1532-1541.
- Zanotti-Fregonara P, Hirvonen J, Lyoo CH, Zoghbi SS, Rallis-Frutos D, Huestis MA, et al. Population-based input function modeling for [(18)F]FMPEP-d 2, an inverse agonist radioligand for cannabinoid CB1 receptors: validation in clinical studies. *PLoS One* 2013;8:e60231.
- Zhang X, Paule MG, Newport GD, Sadovova N, Berridge MS, Apana SM, et al. MicroPET imaging of ketamine-induced neuronal apoptosis with radiolabeled DFNSH. *J Neural Transm* 2011;118:203-211.
- Zimmermann H, Braun N. Ecto-nucleotidases--molecular structures, catalytic properties, and functional roles in the nervous system. *Prog Brain Res* 1999;120:371-385.